AFCRL-72-0665

SYNTHESIS OF LOADED N-PORT SCATTERERS

by

Roger F. Harrington
Joseph R. Mautz

Department of
Electrical and Computer Engineering
Syracuse University
Syracuse, New York 13210

ABSTRACT

This report gives methods for designing reactively loaded N-port
scatterers to have desired scattering pattern characteristics. A method
for obtaining a least-squares approximation to a desired magnitude radi-
ation pattern, with the restriction that port currents are real, is de-
veloped. A procedure for obtaining maximum gain, with the restriction
that the port currents are real, is also described. Conducting bodies
can be reactively loaded to make any real port current the dominant port
mode of that body. If the body is electrically small or of intermediate
size, and if a sufficient number of ports are chosen, then the scattered
field pattern is approximately the same as the synthesized pattern. A
number of numerical examples are given for a body consisting of a wire
triangle with two cross wires, on which four ports are defined. Computer
programs with sample input - output data are given for each procedure
discussed.

CONTENTS

Part One

THEORY AND EXAMPLES

I. INTRODUCTION

The scattering of electromagnetic waves by a body can be controlled by impedance loading of the body, either by lumped loads or by continuous loads. The general problem has been discussed by Schindler, Mack, and Blacksmith [1]. Methods are available for the analysis of lump loaded scatterers [2] and of continuously loaded scatterers [3]. A synthesis procedure for controlling the electromagnetic scattering by continuously loading the body is also available [4]. It makes use of the theory of characteristic modes of a conducting body [5,6]. Similar modes for an N-port scatterer have been defined and used for the analysis of lump loaded scatterers [7].

This report gives methods for synthesizing loaded N-port scatterers to obtain desired scattering patterns or to optimize the radar cross section. The geometry of the scatterer is assumed known and the loads are chosen to control the scattering. The theory makes use of the characteristic modes of loaded N-port scatterers. By a procedure called modal synthesis we can make any set of real port currents a resonant mode of the scatterer. If this resonant mode is the principal contributor to the scattered field, then its field pattern will be essentially the scattering pattern of the loaded scatterer. To synthesize a desired scattering pattern, we first determine the real port current whose field pattern approximates the desired pattern, and then we resonate it. The analogous procedure is used to optimize the scattering cross section.

II. BASIC THEORY

The analysis of loaded N-port scatterers is discussed in reference
[7]. The theory is expressed equally well in terms of either impedance
parameters or admittance parameters. A summary of the basic theory is
given here.

Consider an N-port scatterer loaded by N lumped impedances, or,
more generally, by an N-port load network. The total field $\underset{\sim}{E}$ is the sum
of the impressed field $\underset{\sim}{E}^i$, due to sources external to the scatterer, plus
a scattered field $\underset{\sim}{E}^s$, due to current induced on the scatterer. In the
open-circuit impedance formulation, the scattered field is given by [7]

$$\underset{\sim}{E}^s = \underset{\sim}{E}_0^{oc} - \underset{\sim}{\tilde{E}}^{oc}[Z_S + Z_L]^{-1}\vec{V}^{oc} \tag{1}$$

Here $[Z_S]$ and $[Z_L]$ are the port impedance matrices of the scatterer and
load, respectively, $\vec{V}^{oc}$ is a column matrix of the open circuit port voltages,
$\underset{\sim}{\tilde{E}}^{oc}$ is a row matrix of the fields radiated by unit current sources at the
ports, and $\underset{\sim}{E}_0^{oc}$ is the field scattered when all ports are open circuited.

For a modal analysis, we change the basis to one which diagonalizes
$[Z_S + Z_L]$. In particular, we choose as a basis the eigenvectors $\vec{I}_n$ of

$$[X]\vec{I}_n = \lambda_n[R]\vec{I}_n \tag{2}$$

where $[X]$ and $[R]$ are the Hermitian parts of $[Z_S + Z_L]$, assumed to be
symmetric. The advantages of this choice are:

(a) All eigenvalues λ_n and eigenvectors $\vec{I}_n$ are real. (More
generally, the $\vec{I}_n$ can be equiphasal.)

(b) The eigencurrents $\vec{I}_n$ form an orthonormal set with weight $[R]$,
that is

$$\tilde{I}_m[R]\vec{I}_n = \delta_{mn} \tag{3}$$

(c) The eigencurrents $\vec{I}_n$ form an orthogonal set with respect to [X], that is

$$\tilde{I}_m [X] \vec{I}_n = \delta_{mn} \lambda_n \tag{4}$$

(d) For a loss-free loaded scatterer, the eigenfields $\underset{\sim}{E}(\vec{I}_n)$ form an orthogonal set over the sphere at infinity, that is

$$\frac{1}{\eta} \oiint_{S_\infty} \underset{\sim}{E}^*(\vec{I}_m) \cdot \underset{\sim}{E}(\vec{I}_n) ds = \delta_{mn} \tag{5}$$

Here $\underset{\sim}{E}(\vec{I}_n)$ denotes the field radiated when the eigenvector $\vec{I}_n$ exists at the scatterer ports.

When the eigencurrents $\vec{I}_n$ are chosen as a basis, the solution (1) reduces to

$$\underset{\sim}{E}^s = \underset{\sim}{E}_0^{oc} - \sum_{n=1}^{N} \frac{\tilde{I}_n \vec{V}^{oc}}{1+j\lambda_n} \underset{\sim}{E}(\vec{I}_n) \tag{6}$$

Many examples of the use of (6) for analysis are given in reference [7]. If the scatterer is electrically small or intermediate in size, only a few of the eigenvalues λ_n are of small magnitude, even though there may be many ports. Hence, in a modal solution, only a few of the modes may be required for good accuracy. A mode having $\lambda_n = 0$ is said to be in resonance. In many cases only that mode which is at or near resonance contributes significantly to the scattered field.

The dual short-circuit admittance formulation for the scattered field is [7]

$$\underset{\sim}{E}^s = \underset{\sim}{E}_0^{sc} - \underset{\sim}{\tilde{E}}^{sc} [Y_S + Y_L]^{-1} \vec{I}^{sc} \tag{7}$$

Here $[Y_S]$ and $[Y_L]$ are the port admittance matrices of the scatterer and load, respectively, $\vec{I}^{sc}$ is a column matrix of the short circuit port

4

currents, $\underset{\sim}{E}^{sc}$ is a row matrix of the fields radiated by unit voltage sources at the ports, and $\underset{\sim 0}{E}^{sc}$ is the field scattered when all ports are short circuited. For a modal analysis, the basis is changed to one which diagonalizes $[Y_S + Y_L]$. In particular, we choose as a basis the eigenvectors $\vec{V}_n$ of

$$[B]\vec{V}_n = \mu_n [G]\vec{V}_n \tag{8}$$

where $[B]$ and $[G]$ are the Hermitian parts of $[Y_S + Y_L]$. The advantages of this choice are dual to those listed (a) to (d) above. Finally, when the eigenvoltages $\vec{V}_n$ are chosen as a basis, (7) reduces to

$$\underset{\sim}{E}^s = \underset{\sim 0}{E}^{sc} - \sum_{n=1}^{N} \frac{\tilde{V}_n \vec{I}^{sc}}{1+j\mu_n} \underset{\sim}{E}(\vec{V}_n) \tag{9}$$

Both (6) and (9) are exact formulations of the problem, and either may be used for analysis. However, our synthesis procedures usually involve approximations, in which case (6) and (9) may lead to different results.

III. MODAL SYNTHESIS

In this section the general concept of modal synthesis is discussed. Any real port current (or voltage) can be made an eigencurrent (or eigenvoltage) of the loaded scatterer by choosing the proper load. The procedure is called modal resonance if the eigenvalue of the synthesized mode is zero.

In general, an eigencurrent must satisfy (2) where $[X] = [X_S + X_L]$ and $[R] = [R_S + R_L]$. Rearranging this equation, we have

$$[X_L - \lambda R_L]\vec{I} = - [X_S - \lambda R_S]\vec{I} \tag{10}$$

Both $[X_S]$ and $[R_S]$ are determined by the scatterer geometry, and hence are fixed. If we specify a real $\vec{I}$ and a real λ, then (10) becomes a set of linear equations for determining the elements of $[X_L]$ and $[R_L]$. In general

there are more unknowns than equations, and hence the solution is not unique.
We can choose the load network to be loss-free, in which case (10) reduces
to

$$[X_L]\vec{I} = - [X_S - \lambda R_S]\vec{I} \tag{11}$$

The solution is still not unique in general. We can always choose the load
network to be diagonal, that is

$$[X_L] = [diag\ X_i] \tag{12}$$

In this case the diagonal elements are found from (11) as

$$X_i = - \frac{1}{I_i}\ ([X_S - \lambda R_S]\vec{I})_i \tag{13}$$

Here $(\ )_i$ denotes the i-th component of the enclosed column matrix.
Finally, if we wish to resonate the current $\vec{I}$, we choose $\lambda = 0$ and (13)
reduces to

$$X_i = - \frac{1}{I_i}\ ([X_S]\ \vec{I})_i \tag{14}$$

A real port current may also be resonated by nondiagonal load matrices
$[Z_L]$.

The above discussion applies in the dual sense to port modal
voltages. Analogous to (10), the basic equation to satisfy is

$$[B_L - \mu G_L]\vec{V} = - [B_S - \mu G_S]\vec{V} \tag{15}$$

Again the scatterer geometry determines both $[G_S]$ and $[B_S]$. If we specify
a real $\vec{V}$ and real μ, then (15) becomes a set of linear equations for de-
termining the elements of $[G_L]$ and $[B_L]$. Again there are more unknowns
than equations, and the solution is not unique. Specializations of (15)
analogous to (11) through (14) can be made according to duality. In par-
ticular, for resonance by a loss-free diagonal load matrix $[Y_L] = j[diag\ B_i]$,
we have dual to (14)

$$B_i = -\frac{1}{V_i} ([B_s]\vec{V})_i \tag{16}$$

A real port voltage may also be resonated by nondiagonal load matrices $[Y_L]$.

IV. PATTERN SYNTHESIS

In this section we consider synthesis procedures for determining the real port current $\vec{I}$ (or port voltage $\vec{V}$) whose radiation field pattern approximates a desired field pattern. The method developed for general surfaces [4] can be used for N-port scatterers with only minor changes in the theory. However, this synthesis procedure requires the desired field pattern to be specified in both magnitude and phase. For most applications the phase of the field pattern is unimportant, and better approximations can be obtained by specifying only the magnitude of the field pattern. This is especially true for our problem because of the constraint that the port current be real. We will develop the theory in terms of N-port systems, but it also applies to surfaces, such as considered in reference [4].

The problem is one of mixed antenna synthesis, as defined by Bakhrakh and Troytskiy [8]. The method of solution is similar to that used by Choni [9]. We desire to obtain the real port current $\vec{I}$ whose radiation field $\underset{\sim}{E}$ approximates in magnitude a real pattern $\underset{\sim}{F}$ on the radiation sphere. Let E^m denote a component of $\underset{\sim}{E}$ at point m on the radiation sphere, and F^m the corresponding component of $\underset{\sim}{F}$ at the same point. Given M points, we define the error of synthesis to be

$$\varepsilon = \sum_{m=1}^{M} \left| |E^m| - F^m \right|^2 \tag{17}$$

Next, let $\{\vec{I}_n\}$ be a basis of real port currents, and express the port current as

$$\vec{I} = \sum_{n=1}^{N} \alpha_n \vec{I}_n \tag{18}$$

where α_n are real constants to be determined. The radiation field of $\vec{I}$ is

$$\underset{\sim}{E} = \sum_{n=1}^{N} \alpha_n \underset{\sim}{E}_n \qquad (19)$$

where $\underset{\sim}{E}_n$ is the radiation field produced by the corresponding $\vec{I}_n$. In terms of (19), the error (17) becomes

$$\varepsilon = \sum_{m=1}^{M} \left| \left| \sum_{n=1}^{N} \alpha_n E_n^m \right| - F^m \right|^2 \qquad (20)$$

We wish to determine the real α_n which minimize ε. It is sometimes convenient to use fewer basis functions than ports, in which case the N of (18) to (20) is the number of basis functions instead of the number of ports.

To circumvent the troublesome inner magnitude operation in (20), we first consider the more general function

$$\varepsilon(\vec{\alpha},\vec{\beta}) = \sum_{m=1}^{M} \left| \sum_{n=1}^{N} \alpha_n E_n^m - F^m e^{j\beta_m} \right|^2 \qquad (21)$$

This is the error function used when the desired field pattern is specified both in magnitude F and in phase β. Hence, for β_m fixed, the α_n for minimum ε are given by the analysis of reference [4]. When the α_n are fixed the minimum ε is obviously obtained when both quantities within the magnitude signs of (21) are in phase for each m, or

$$\beta_m = \text{angle of } \sum_{n=1}^{N} \alpha_n E_n^m \qquad (22)$$

Because (21) is more general than (20), its minimum is less than or equal to that of (20). But under condition (22), the ε of (21) is equal to that of (20). Therefore (20) and (21) have the same minimum.

An iterative procedure for minimizing (21) proceeds as follows:

1. Assume starting values for $\beta_1, \beta_2, \ldots, \beta_M$.

2. Keep the β_m fixed and calculate the α_n which minimize ε according to the theory of [4].

3. Keep the α_n fixed and calculate the β_m which minimize ε according to (22).

4. Go to step 2.

This procedure eventually converges because steps 2 and 3 cannot increase ε. While the procedure obtains absolute minima in $\vec{\alpha}$ space and in $\vec{\beta}$ space, it does not necessarily obtain the absolute minimum in the catenated space $(\vec{\alpha}, \vec{\beta})$. The procedure in general converges to a stationary point, usually a local minimum, which may or may not be the global minimum.

We now describe steps 2 and 3 in more detail. When $\vec{\beta}$ is constant, $\varepsilon(\vec{\alpha}, \vec{\beta})$ is quadratic in $\vec{\alpha}$ and thus has only one stationary point. This is the absolute minimum located at [4]

$$\vec{\alpha} = [\text{Re}(\widetilde{E}*E)]^{-1}[\text{Re}(\widetilde{E}*Fe^{j\beta})] \tag{23}$$

where the matrices are

$$E = [E_n^m]_{M \times N} \tag{24}$$

$$Fe^{j\beta} = [F^m e^{j\beta_m}]_{M \times 1} \tag{25}$$

When $\vec{\alpha}$ is constant, we adjust the phase $\vec{\beta}$ according to (22). An alternative way of expressing this is

$$e^{j\beta_m} = \frac{(E\vec{\alpha})_m}{|(E\vec{\alpha})_m|} \tag{26}$$

where $(E\vec{\alpha})_m$ denotes the m-th component of the column vector $E\vec{\alpha}$. Note that, since only the exponential (26) is used in the iteration procedure, we need never calculate the β_m.

The synthesis procedure in terms of port voltage $\vec{V}$ is the same except for a change in definition of various quantities. Instead of (18), we express the port voltage as

$$\vec{V} = \sum_{n=1}^{N} \alpha_n \vec{V}_n \qquad (27)$$

where $\{\vec{V}_n\}$ is a real basis and α_n are real constants to be determined. Equation (19) remains the same, except $\underset{\sim}{E}_n$ is the radiation field produced by the corresponding $\vec{V}_n$. The rest of the theory applies unchanged.

V. EXAMPLES – PATTERN SYNTHESIS

The theory is applicable to a large variety of problems, and even when the problem is specified there still remains the choice of the formulation (open-circuit or short-circuit) and of the basis functions. For the geometry we choose the wire triangle with two cross wires shown in Fig. 1. This is the same object used in the previous report on modal analysis of N-port systems [7]. The tip angle is 30°, the parameter a is one wavelength at a frequency f_o, and the wire diameter is a/100. The four points at which the wires cross the z axis are input ports, labeled (1), (2), (3), and (4). All computations are made using 38 triangle functions in a Galerkin solution. (The computer input data is given in Part two, Section II of reference [7].)

The magnitude of the pattern chosen for synthesis is

$$F_\phi = |\cos \theta| \quad \text{in the x=0 plane,} \qquad (28)$$

$$F_\theta = |\cos \theta| \quad \text{in the y=0 plane.} \qquad (29)$$

Twelve points are chosen for the least-squares pattern synthesis as follows: For F_ϕ in the x=0 plane,

$$\theta = 0, \ 30°, \ 60°, \ 90°, \ 120°, \ 150°, \ 180° \qquad (30)$$
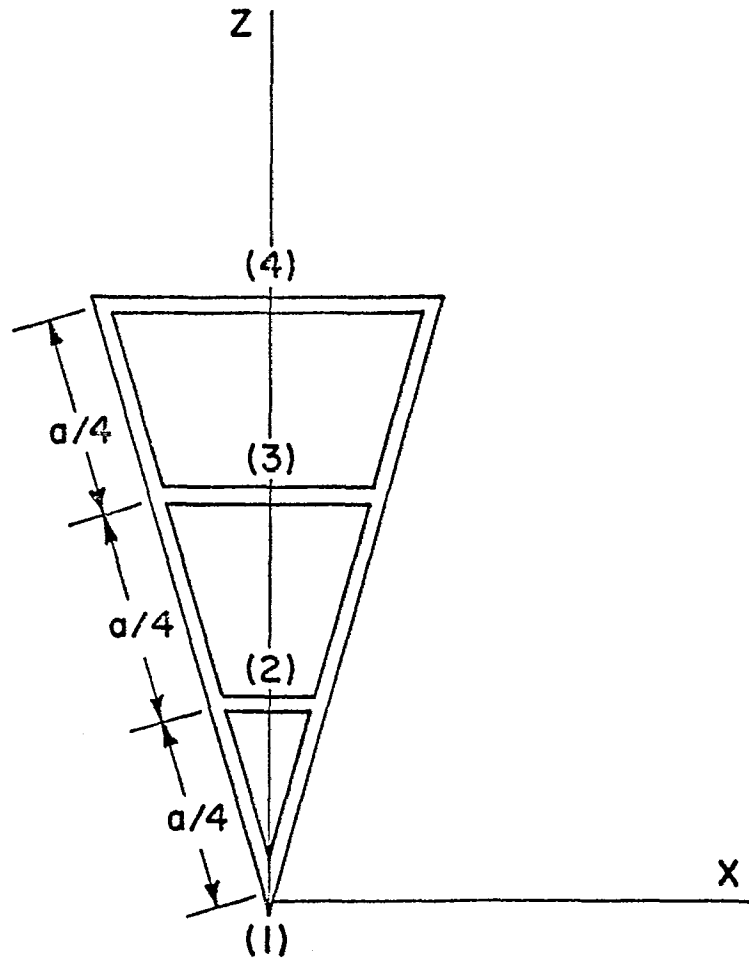
Fig. 1. Wire triangle with cross wires, tip angle = 30°,
a = one wavelength, wire diameter = a/100.

and for F_θ in the y=0 plane,

$$\theta = 30°, \ 60°, \ 90°, \ 120°, \ 150° \qquad\qquad (31)$$

The pattern functions F_θ at 0 and 180° in the y=0 plane are the same as F_ϕ at 0 and 180° in the x=0 plane, and hence are not included in (31). The phase angles of the field were chosen to be zero at all points in the first iteration of the pattern synthesis procedure.

For the first example we use port currents as the basis for pattern synthesis. To illustrate convergence, first one, then two, then three and finally four port currents are used. They are added in the order in which the ports are labeled in Fig. 1. This order is arbitrary, and any other order could be chosen if desired. Figure 2 illustrates the results of this synthesis procedure. The solid curves show the magnitude of the synthesized E_ϕ and E_θ in the x=0 and y=0 planes, respectively, and the crosses show the desired field magnitudes. The port currents for the final synthesized pattern are

$$I_1 = 0.3428$$

$$I_2 = 0.2923 \qquad\qquad (32)$$

$$I_3 = -0.1048$$

$$I_4 = -0.0013$$

Note that there is little change between the synthesized patterns of Fig. 2c and Fig. 2d. This is reflected in the relative smallness of I_4 above. Hence, for this particular synthesis approach, one can do almost as well by using only three ports and leaving the fourth one open circuited. It is to be emphasized that the synthesis procedure is an optimum seeking one, usually having several local optima. Hence, starting from different initial phases for the field, or using a different order of iteration, we may arrive at a different final synthesis.

12
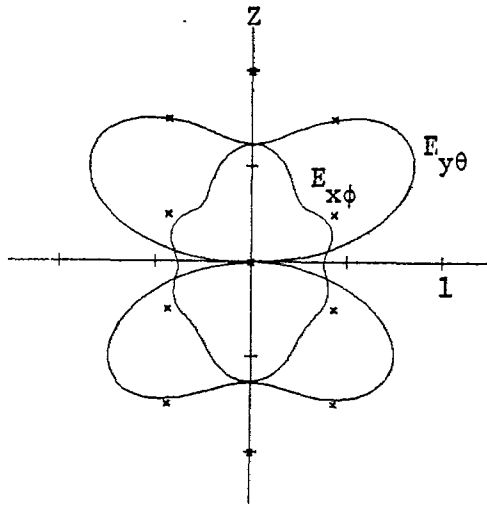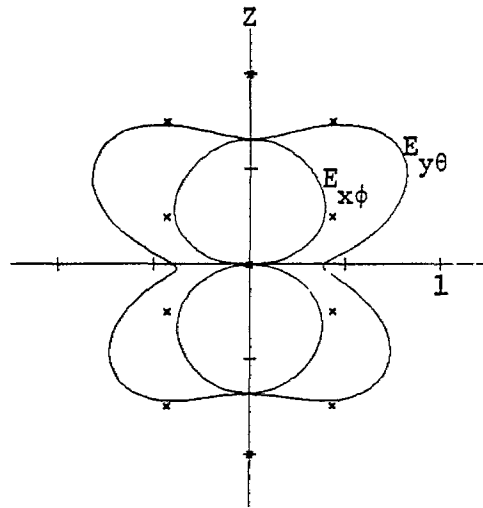
(a) one port current
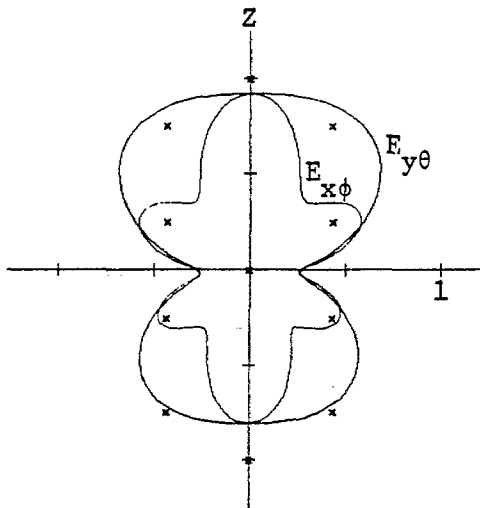
(b) two port currents

(c) three port currents

(d) four port currents

Fig. 2. Field magnitude pattern synthesis using real port currents
as a basis. Crosses denote the desired pattern. Curves
labeled $E_{x\phi}$ denote $|E_\phi|$ in the x=0 plane. Curves labeled
$E_{y\theta}$ denote $|E_\theta|$ in the y=0 plane.

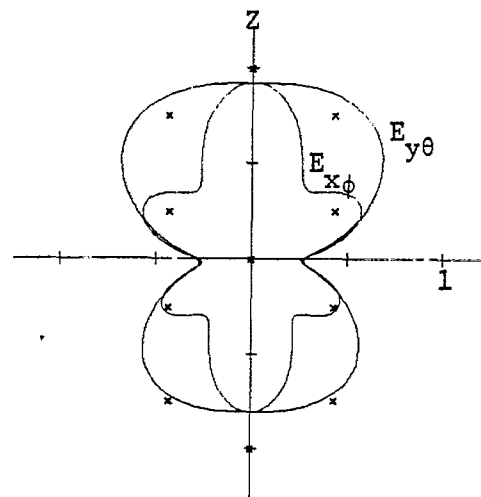Once the desired real port currents are obtained, they can be resonated by the procedure of Section III. This has been done for each of the synthesized patterns of Fig. 2. Since port currents were used as a basis, this means that in Fig. 2a a reactive load was placed only at port (1), in Fig. 2b at ports (1) and (2), in Fig. 2c at ports (1), (2), and (3), and in Fig. 2d at all four ports. It is understood that ports at which no reactive load is placed are open circuited. The resultant scattering patterns are shown in Fig. 3. The plots are in terms of $\sqrt{\sigma}/\lambda$, since this is the field magnitude which was used in the synthesis procedure. In each case the incident wave is an x-polarized plane wave propagating in the z-direction (incident on the 30° tip angle). Note that the scattering patterns of Figs. 3a, 3b, 3c, and 3d are similar to the synthesized patterns of Figs. 2a, 2b, 2c, and 2d, respectively. The degree to which the scattering patterns are the same as the synthesized patterns depends upon the smallness of the "background scattering," that is, of the $\underset{\sim}{E}_0^{OC}$ term in (6). In the present problem, for the open-circuited scatterer of Fig. 1,

$$\sigma/\lambda^2 = 0.0177 \qquad (33)$$

In contrast σ/λ^2 is of the order unity for the loaded scatterer. Hence, our assumption that the $\underset{\sim}{E}_0^{OC}$ term is small is fully justified in this case. The reactive loads used in the final loaded scatterer (Fig. 3d) are

$$X_1 = -100.3$$

$$X_2 = -546.7$$

$$X_3 = -1448. \qquad (34)$$

$$X_4 = 47,370.$$

Note that X_4 is large, indicating that port (4) is almost an open circuit. It is an open circuit in the scatterer of Fig. 3c, but the other loads are then slightly different from those of (34). This again indicates that port (4) is relatively unimportant for this particular synthesis procedure.

14
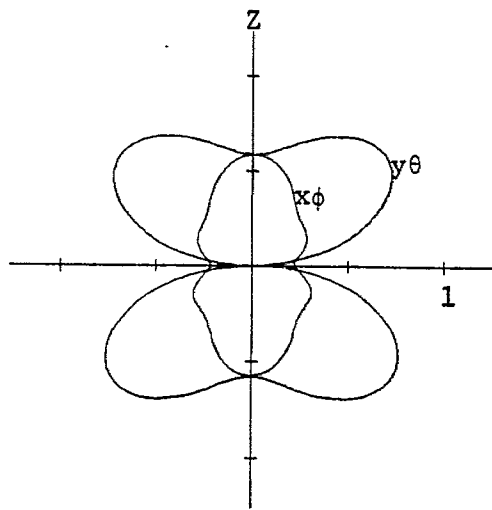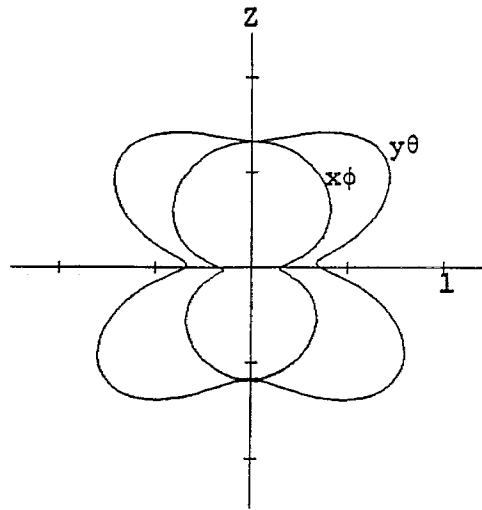
(a) one port current
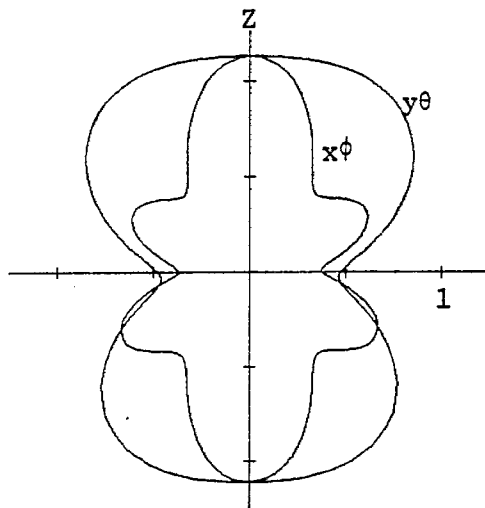
(b) two port currents

(c) three port currents
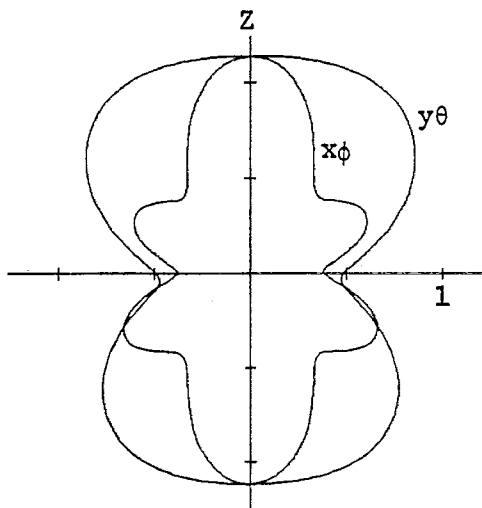
(d) four port currents

Fig. 3. Bistatic scattering patterns $(\sqrt{\sigma}/\lambda)$ for the wire object of
Fig. 1 loaded to resonate the port currents which synthesize
the patterns of Fig. 2. Curves labeled xϕ denote ϕ polariza-
tion in the x=0 plane. Curves labeled yθ denote θ polariza-
tion in the y=0 plane.

In most practical applications one seeks scatterers having desirable scattering characteristics over some reasonably broad frequency band. The synthesis procedure is basically a single frequency one, with no consideration given as yet to variation with frequency. As an indication of frequency sensitivity, we have calculated the backscattering cross section per wavelength squared (σ/λ^2) vs. frequency over the range $f = 0.8f_o$ to $1.2f_o$, where f_o is the design frequency. Figure 4 shows curves for the same loaded scatterers as considered in Fig. 3. In each case the load is considered to be an inductance if X_i is positive at f_o, or a capacitance if X_i is negative at f_o. Note that even the singly-loaded case, Fig. 4a, has considerable variation of σ/λ^2 vs. frequency. Hence, we conclude that our synthesized loaded scatterers are relatively frequency sensitive. (Any non-smoothness of the frequency plots are due to relatively large increments in frequency used over parts of the frequency range.)

The same synthesis problem is next treated using the modal currents of the open-circuit formulation as the basis. Qualitatively speaking, we expect the modal currents corresponding to the smaller eigenvalues to have broader band characteristics. Hence, if only currents with small eigenvalues are used, structures with broader band characteristics should result. To test this hypothesis, we added the modal currents in the order of increasing magnitude of eigenvalues. These mode eigenvalues and eigencurrents (normalized to maximum value unity) are tabulated in the following table.

Table 1. Eigenvalues λ_n and eigencurrents $\vec{I}_n$ for the wire object of Fig. 1.

n	λ_n	Port (1)	Port (2)	Port (3)	Port (4)
1	-0.1552	-0.1338	0.4326	0.8419	1.0000
2	-10.12	-0.6078	1.0000	0.8054	-0.6458
3	-50.54	1.0000	-0.5374	0.0137	0.0740
4	816.4	0.5441	1.0000	-0.2839	0.0778
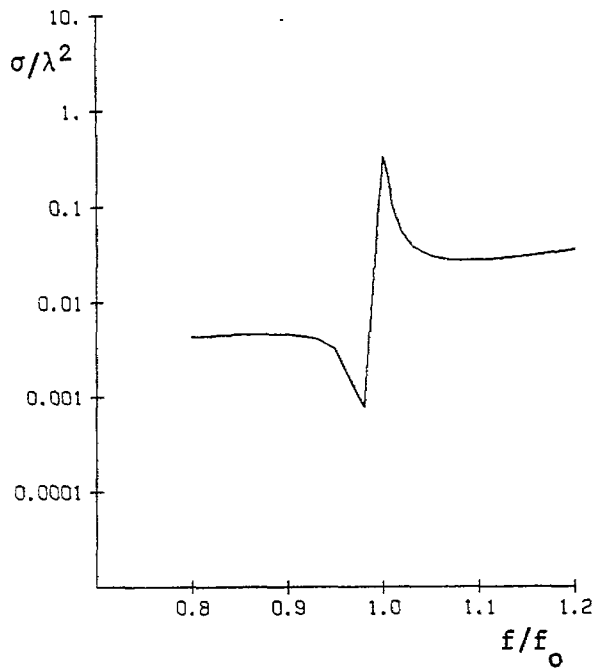
(a) one port current
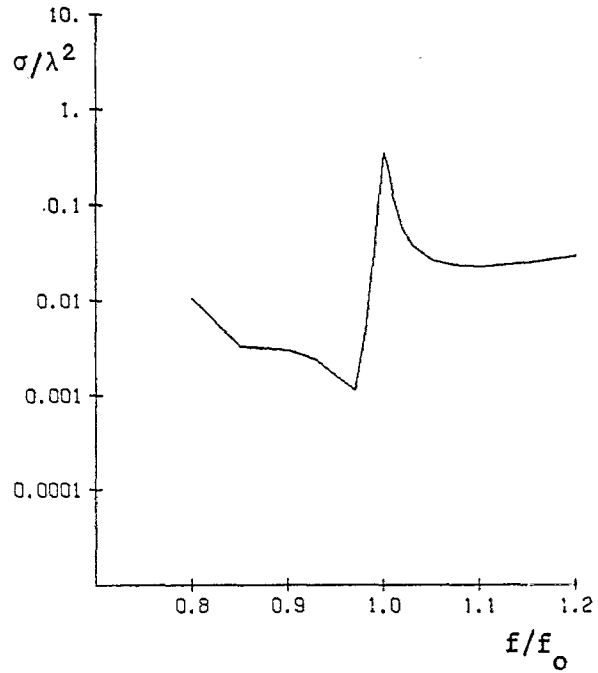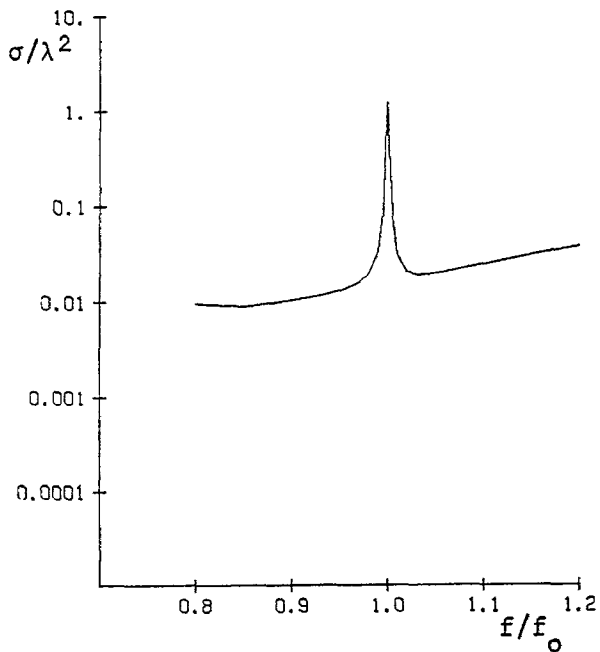
(b) two port currents

(c) three port currents
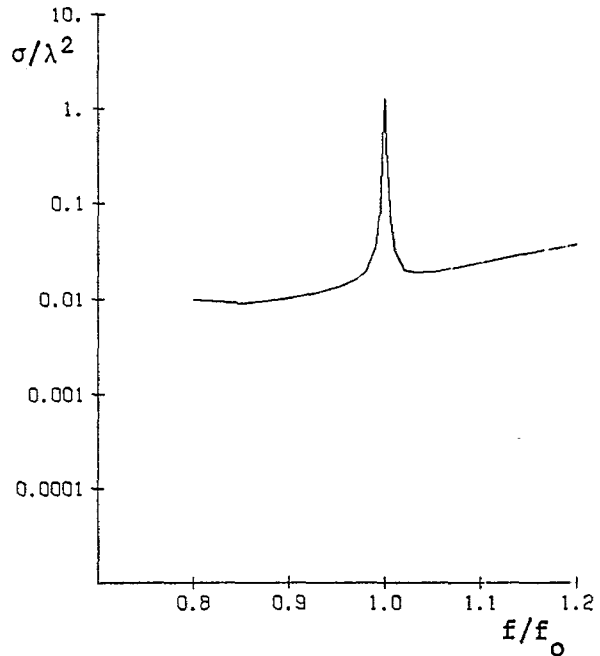
(d) four port currents

Fig. 4. Backscattering (σ/λ^2) vs. frequency (f/f_o) for the same loaded scatterers as Fig. 3.

(a) one mode current

(b) two mode currents

(c) three mode currents

(d) four mode currents
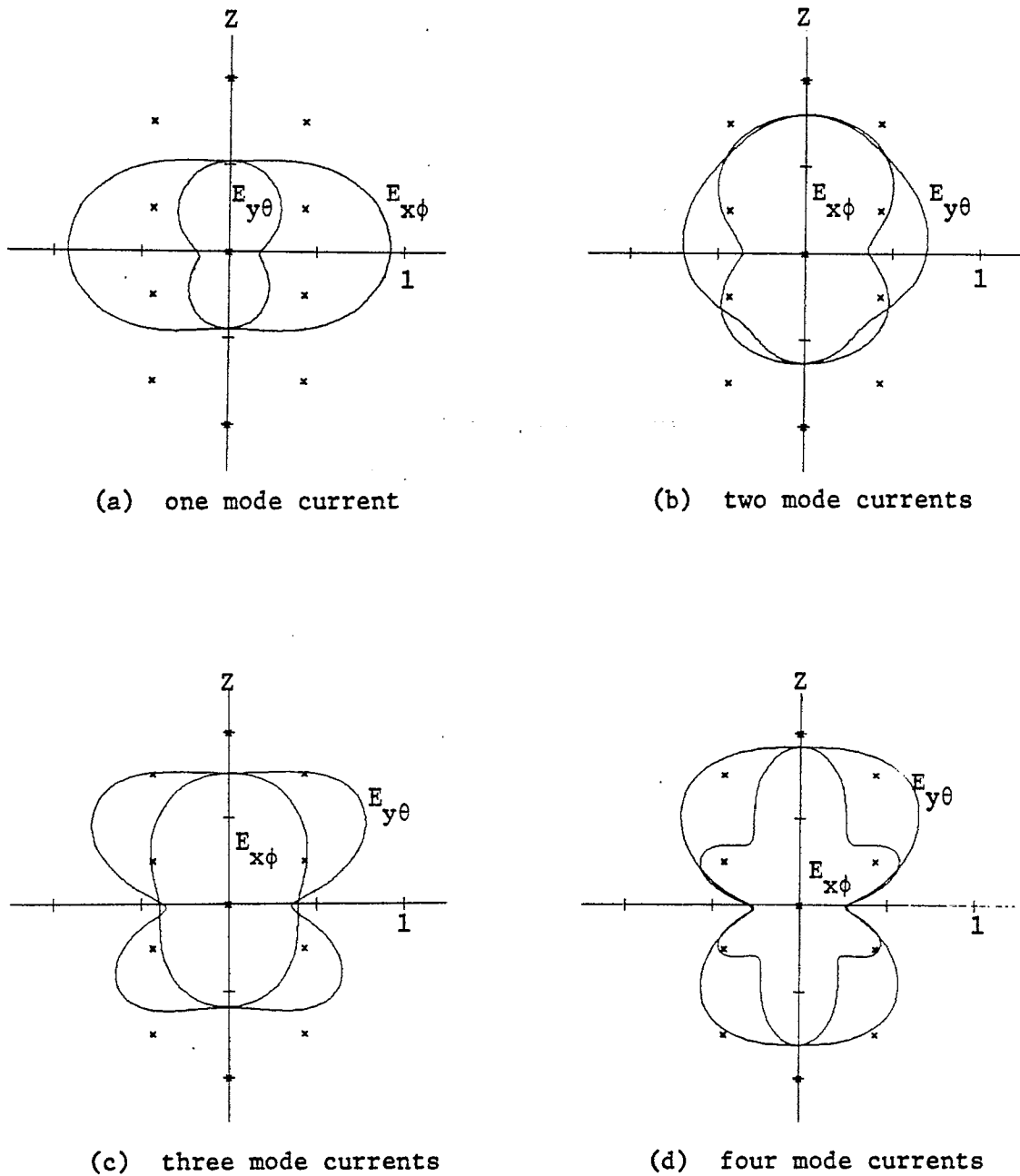
Fig. 5. Field magnitude pattern synthesis using real mode currents as a basis. Crosses denote the desired pattern. Curves labeled $E_{x\phi}$ denote $|E_\phi|$ in the x=0 plane. Curves labeled $E_{y\theta}$ denote $|E_\theta|$ in the y=0 plane.

18
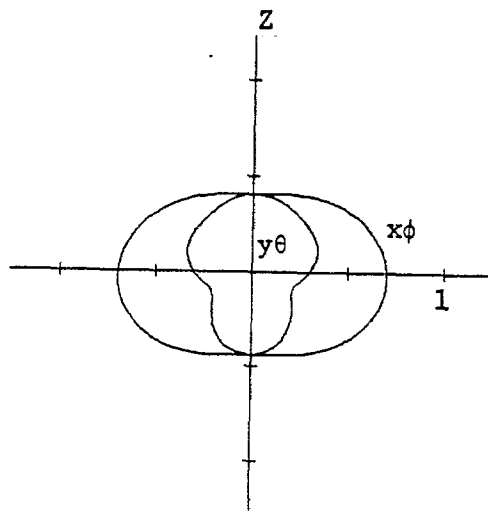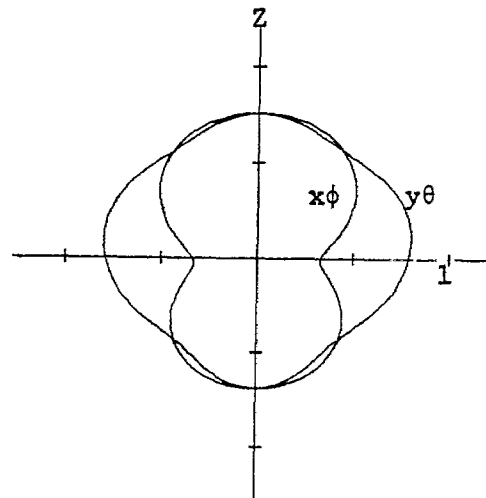
(a) one mode current
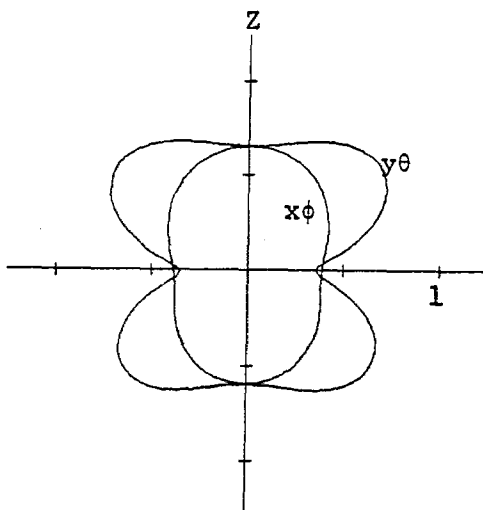
(b) two mode currents

(c) three mode currents
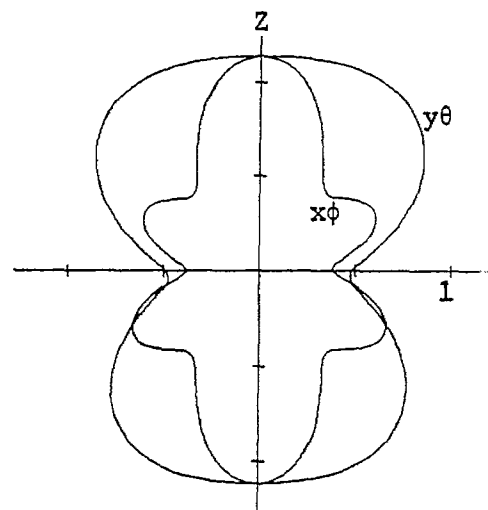
(d) four mode currents

Fig. 6. Bistatic scattering patterns ($\sqrt{\sigma}/\lambda$) for the wire object of Fig. 1 loaded to resonate the port currents which synthesize the patterns of Fig. 5. Curves labeled xϕ denote ϕ polarization in the x=0 plane. Curves labeled yθ denote θ polarization in the y=0 plane.

We used first one, then two, then three, and then all four eigencurrents in the synthesis procedure. The results are shown in Figs. 5a to 5d, respectively. Again the solid curves are the magnitude of the synthesized E_ϕ in the x=0 plane and E_θ in the y=0 plane, while the crosses are the desired field magnitudes. The synthesized pattern using only one basis function, Fig. 5a, is just the pattern of the single mode current $\vec{I}_1$. This mode has components of current at all ports, as shown in the first row of Table 1. In fact, each synthesized pattern, Figs. 5a, 5b, 5c, 5d, now results from currents at all ports. The final synthesized pattern, Fig. 5d, is the same as the final synthesized pattern using port currents, Fig. 2d. However, the final patterns in the two cases do not necessarily have to be the same, since the synthesis method is iterative and may arrive at a different local optimum point.

Again, once we have a desired real current it can be resonated by the procedure of Section III. The currents producing each of the synthesized patterns of Fig. 5 have been resonated in this way. This now involves placing a reactive load at each port in each case. The scattering patterns for the reactively loaded scatterers are shown in Fig. 6. As before, these plots are of $\sqrt{\sigma}/\lambda$, which is field magnitude as used in the synthesis procedure. The incident wave in each case is x-polarized and z-propagating. Again, note that the scattering patterns of Figs. 6a, 6b, 6c, and 6d are similar to the synthesized patterns of Figs. 5a, 5b, 5c, and 5d, respectively. The reactive loads used in the final case are essentially the same as (34), since we arrived at the same optimum point. Note that each scatterer of Fig. 6 involves loads at all ports. This is in contrast to the preceding case where only one load was used in Fig. 3a, two in Fig. 3b, and three in Fig. 3c.

We next wish to demonstrate that broader band behavior results when a partial modal basis is used for the current. Figure 7 shows graphs of backscattering σ/λ^2 vs. frequency for the loaded scatterers of Fig. 6. Again the load is considered to be an inductor if X_i is positive at f_o, or a capacitor if X_i is negative at f_o. Note that the

20
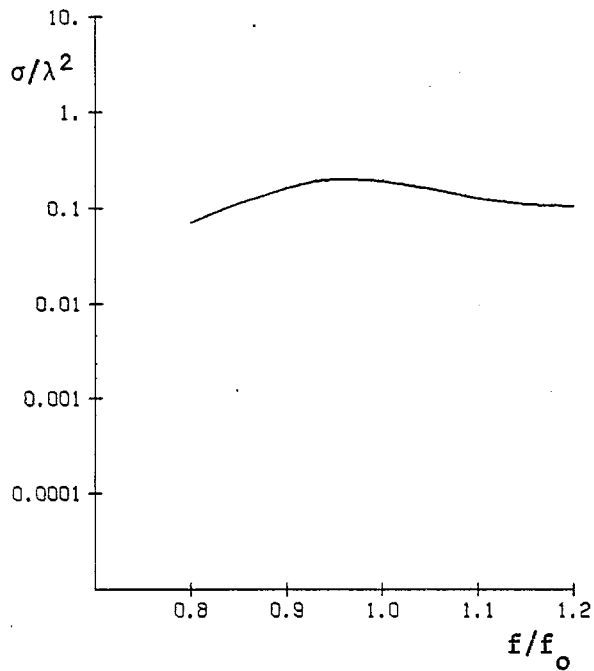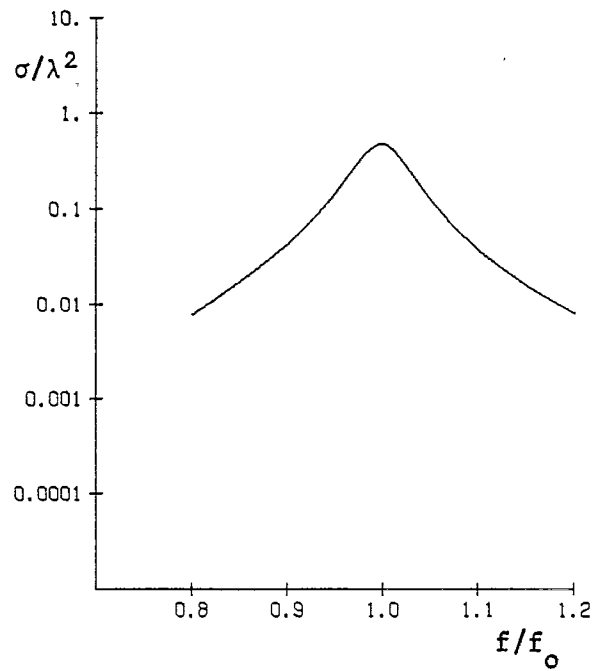
(a)   one mode current
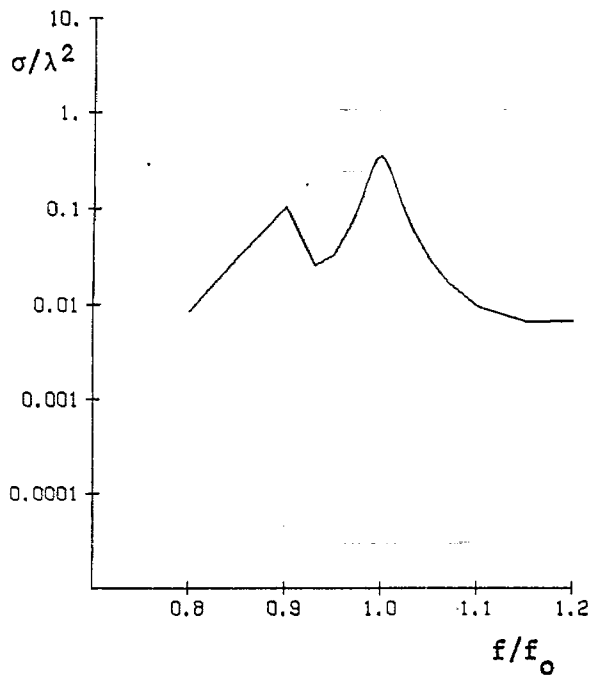
(b)   two mode currents

(c)   three mode currents
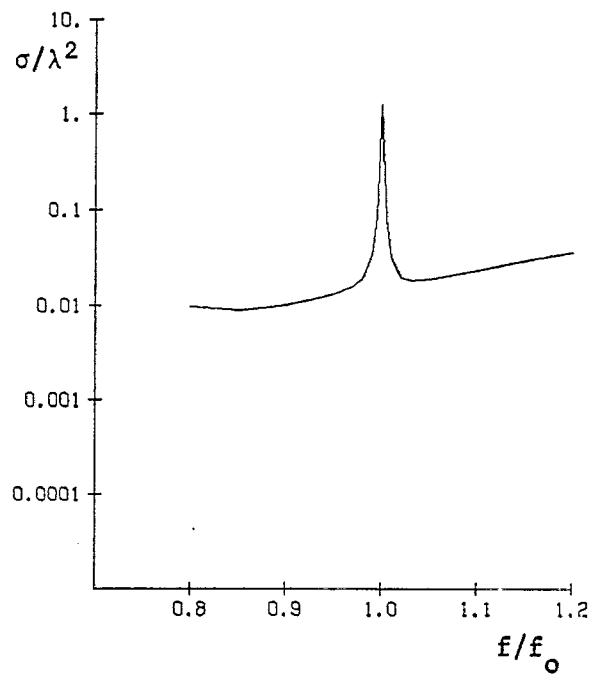
(d)   four mode currents

Fig. 7.   Backscattering (σ/λ^2) vs. frequency (f/f_o) for the same loaded scatterers as Fig. 6.

single mode case, Fig. 7a, gives extremely broadband scattering. The two mode case, Fig. 7b, is still relatively broadband, the three mode case, Fig. 7c, less so, and the four mode case, Fig. 7d, quite narrow band. The four mode case is, in fact, identical to Fig. 4d, the final design being the same.

Other bases for the current can be used in the synthesis procedure. For example, the mode currents for some particular loaded structure can be used [7]. For the broadest band behavior, we can use the Q mode currents, defined in a manner analogous to that for complete conducting bodies [4]. In particular, the Q mode currents $\vec{I}_n$ are defined by

$$\omega [X'] \vec{I}_n = Q_n [R] \vec{I}_n \qquad (35)$$

where $[X']$ is the angular frequency derivative of the port matrix $[X]$. For computation, we used a finite difference approximation to $[X']$. The Q mode currents are then obtained from (35) by the same method used to solve (2) for the ordinary mode currents. It turns out that, for the particular scatterer of Fig. 1, the Q mode currents did not differ greatly from the ordinary mode currents. The eigenvalues Q_n are different, but the ordering according to magnitude of Q_n remained the same as for the λ_n eigenvalues. Hence, computations using Q mode currents were similar to those of Figs. 5 to 7. Plots of the resulting synthesized patterns and scattering are therefore not shown explicitly. Suffice it to say that the scatterers of Figs. 6 and 7 are, for most practical purposes, the broadest band obtainable.

A set of curves similar to Figs. 2 to 7 has been prepared using the short-circuit formulation and port voltages. The results are qualitatively similar, except that the correspondence of the scattering patterns for loaded scatterers to the corresponding synthesized patterns is not quite as good. This is because the "background scattering" for the short-circuited scatterer, that is, the $\underset{\sim}{E}_0^{sc}$ term in (9), is not as small as the analogous $\underset{\sim}{E}_0^{oc}$ term in (6). In fact, for the short-circuited scatterer of Fig. 1,
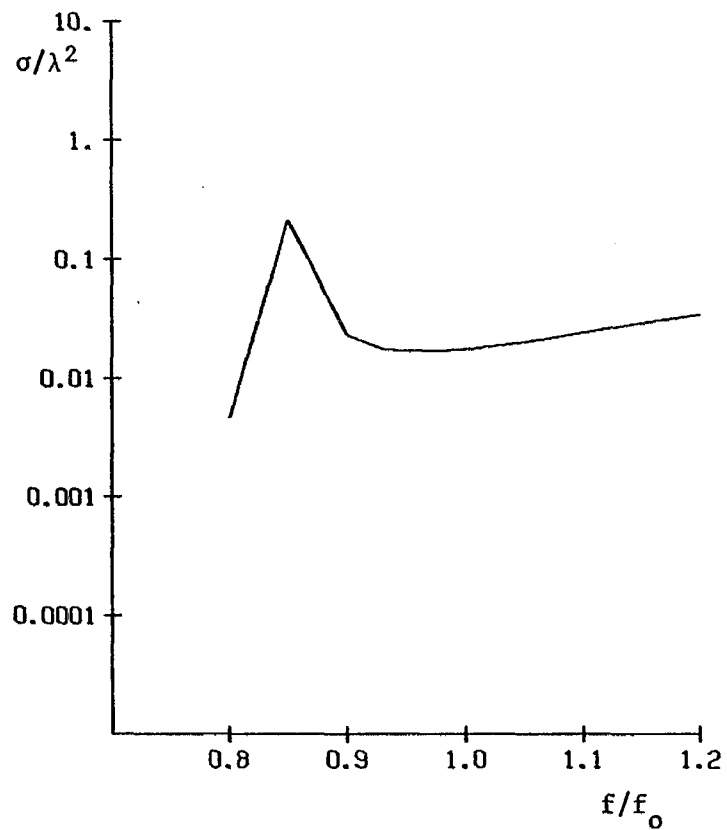
(a) open-circuited scatterer
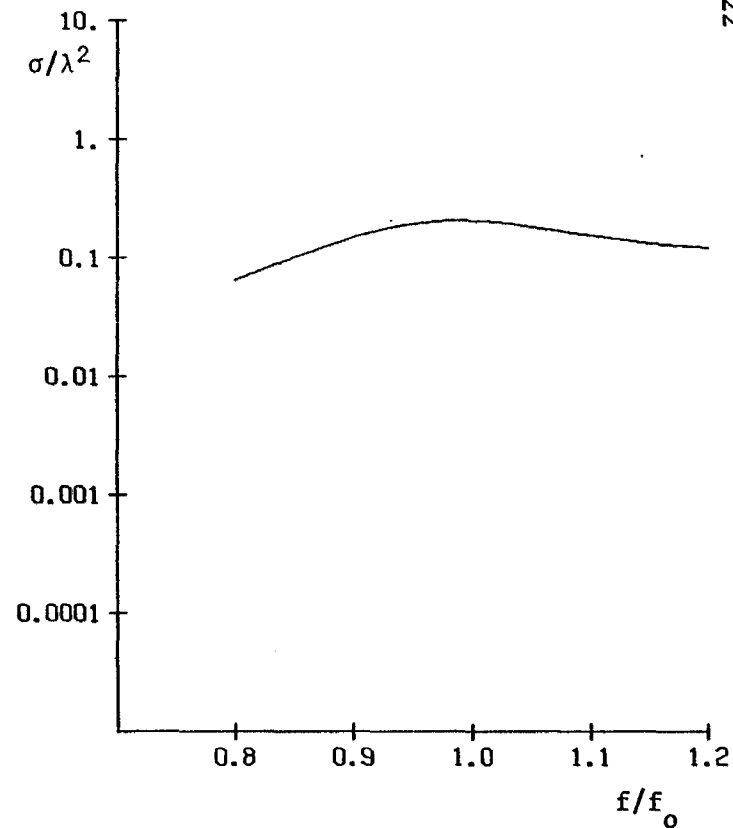
(b) short-circuited scatterer

Fig. 8. Backscattering (σ/λ^2) vs. frequency (f/f_o) for the wire object of Fig. 1 when (a) ports are open circuited, and (b) ports are short circuited.

$$\sigma/\lambda^2 = 0.2011 \tag{36}$$

which is significantly larger than (33) for the open-circuited scatterer. For reference, the curves for the short-circuit formulation are given in Appendix A. These correspond to Figs. 2 to 7 for the open-circuit formulation. Finally, so that the reader can compare the behavior of loaded scatterers to the same scatterer unloaded, plots of the open-circuited and short-circuited backscattering σ/λ^2 vs. frequency are given in Fig. 8.

VI. MAXIMUM RADAR CROSS SECTION

Another problem of interest is that of maximizing the radar cross section of a loaded scatterer. In terms of the open-circuit modal analysis, the bistatic radar cross section is given by [7, Eqs. (69) and (74)]

$$\sigma = \frac{\omega^2 \mu^2}{4\pi} \left| F_0^{oc} + \sum_{n=1}^{N} \frac{\alpha_n^r \alpha_n^t}{1+j\lambda_n} \right|^2 \tag{37}$$

Here F_0^{oc} is the term due to scattering by the open-circuited scatterer, and α_n^r and α_n^t are mode excitation coefficients for the n-th mode due to excitation from the receiver and transmitter, respectively. It is desired to reactively load the scatterer to resonate a port current $(\lambda_1 = 0)$ such that its contribution is the only significant term in (37). Then

$$\sigma \approx \frac{\omega^2 \mu^2}{4\pi} \left| \alpha_1^r \alpha_1^t \right|^2 \tag{38}$$

We here consider only the case of backscattering, whence $\alpha_1^r = \alpha_1^t$. The coefficient α_1^r is given by [7, Eq. (55)] with the port current normalized according to $\tilde{I}^*[R]\vec{I} = 1$. A formula for $\left| \alpha_1^r \right|^2$ which is insensitive to the amplitude of $\vec{I}$ is therefore

$$\rho = \left| \alpha_1^r \right|^2 = \frac{\left| \tilde{I}\vec{V}^{oc} \right|^2}{\tilde{I}^*[R]\vec{I}} \tag{39}$$

24

where $\vec{V}^{oc}$ is the open-circuit port voltage produced by a unit plane wave from the receiver. The problem is now to find the real port current $\vec{I}$ which maximizes (39). Once the desired $\vec{I}$ is found, it can be resonated by the method of Section III.

The parameter ρ is also proportional to the power gain g of the current $\vec{I}$, the explicit relationship being [10]

$$g = \frac{k^2 \eta}{4\pi} \rho \tag{40}$$

Hence, maximization of radar cross section is equivalent to the maximization of gain, but with the restriction that $\vec{I}$ is real. In the more general case of bistatic scattering, (38) can be written as

$$\sigma \approx \frac{\lambda^2}{\pi} g^r g^t \tag{41}$$

where g^r and g^t are the power gains in the directions of the receiver and transmitter, respectively. Thus, maximization of bistatic radar cross section is equivalent to maximizing the product of two gains, again with the restriction that $\vec{I}$ is real. The relationship (41) was previously derived for one-port loaded scatterers in reference [2].

The optimization of Rayleigh quotients of the form (39) when $\vec{I}$ is restricted to the real field is considered in reference [4]. In this case the maximum ρ is

$$\rho_r = \text{Re}(\widetilde{V}^{oc})[R]^{-1}\{\text{Re}(\vec{V}^{oc}) + c \ \text{Im}(\vec{V}^{oc})\} \tag{42}$$

and the associated port current is

$$\vec{I}_r = [R]^{-1}\{\text{Re}(\vec{V}^{oc}) + c \ \text{Im}(\vec{V}^{oc})\} \tag{43}$$

In (42) and (43), c is chosen to give the larger ρ_r from the two numbers

$$c = -a \pm \sqrt{a^2 + 1} \tag{44}$$

where

$$a = \frac{\text{Re}[\tilde{V}^{oc}][R]^{-1}\text{Re}(\vec{V}^{oc}) - \text{Im}(\tilde{V}^{oc})[R]^{-1}\text{Im}(\vec{V}^{oc})}{2\,\text{Re}(\tilde{V}^{oc})[R]^{-1}\text{Im}(\vec{V}^{oc})} \qquad (45)$$

Even though $\vec{I}$ must be real (or equiphase) for (39) to be valid, it is of interest to compare the above result with the maximum ρ that could be obtained if $\vec{I}$ were complex. This problem is treated in reference [10], the maximum ρ being

$$\rho_o = \tilde{V}^{oc}[R]^{-1}\vec{V}^{oc*} \qquad (46)$$

and the associated port current being

$$\vec{I}_o = [R]^{-1}\vec{V}^{oc*} \qquad (47)$$

It has been shown that the maximum ρ for real port currents is at least one-half that for complex port currents, and the two cases are equal if $\vec{V}^{oc}$ is equiphasal [4].

The analysis can alternatively be carried out in terms of short-circuit parameters and port voltages. In this case the appropriate starting formula is [7, Eqs. (74) and (76)]. It is now desired to susceptively load the scatterer to resonate ($\mu_1 = 0$) a port voltage such that it is the only significant term in the bistatic radar cross section formula. Analogous to (38), we then have

$$\sigma \approx \frac{\omega^2 \mu^2}{4\pi}\left|\beta_1^r \ \beta_1^t\right|^2 \qquad (48)$$

where β_1^r and β_1^t are the mode excitation coefficients for the resonant mode. Again we consider only the case of backscattering, whence $\beta_1^r = \beta_1^t$. The coefficient β_1^r is given by [7, Eq. (63)], with the port voltage normalized according to $\tilde{V}*[G]\vec{V} = 1$. Therefore, analogous to (39), we have

$$\rho = |\beta_1^r|^2 = \frac{|\widetilde{V}\vec{I}^{sc}|^2}{\widetilde{V}*[G]\vec{V}} \tag{49}$$

where $\vec{I}^{sc}$ is the short-circuit port current produced by a unit plane wave from the receiver. The problem is now to find the real port voltage $\vec{V}$ which maximizes (49). The maximization procedure is identical to that used in the preceding case, except for an interchange of symbols. Hence, if we replace $\vec{V}^{oc}$ by $\vec{I}^{sc}$, $\vec{I}$ by $\vec{V}$, and [R] by [G], equations (42) to (47) remain valid in the present case. Once the desired real $\vec{V}$ is obtained it can be resonated by the methods of Section III. Because of the approximations involved, the solution in terms of $\vec{V}$ will not give exactly the same radar cross section as the solution in terms of $\vec{I}$, but the two cross sections are usually very close.

We can think of the preceding solution as the maximization of ρ when $\vec{I}$ (or $\vec{V}$) is expressed in terms of the port basis. It is of interest to consider the solution when an arbitrary basis is used, or even when an incomplete basis is used. To accomplish this, let $\{\vec{I}_n\}$ denote a real basis and let

$$\vec{I} = \sum_{n=1}^{N} \alpha_n \vec{I}_n \tag{50}$$

where the α_n are real constants to be determined. Then

$$\widetilde{I}\vec{V}^{oc} = \sum_{n=1}^{N} \alpha_n \widetilde{I}_n \vec{V}^{oc} = \widetilde{\alpha}\hat{V}^{oc} \tag{51}$$

where $\widetilde{\alpha}$ is a row vector of the α_n and $\hat{V}^{oc}$ is the new voltage vector

$$\hat{V}^{oc} = [\widetilde{I}_n]\vec{V}^{oc} \tag{52}$$

Here $[\widetilde{I}_n]$ is the matrix with rows equal to $\widetilde{I}_n$. Similarly,

$$\widetilde{I}*[R]\vec{I} = \sum_{m=1}^{N} \sum_{n=1}^{N} \alpha_m \widetilde{I}_m [R]\vec{I}_n \alpha_n$$

$$= \widetilde{\alpha}[\hat{R}]\vec{\alpha} \tag{53}$$

where $[\hat{R}]$ is the new resistance matrix with elements

$$\hat{R}_{mn} = \widetilde{\vec{I}}_m [R] \vec{I}_n \tag{54}$$

In terms of the new basis, the ρ of (39) becomes

$$\rho = \frac{\left| \widetilde{\vec{\alpha}} \hat{V}^{oc} \right|^2}{\widetilde{\vec{\alpha}} [\hat{R}] \vec{\alpha}} \tag{55}$$

which is again the same form as (39). Hence, the optimization of ρ proceeds as before. The theory also remains valid if the basis $\{\vec{I}_n\}$ is incomplete. In this case the N of the above equations becomes the number of basis functions instead of the number of ports. A change of basis for the solution in terms of port voltages is accomplished in a similar way.

VII. EXAMPLES - MAXIMUM CROSS SECTION

Representative computations of maximum radar cross section have been made for the 4-port wire object of Fig. 1. Again the choices of the formulation and of the basis are arbitrary. For the first example we use the open-circuit formulation and port currents for the basis. Gain is optimized using first one port, then two, then three, and finally four real port currents. The ports are added in the order in which they are numbered in Fig. 1, which is arbitrary. Once the real port currents are found, they are resonated by the method of Section III. This results in a reactively loaded scatterer which gives approximately the maximum backscattering radar cross section in the direction that gain was maximized. Table 2 summarizes these results. The first column shows the ports used in the gain maximization, which are also those ports loaded when the scatterer is resonated. The second column gives the maximum x-polarized gain in the -z direction for real currents at the excited ports. The third column gives the x-polarized backscattering cross section for the resonated scatterer in the -z direction. In this case, those ports not used in the optimization procedure are open circuited.
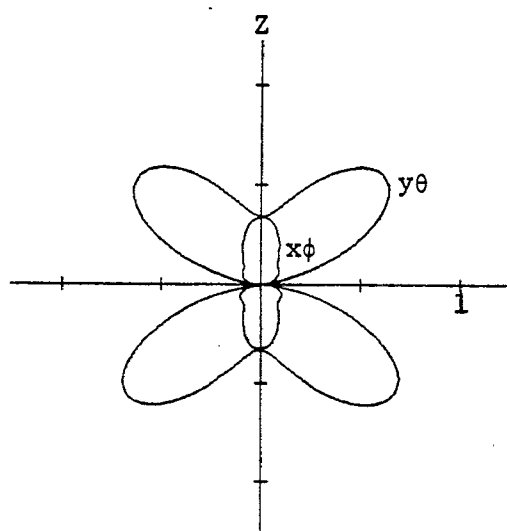
(a) one port current
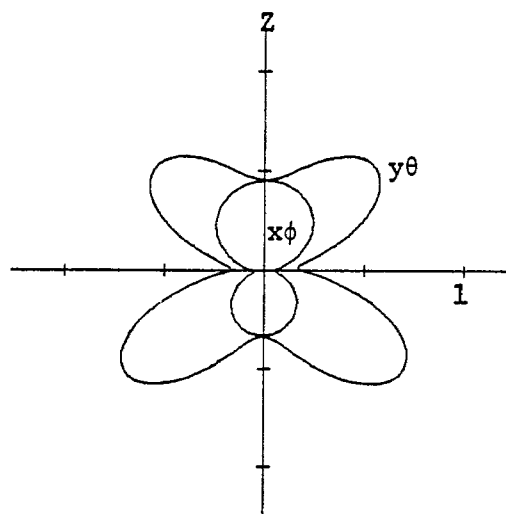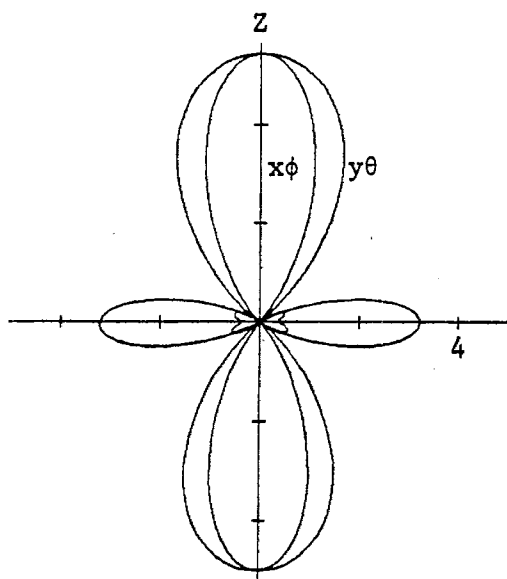
(b) two port currents

(c) three port currents
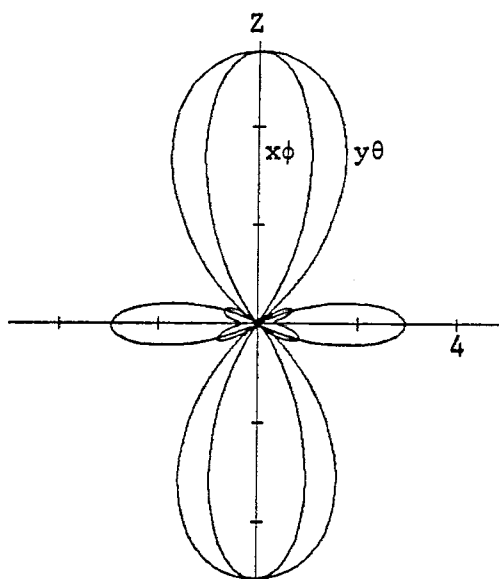
(d) four port currents

Fig. 9. Bistatic scattering patterns (σ/λ^2) for the wire object of Fig. 1 loaded for maximum gain in the -z direction. Curves labeled xϕ denote ϕ polarization in the x=0 plane. Curves labeled yθ denote θ polarization in the y=0 plane.

Table 2. Maximum gain and backscattering cross section
when port currents are used as a basis.

Ports Used	Maximum Gain	Cross Section
1	1.017	0.3293 λ^2
1,2	1.185	0.3322 λ^2
1,2,3	3.972	5.005 λ^2
1,2,3,4	4.033	5.160 λ^2

The bistatic radar cross section patterns (σ/λ^2) for the loaded scatterers of Table 2 are shown in Fig. 9. The curves labeled xϕ are for the ϕ-polarized scattered field in the x=0 plane, and those labeled yθ are for the θ-polarized scattered field in the y=0 plane. When only port 1 is loaded, Fig. 9a, the maximum gain pattern is the same as the field synthesis pattern, Fig. 3a. (Note, however, that Fig. 3a is a plot of $\sqrt{\sigma}/\lambda$, whereas Fig. 9a is of σ/λ^2.) When ports 1 and 2 are loaded, the scattering pattern is still not very directive in the desired -z direction. When ports 1,2, and 3 are loaded (Fig. 9c), the scattering pattern becomes highly directive in the -z direction. Finally, there is little improvement over the three port case when all four ports are loaded, Fig. 9d. The reactive loads for this final case are as follows

$$X_1 = -693.2$$

$$X_2 = -361.7$$

$$X_3 = -933.9 \tag{56}$$

$$X_4 = -4949.$$

Note that X_4 is large compared to the other loads, which we would expect since there is little change when it is open circuited. Plots of the gain patterns for maximum gain, corresponding to Figs. 2 and 5 in the pattern
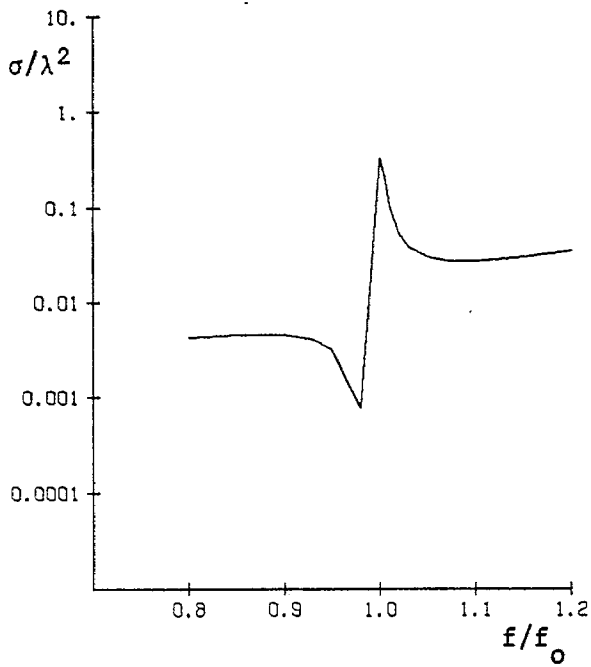
(a) one port current
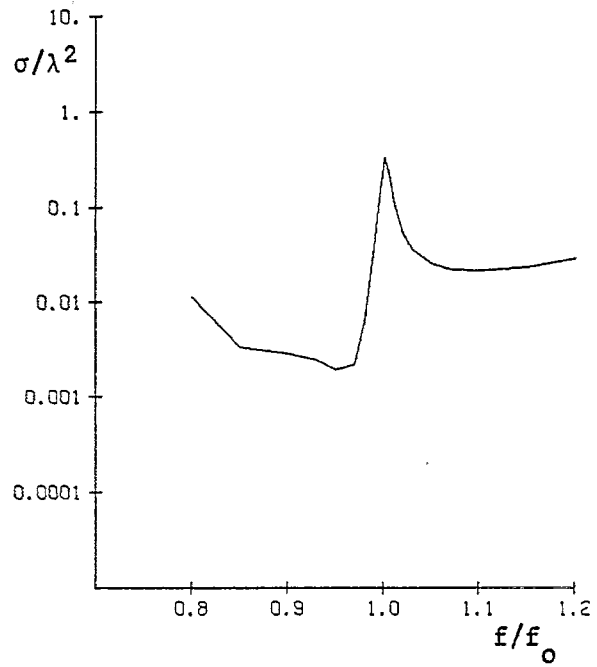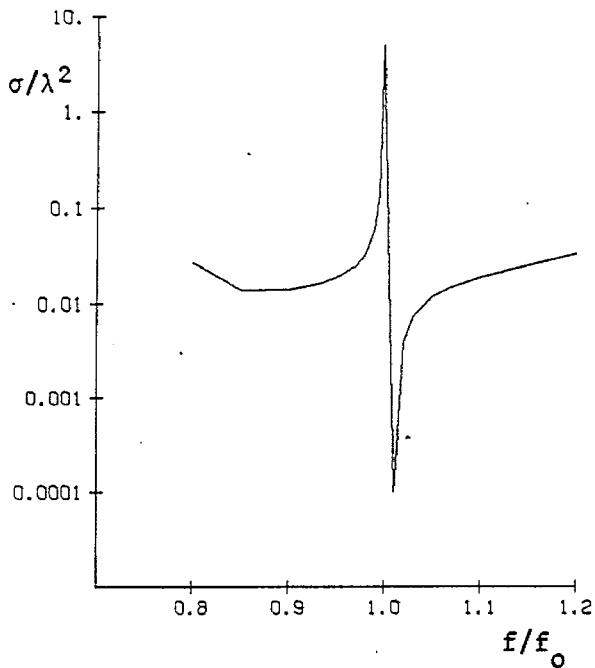
(b) two port currents

(c) three port currents
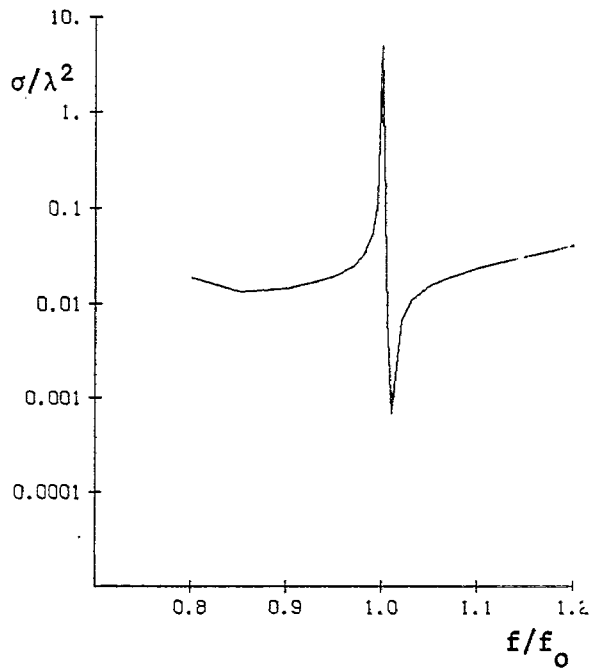
(d) four port currents

Fig. 10. Backscattering (σ/λ^2) vs. frequency (f/f_o) for the same
loaded scatterers as Fig. 9.

synthesis problem, are not shown. They are similar in form to the correspond-
ing scattering patterns of Fig. 9.

The behavior of the synthesized scatterers over a frequency bandwidth
is also important, just as in the pattern synthesis case. Figure 10 shows
the variation of σ/λ^2 vs. frequency over the range $f = 0.8f_o$ to $1.2f_o$, where
f_o is the design frequency, for the four cases of Table 2. Again a load is
considered to be an inductor if X_i is positive at f_o, or a capacitor if X_i
is negative at f_o. Note that each scatterer is relatively narrow band, with
the frequency sensitivity increasing as the number of loads is increased.
Note also that the one-port optimization result, Fig. 10a, is the same as
the one-port synthesis result, Fig. 4a. This is because only one basis
function is used in each case.

The gain optimization problem is next treated using the modal currents
of the unloaded body as the basis. These modal currents are again those
listed in Table 1. The currents are added to the optimization procedure in
the order of increasing $|\lambda_n|$, just as in the previous pattern synthesis
problem. Again the x-polarized gain in the $-z$ direction is maximized, and
Table 3 summarizes the results. The first column shows the number of modes
used, the second column gives the maximum gain obtained, and the third
column lists the back-scattering cross section obtained when the scatterer
is resonated. Note that the fourth rows of Tables 2 and 3 are identical
since a complete basis was used in both cases. Also, it should be empha-
sized that for each case of Table 3 reactive loads are placed at all ports
in contrast to the case of Table 2 where loads are placed only at those
ports used in the basis.
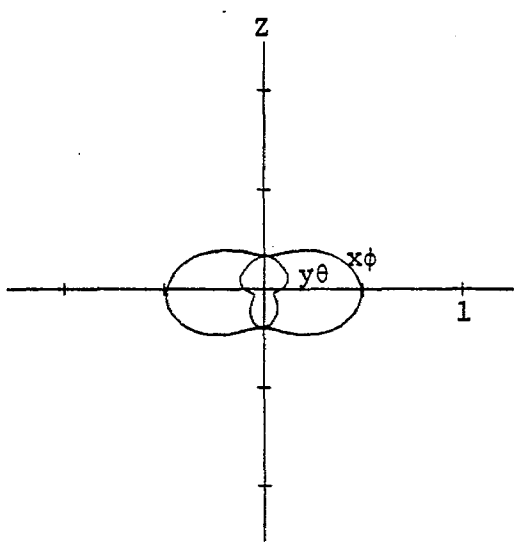
(a)   one mode current
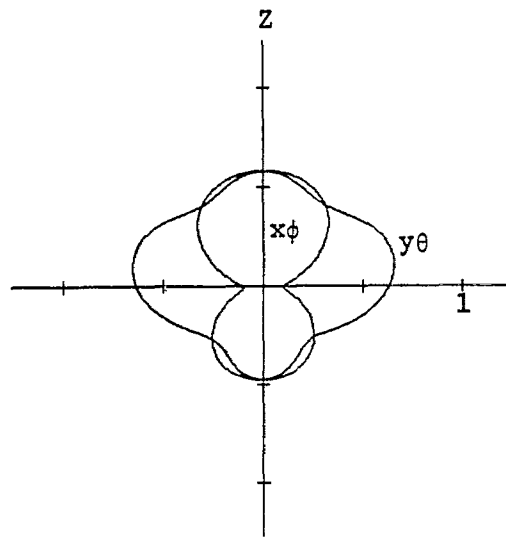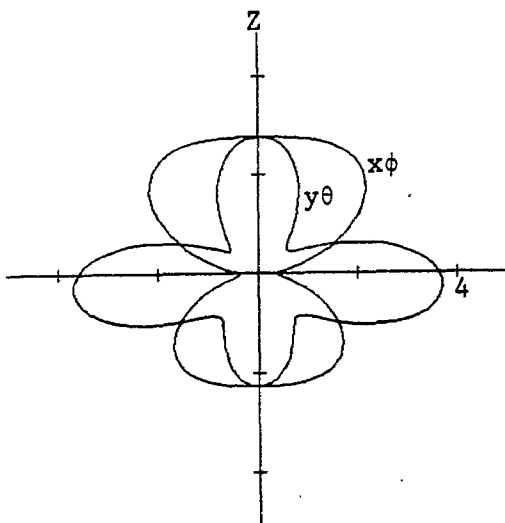
(b)   two mode currents

(c)   three mode currents
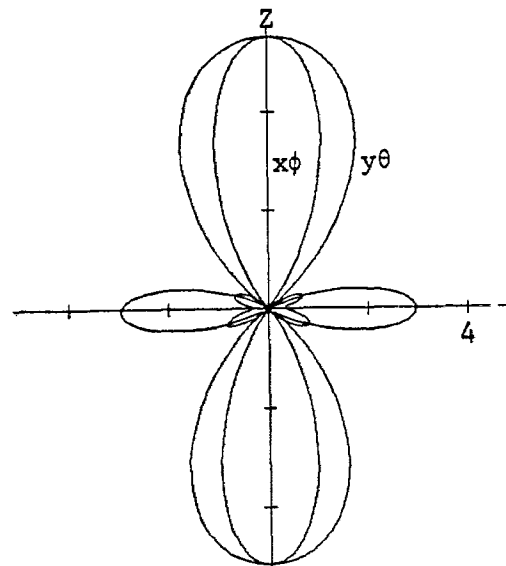
(d)   four mode currents

Fig. 11.   Bistatic scattering patterns (σ/λ^2) for the wire object of
Fig. 1 loaded for maximum gain in the -z direction.   Curves
labeled xϕ denote ϕ polarization in the x=0 plane.   Curves
labeled yθ denote θ polarization in the y=0 plane.

Table 3. Maximum gain and backscattering cross section
when mode currents are used as a basis

Modes Used	Maximum Gain	Cross Section
One	0.609	$0.1934 \ \lambda^2$
Two	1.044	$0.4757 \ \lambda^2$
Three	1.554	$0.5659 \ \lambda^2$
Four	4.033	$5.160 \ \ \lambda^2$

The bistatic radar cross section patterns (σ/λ^2) are shown in Fig. 11 for the loaded scatterers listed in Table 3. The curves are labeled in the same manner as those of Fig. 9. Again the one-mode case, Fig. 11a $(\sigma/\lambda^2$ plotted) is the same as the one-mode synthesis case, Fig. 6a $(\sqrt{\sigma}/\lambda$ plotted). It is also, of course, just the bistatic scattering pattern obtained by directly resonating the dominant mode current. The two-mode case, Fig. 11b, has a significantly higher cross section in the desired minus z-direction than does the one-mode case. The improvement in backscattering cross section in the three-mode case, Fig. 11c, is small over the two-mode case. Finally, the four-mode case, Fig. 11d, is identical to the four-port case of Fig. 9d, since a complete current basis is used in both cases. Also, the final loading reactances must be the same for these two cases. Hence, the loads (56) are also those used in the final four-mode synthesis procedure.

The broadband behavior of the loaded scatterers listed in Table 3 is summarized by the curves of Fig. 12. The one-mode case is, of course, the same in the pattern synthesis problem as in the gain optimization problem, hence Fig. 12a is identical to Fig. 7a. The two-mode case, Fig. 12b, is more narrow band than the one-mode case, but the improvement in backscattering cross section is significant. The three-mode case, Fig. 12c, is still more narrow band, and the improvement in backscattering cross section over the two-mode case is only slight. Finally, the four-
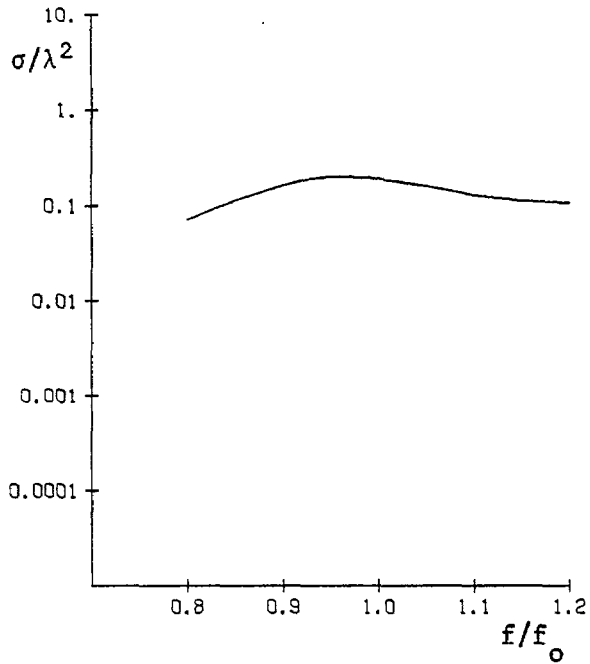
(a) one mode current
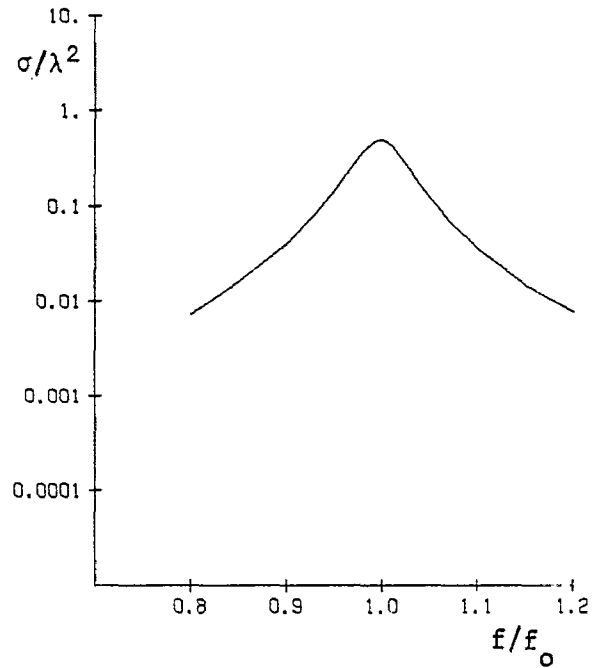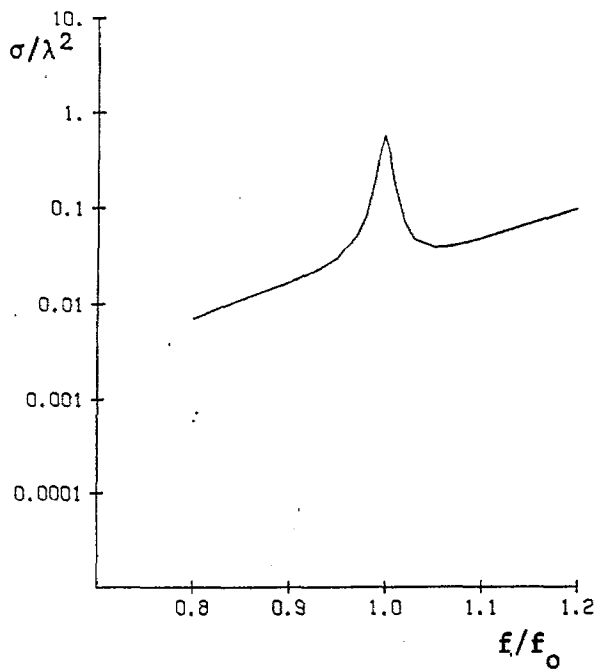
(b) two mode currents

(c) three mode currents
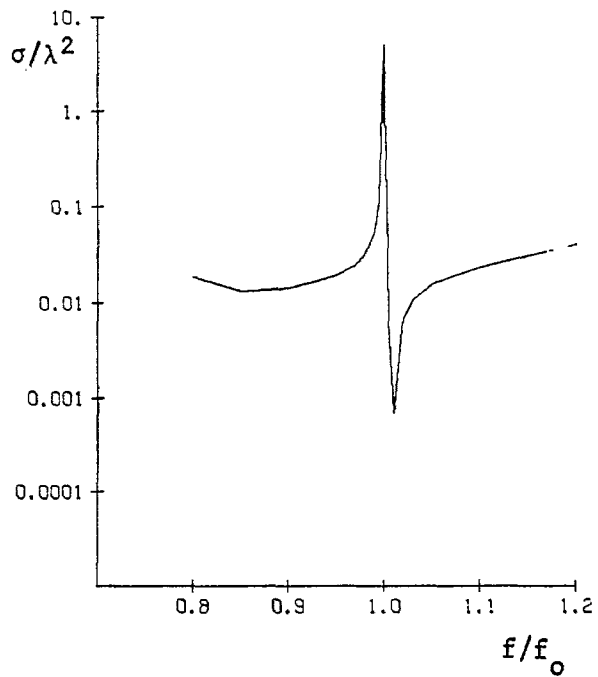
(d) four mode currents

Fig. 12. Backscattering (σ/λ^2) vs. frequency (f/f_o) for the same loaded scatterers as Fig. 11.

mode case, Fig. 12d, is very frequency sensitive, and, in fact, is identical
to the four-port case of Fig. 10d.

We can use still other bases for gain optimization if desired. Con-
ceptually, the broadest band behavior should result when the Q-mode currents,
defined by (35), are used as a basis in order of increasing $|Q_n|$. However,
as noted earlier, for this problem there are no significant differences be-
tween the ordinary mode currents used above and the Q mode currents defined
by (35). Hence, results using the Q-mode currents for gain optimization were
very similar to those of Table 3 and Figs. 11 and 12, and are not shown
separately.

Finally, all of the examples of this section can be run for the dual
formulation in terms of short circuit parameters and port voltages. The
results are qualitatively similar to those obtained using the open-circuit
formulation. However, as noted in the synthesis problem, the "background
scattering" for the short-circuit formulation is larger than for the open-
circuit formulation. Thus, neglecting this term is a somewhat poorer
approximation for the particular problem being treated. For reference, the
results for optimum gain and backscattering cross section using the short-
circuit formulation are summarized in Appendix B.

VIII. DISCUSSION

Given an N-port conducting body, any set of real port currents can
be resonated by reactive loads according to the concepts of Section III.
If the resonated current provides the major contribution to the scattered
field, then the reactively loaded object will have a scattering pattern
approximately equal to the radiation pattern of the same object excited
by the given set of port currents. Various synthesis and optimization
procedures can be used to obtain real port currents whose fields have de-
sirable radiation characteristics. In this report we give two such procedures,
one which synthesizes a desired field pattern, and the other which optimizes
power gain.

The synthesis procedure involves a specification of the radiation field in magnitude only, and then uses an iterative procedure to determine the phase which minimizes a certain error parameter. The problem is basically nonlinear, and by using different starting points we sometimes arrive at different ending points (local minima). Some examples of this for the wire object of Fig. 1 are given in Appendix C.

In the optimization procedure, the power gain is maximized subject to the condition that the port currents are real. The solution in this case is unique. When resonated by reactive loads, this maximizes the backscattering radar cross section under the assumption that only the resonated mode contributes to the scattering. Other modes are usually negligible when the scatterer is electrically small or of intermediate size, but not if it is electrically large. There is also a background term present, the term $\underset{\sim}{E}_0^{oc}$ in the open-circuit formulation (6) or the term $\underset{\sim}{E}_0^{sc}$ in the short-circuit formulation (7). In the first case, $\underset{\sim}{E}_0^{oc}$ can usually be made small if enough open-circuits are placed on the body. The term $\underset{\sim}{E}_0^{sc}$ is probably harder to make small in general, since this involves placing short circuits on the body. Sometimes $\underset{\sim}{E}_0^{oc}$ may be small and $\underset{\sim}{E}_0^{sc}$ large, in which case the open-circuit formulation should be used. For other bodies the reverse may be true, in which case the short-circuit formulation is preferable.

APPENDIX A

PATTERN SYNTHESIS, SHORT-CIRCUIT FORMULATION

The examples of this Appendix are dual to those of Section V. The wire object considered is the same, Fig. 1, as for the short-circuit formulation. For pattern synthesis, the magnitude pattern is again given by (28) and (29). The points chosen for the least-squares solution are again given by (30) and (31). The first example uses port voltages as a basis, with convergence illustrated by choosing first one, then two, then three, and finally four ports. Figure 13 shows the results presented in the same manner as in Fig. 2 for the dual case. The port voltages for the final synthesized pattern are

$$V_1 = 161.4$$

$$V_2 = 214.4$$

$$V_3 = -117.3 \tag{57}$$

$$V_4 = 27.3$$

Note that the synthesized patterns in each case are considerably different from the corresponding patterns of Fig. 2. This is because the radiation fields resulting from voltages applied to ports with all other ports short circuited are different from those resulting from currents applied to ports with all other ports open circuited. We should expect the two formulations to give different synthesized patterns because the space of pattern functions for real port voltages is different from that for real port currents.

Next the computed real port voltages are resonated by the procedure of Section III. Figure 14 shows the resulting bistatic scattering patterns for when the four cases of Fig. 13 are resonated. For Fig. 14a, we have a susceptance at port 1 and the other three ports are short circuited. For Fig. 14b, susceptances are at ports 1 and 2, and short circuits at ports 3

38
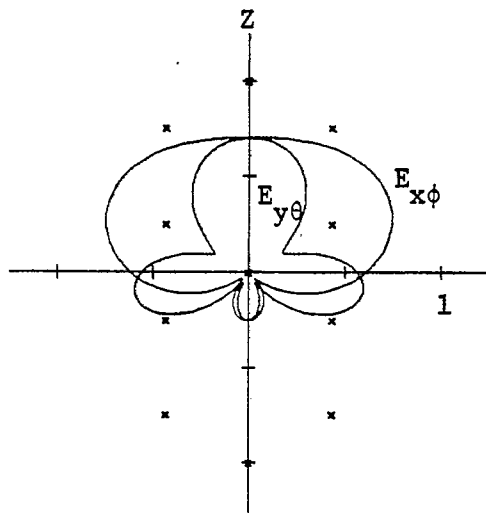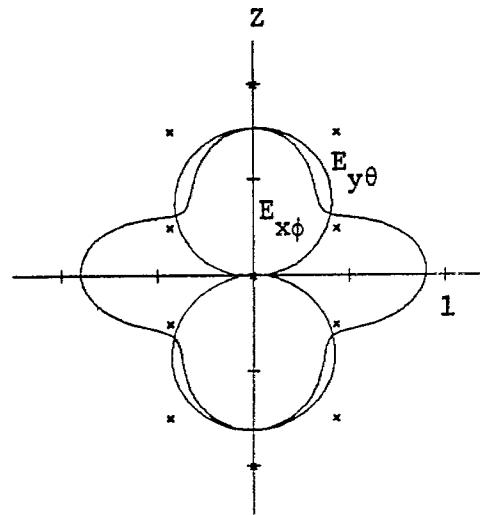
(a)   one port voltage
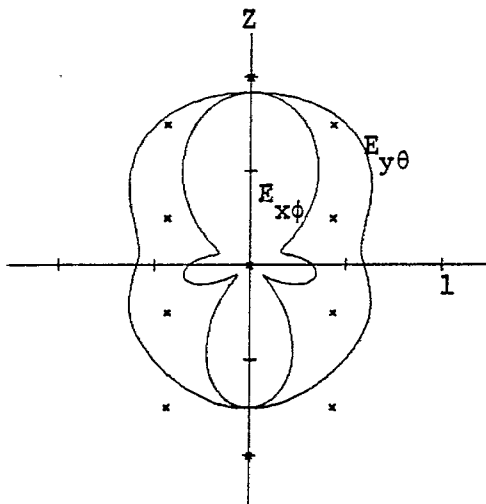
(b)   two port voltages

(a)   three port voltages
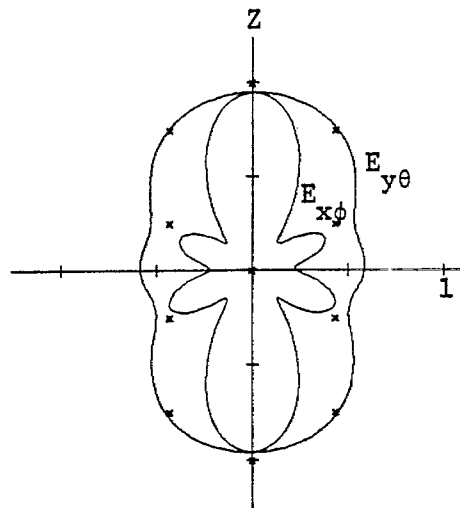
(d) four port voltages

Fig. 13.   Field magnitude pattern synthesis using real port
voltages as a basis.   Crosses denote the desired
pattern.   Curves labeled $E_{x\phi}$ denote $|E_\phi|$ in the
x=0 plane.   Curves labeled $E_{y\theta}$ denote $|E_\theta|$ in the
y=0 plane.

(a) one port voltage

(b) two port voltages

(c) three port voltages

(d) four port voltages

Fig. 14. Bistatic scattering patterns ($\sqrt{\sigma}/\lambda$) for the wire object of Fig. 1 loaded to resonate the port voltages which synthesize the patterns of Fig. 13. Curves labeled xϕ denote ϕ polarization in the x=0 plane. Curves labeled yθ denote θ polarization in the y=0 plane.

40
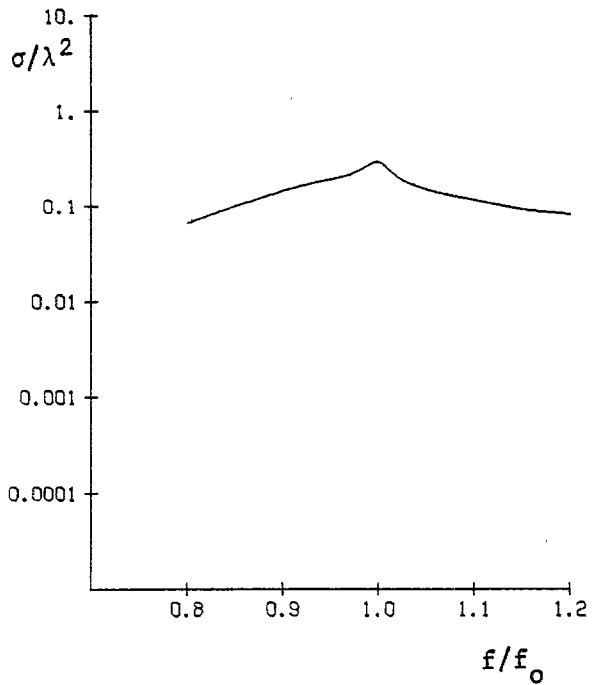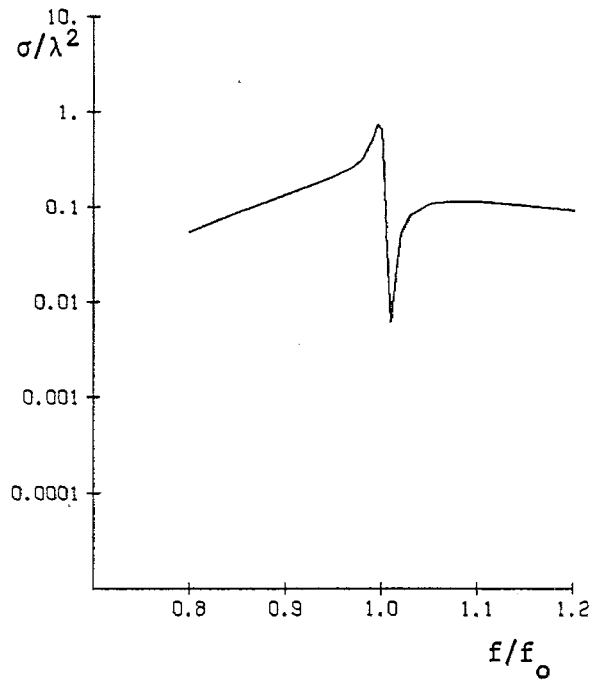
(a) one port voltage
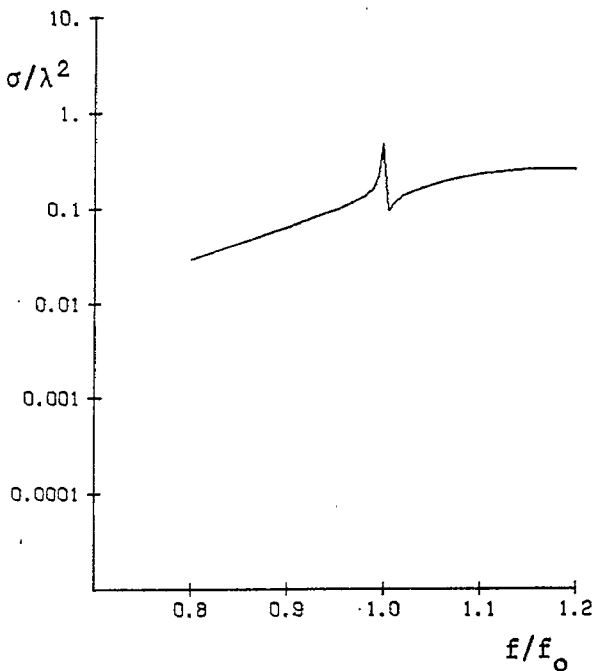
(b) two port voltages

(c) three port voltages
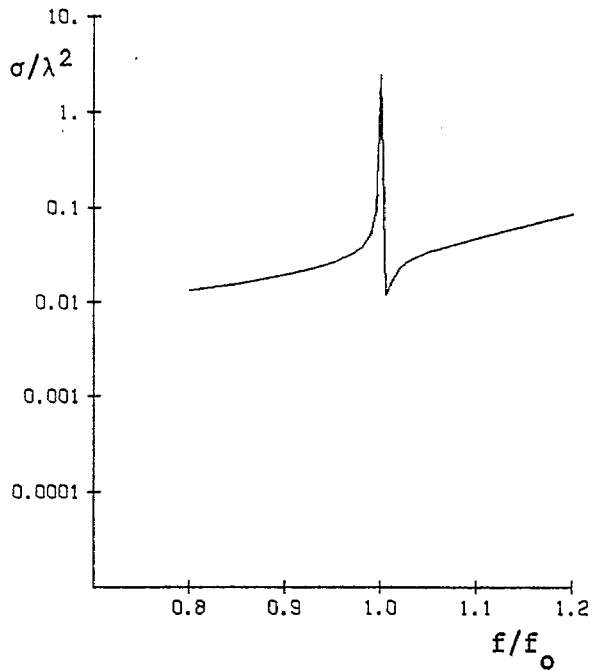
(d) four port voltages

Fig. 15. Backscattering (σ/λ^2) vs. frequency (f/f_o) for the same
loaded scatterers as Fig. 14.

and 4. For Fig. 14c, susceptances are at the first three ports, and a short circuit at the fourth. Finally, for Fig. 14d susceptances are at all four ports. The loads used in the final case are

$$B_1 = 0.000927$$

$$B_2 = 0.002884$$

$$B_3 = 0.001355$$

$$B_4 = 0.001246$$

(58)

They are, of course, different for the intermediate cases.

The frequency sensitivity of the synthesized scatterers is illustrated by Fig. 15. In each case, when a load B_i is positive at the design frequency f_o it is considered to be a capacitor, or when B_i is negative at f_o it is considered to be an inductor. Note that the one-port case, Fig. 15a, happens to be broadband, although we did not design it to be so. The other three cases, Figs. 15b to 15d, are all relatively narrow band.

The second example of this Appendix uses the modal voltages of the body as the basis for the optimization procedure. These mode eigenvalues and eigenvoltages (normalized to maximum value unity) are given in the following table.

Table 4. Eigenvalues μ_n and eigenvoltages $\vec{V}_n$
for the wire object of Fig. 1.

n	μ_n	Port (1)	Port (2)	Port (3)	Port (4)
1	0.1552	-0.0205	0.1158	0.6425	1.0000
2	10.12.	0.1904	0.2524	1.0000	-0.9256
3	50.54	1.0000	-0.2887	0.7884	-0.4050
4	-816.2	0.5313	1.0000	-0.6749	0.2066

Note that the μ_n of Table 4 are equal to $-\lambda_n$ of Table 1, as proved in [7].

42

(a)   one mode voltage

(b)   two mode voltages

(c)   three mode voltages

(d)   four mode voltages
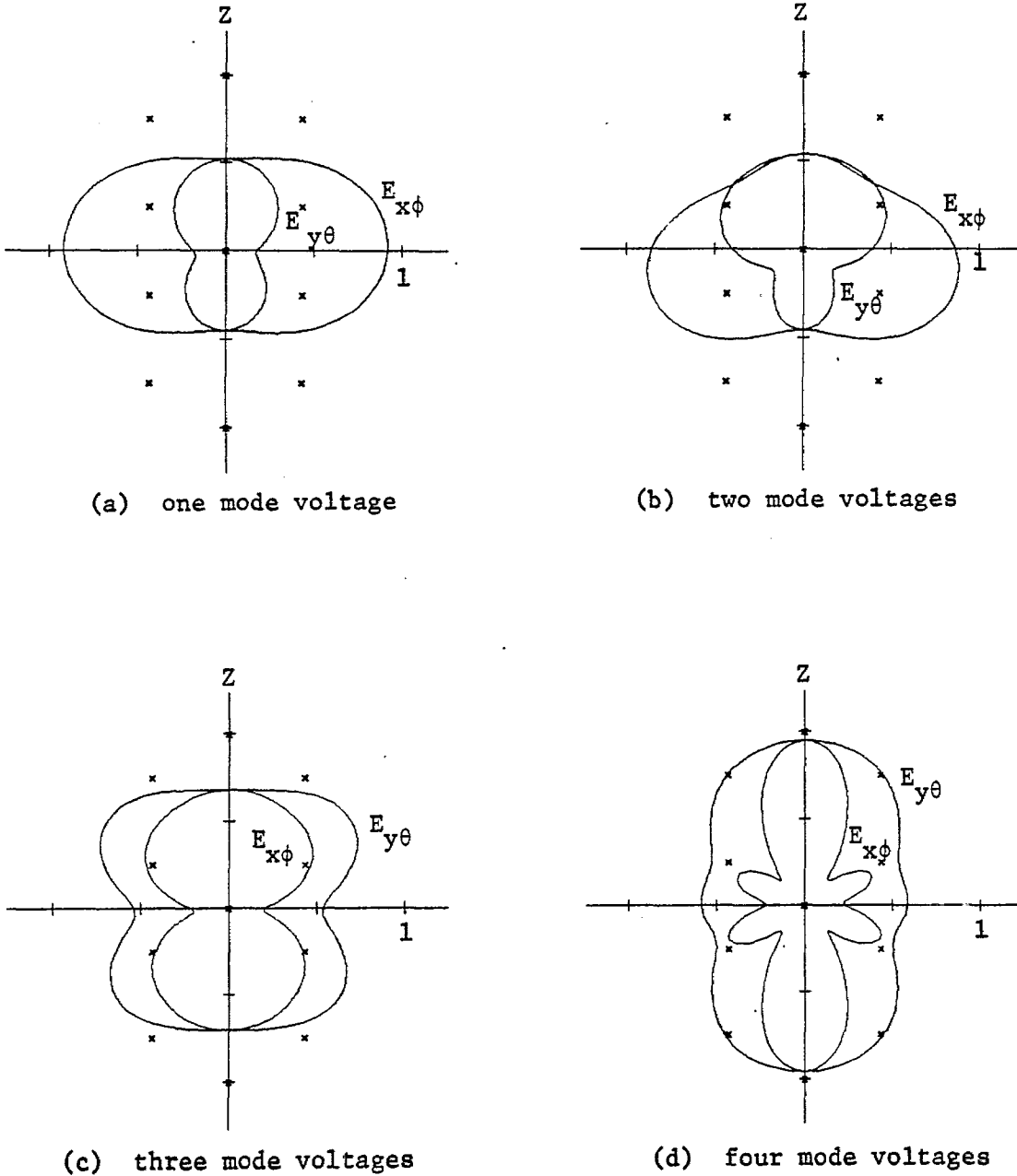
Fig. 16.   Field magnitude pattern synthesis using real mode voltages as
a basis.   Crosses denote the desired pattern.   Curves labeled
$E_{x\phi}$ denote $|E_\phi|$ in the x=0 plane.   Curves labeled $E_{y\theta}$ denote
$|E_\theta|$ in the y=0 plane.

(a) one mode voltages

(b) two mode voltages

(c) three mode voltages

(d) four mode voltages
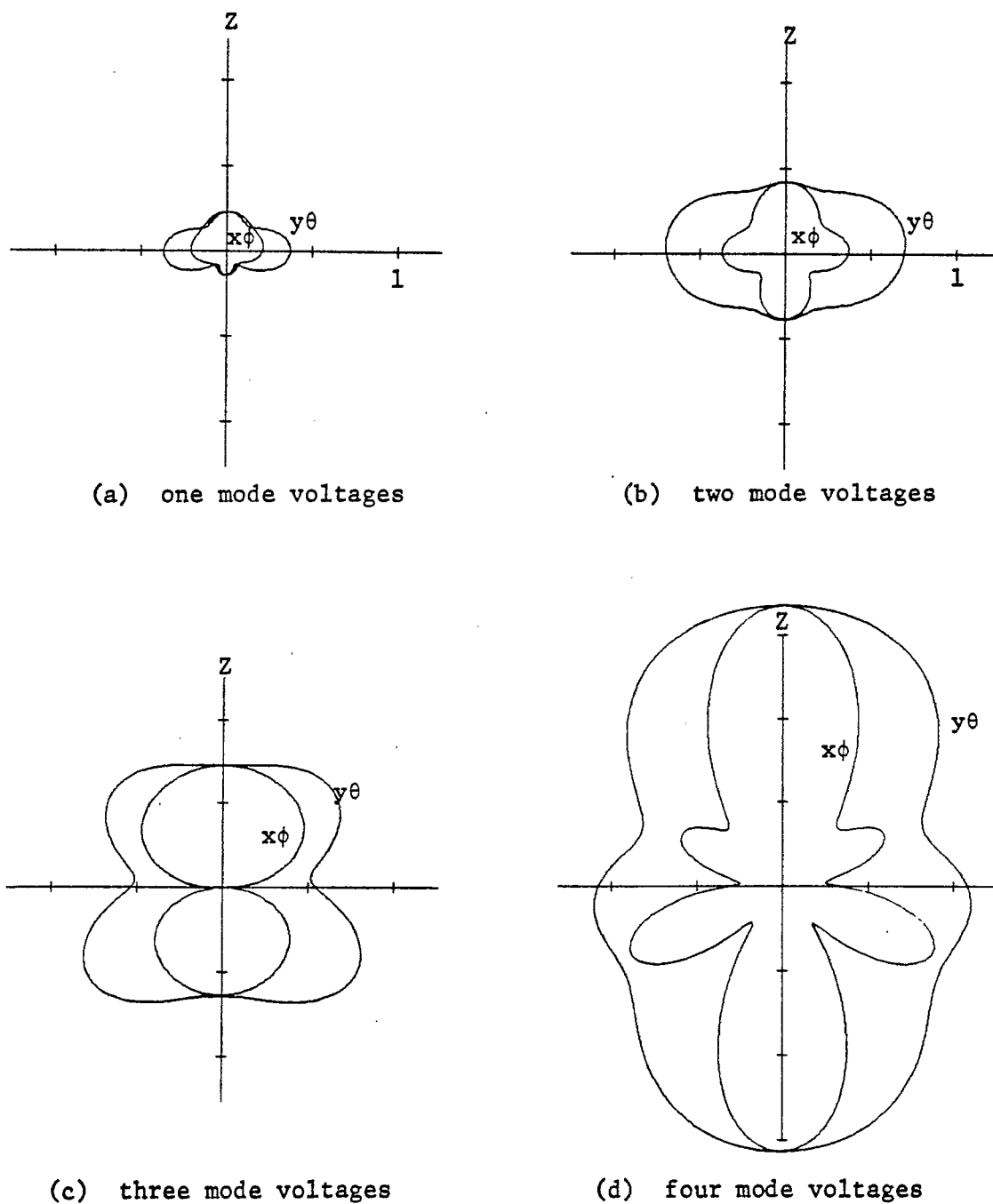
Fig. 17. Bistatic scattering patterns $(\sqrt{\sigma}/\lambda)$ for the wire object of Fig. 1 loaded to resonate the port voltages which synthesize the patterns of Fig. 16. Curves labeled xϕ denote ϕ polarization in the x=0 plane. Curves labeled yθ denote θ polarization in the y=0 plane.

44
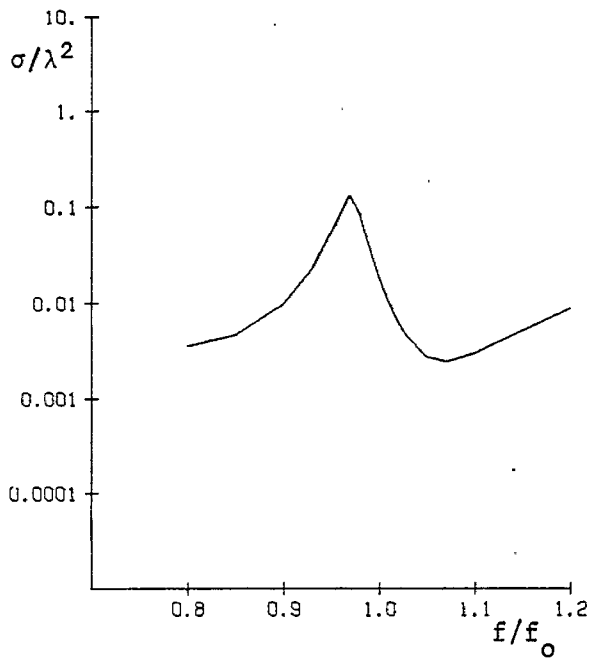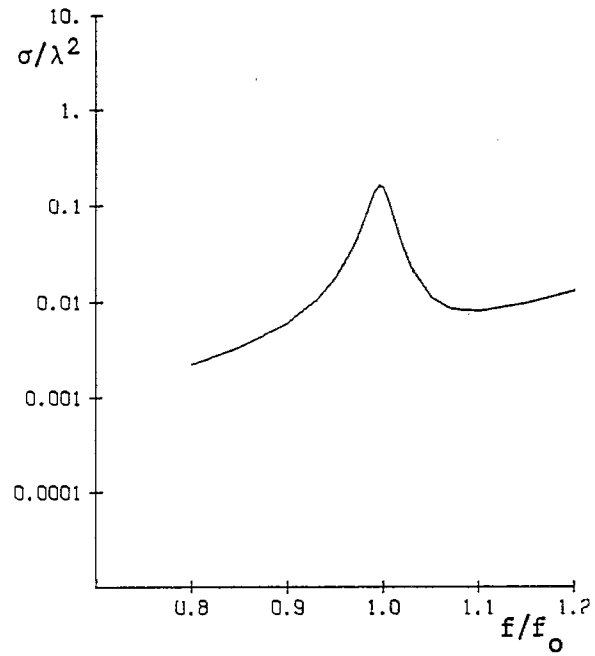
(a) one mode voltage
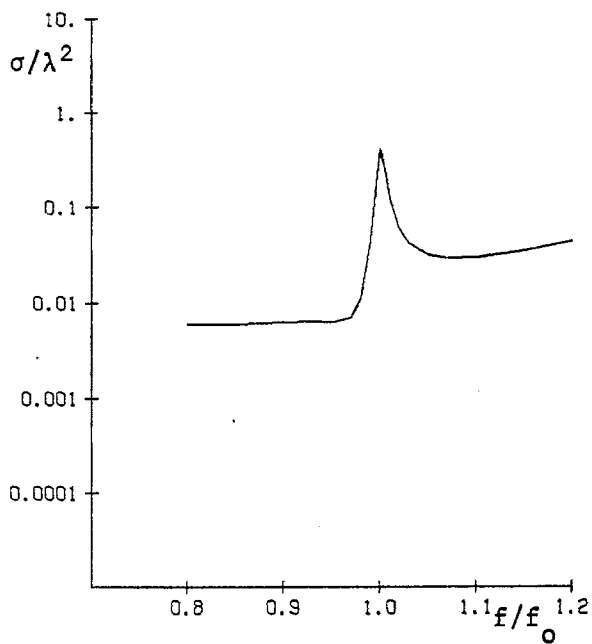
(b) two mode voltages

(c) three mode voltages
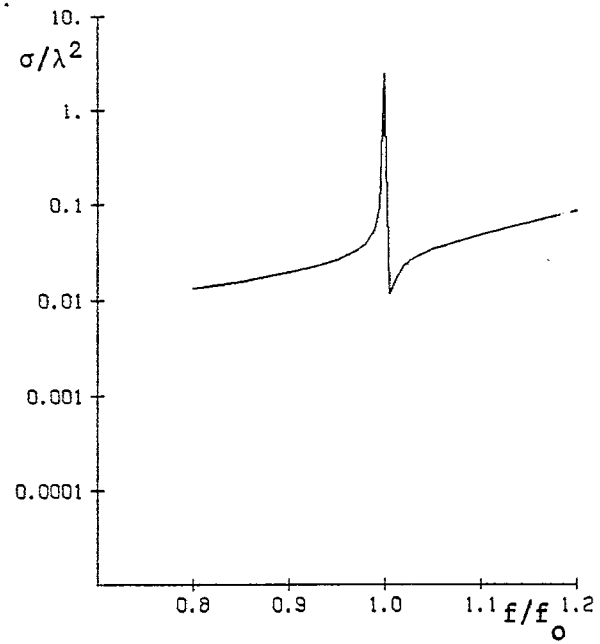
(d) four mode voltages

Fig. 18. Backscattering (σ/λ^2) vs. frequency (f/f_o) for the same loaded scatterers as Fig. 17.

Again the synthesis procedure was run using first one, then two, then three, and finally all four eigencurrents in the basis. The results are shown in Figs. 16a to d, respectively. The synthesized pattern using only one basis function, Fig. 16a, is just the field pattern of the first mode alone. The synthesized pattern using all mode functions, Fig. 16d, is the same as that using all port bases, Fig. 13d. This final correspondence is somewhat fortuitous, since the two procedures could arrive at different points of local optima.

The real port voltages are next resonated by susceptive loads according to the procedure of Section III. Figure 17 shows the bistatic scattering patterns when each case of Fig. 16 is resonated. This time there are susceptances at each port for all cases, regardless of the number of basis functions. The susceptances used in the final case, the scatterer for Fig. 17d, are the same as those given by (58). This is because we have arrived at the same solution as we did using the port voltage basis.

Finally, the frequency sensitivity of the synthesized scatterers is illustrated by Fig. 18. Again a load B_i is considered to be a capacitor if positive at f_o, or an inductor if negative at f_o. The frequency sensitivity of the loaded scatterers is seen to increase as the number of modes used in the synthesis procedure is increased (in the order of increasing $|\mu_n|$). It is interesting to note that the one-port loaded scatterer of Fig. 15a is considerably more broadband then the one-mode synthesized scatterer of Fig. 18a. In fact, it is not greatly different from the scattering when all ports are short circuited, Fig. 8b. In this case the "background scattering" is of the same order of magnitude as that from the synthesized scatterer, violating our assumption that it should be small.

46
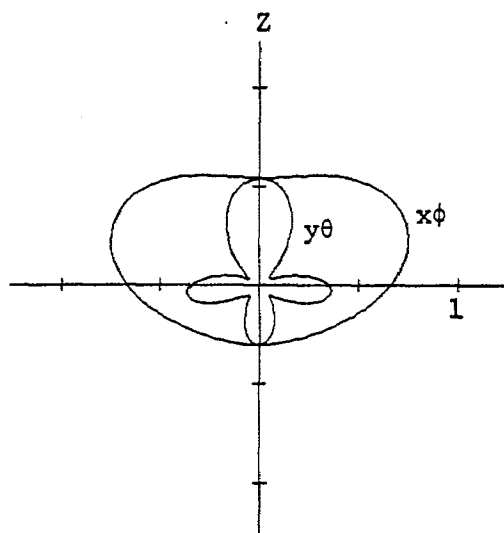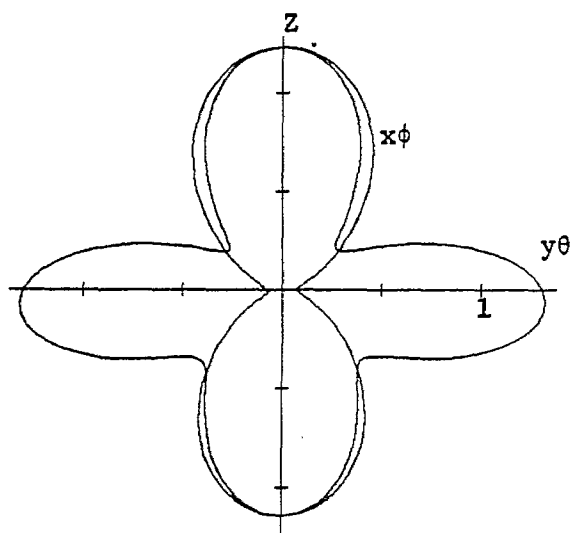
(a) one port voltage
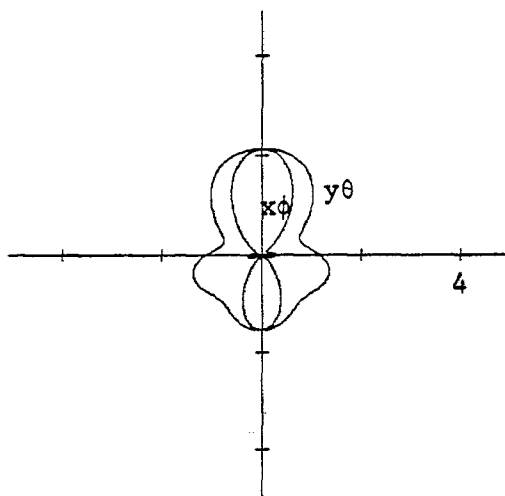
(b) two port voltages

(c) three port voltages
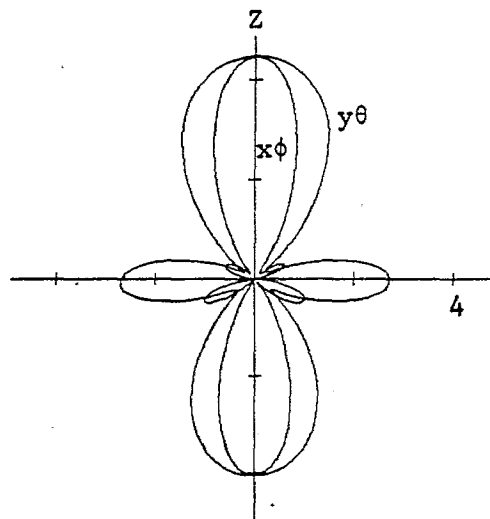
(d) four port voltages
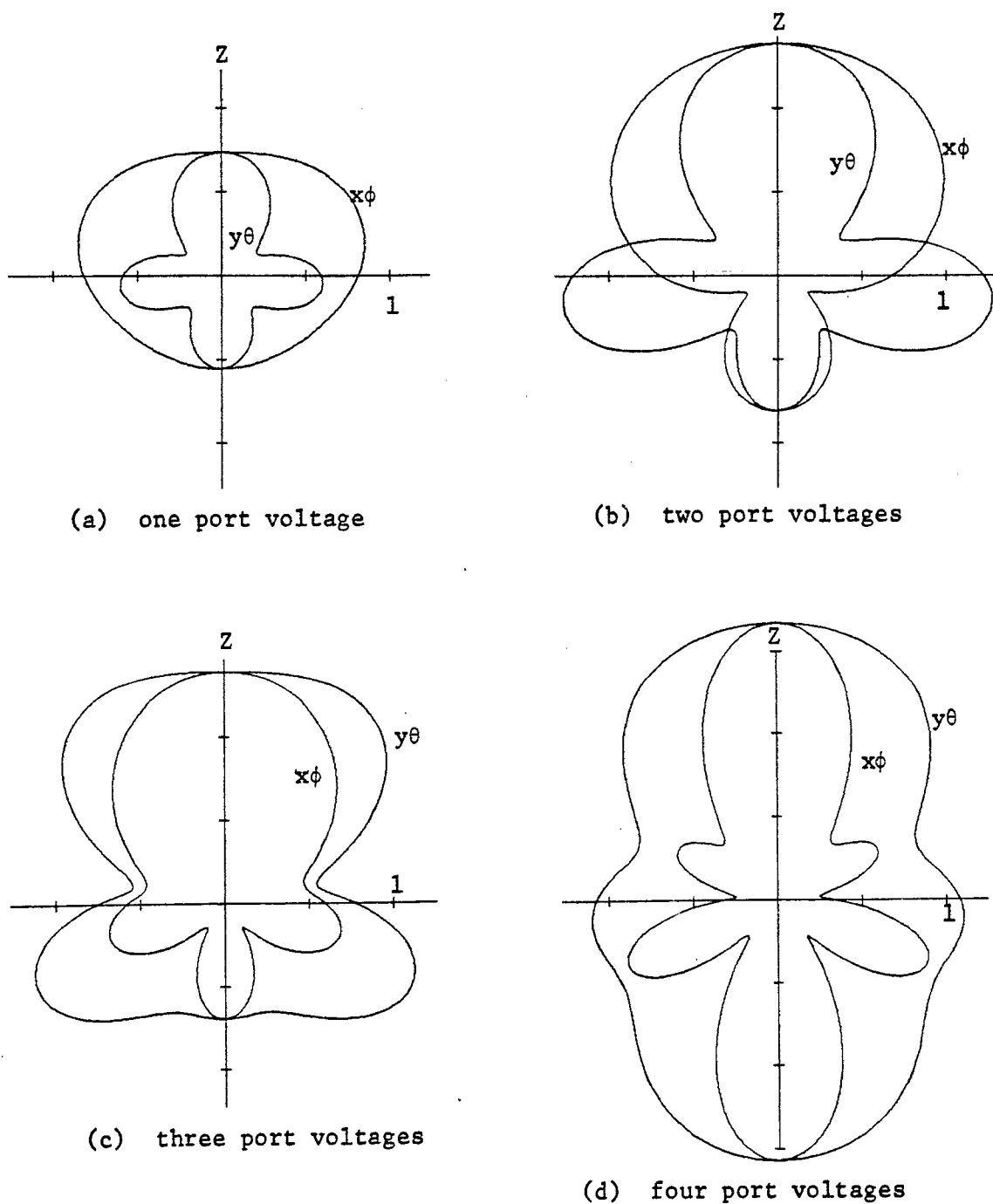
Fig. 19. Bistatic scattering patterns (σ/λ^2) for the wire object of
Fig. 1 loaded for maximum gain in the -z direction. Curves
labeled xϕ denote ϕ polarization in the x=0 plane. Curves
labeled yθ denote θ polarization in the y=0 plane.

APPENDIX B

MAXIMUM CROSS SECTION, SHORT-CIRCUIT FORMULATION

The examples of this Appendix are dual to those of Section VII. The
wire object, Fig. 1, is the same, but the short-circuit formulation is used
for gain maximization. The theory is dual to that summarized in Section VI.
The first example uses port voltages as a basis. Gain is optimized using
first one port, then two, then three, and finally all four ports, added in
the order in which they are numbered in Fig. 1. Once the real port voltages
for maximum gain are found, they are resonated by the method of Section III.
The result is a loaded scatterer having approximately maximum (for the ports
used) backscattering. Table 5 summarizes these results. The first column
shows the ports used, the second column gives the maximum gain for real cur-
rents, and the third column gives the backscattering cross section of the
resonated scatterer.

Table 5. Maximum gain and backscattering cross sections
when port voltages are used as a basis,

Ports Used	Maximum Gain	Cross Section
1	2.418	0.3054 λ^2
1,2	2.458	1.139 λ^2
1,2,3	2.753	1.546 λ^2
1,2,3,4	3.730	4.046 λ^2

The bistatic radar cross section patterns (σ/λ^2) for the loaded
scatterers of Table 5 are shown in Fig. 19. The curves labeled $\sigma_{x\phi}/\lambda^2$
are for the ϕ-polarized scattered field in the x=0 plane, and those
labeled $\sigma_{y\theta}/\lambda^2$ are for the θ-polarized scattered field in the y=0 plane.
Figure 19a is for the case of only one port loaded, Fig. 19b two ports,
Fig. 19c three ports, and Fig. 19d four ports. The susceptive loads for
the final case, Fig. 19d, are

48
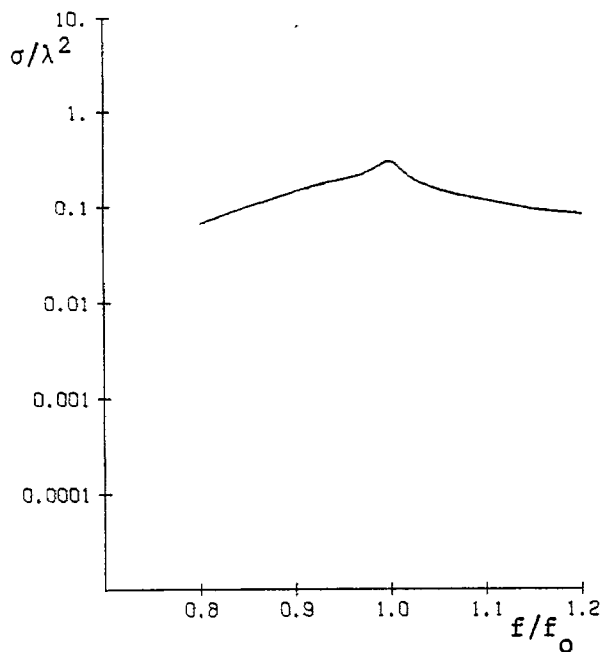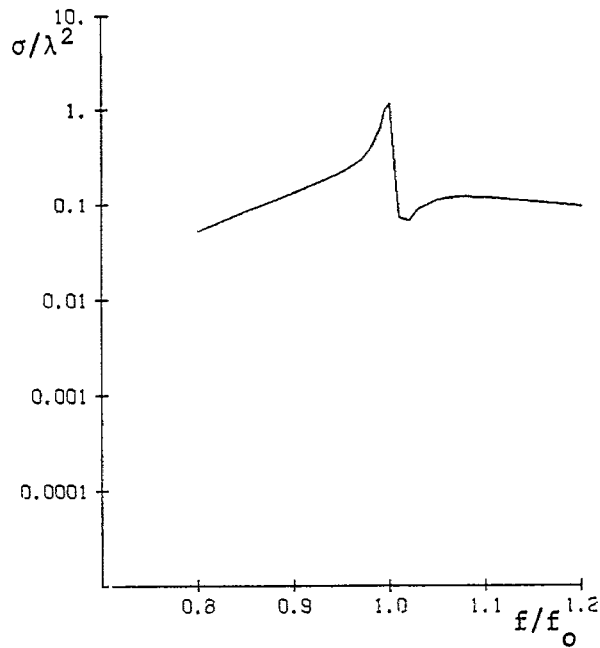
(a) one port voltage
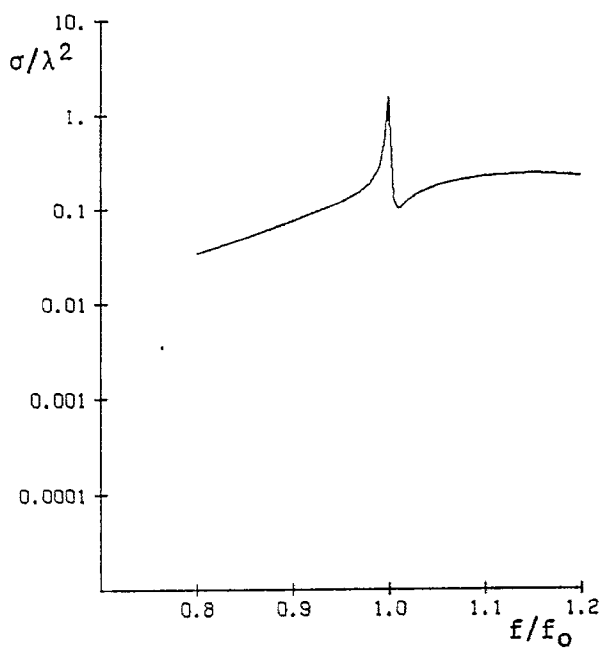
(b) two port voltages

(c) three port voltages
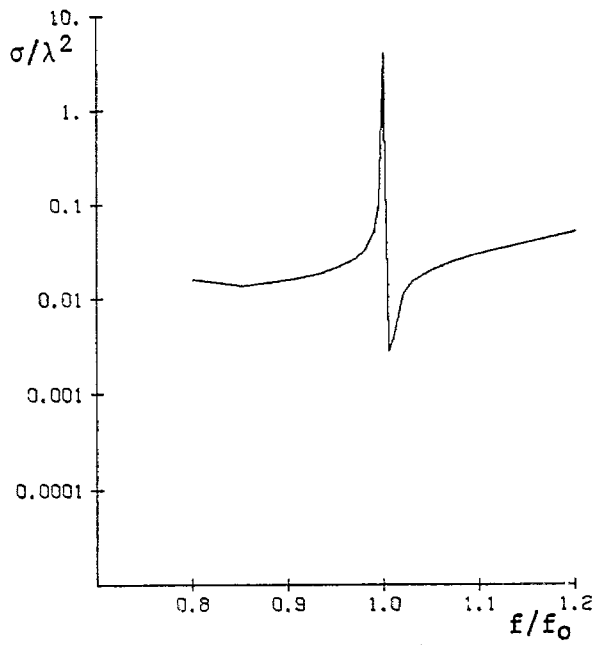
(d) four port voltages

Fig. 20. Backscattering (σ/λ^2) vs. frequency (f/f_o) for the same loaded scatterers as Fig. 19.
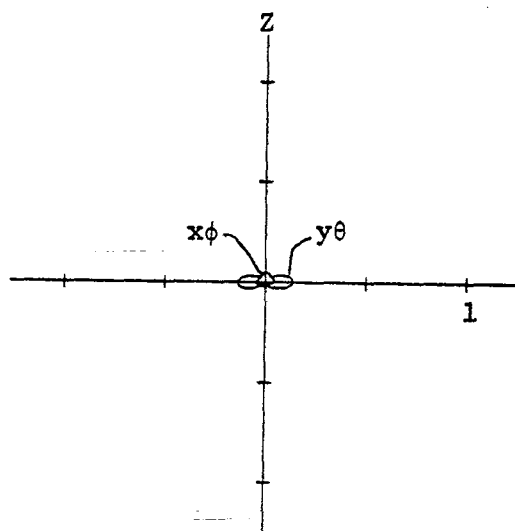
(a)   one mode voltage
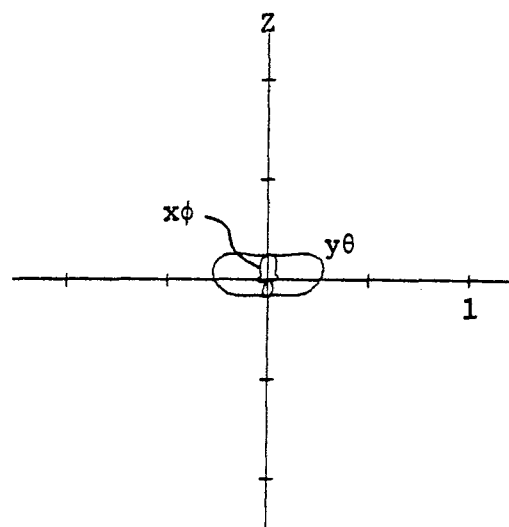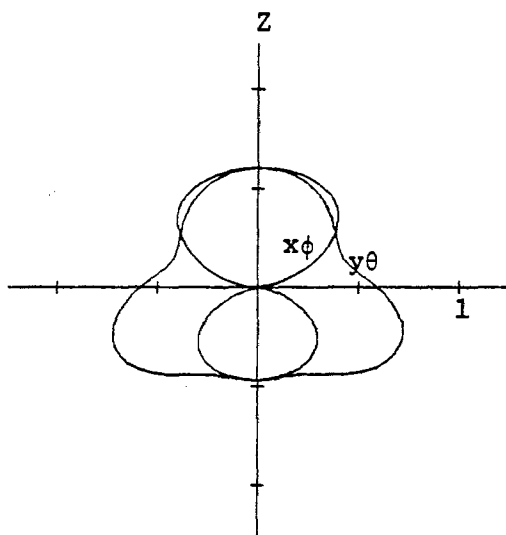
(b)   two mode voltages

(c)   three mode voltages
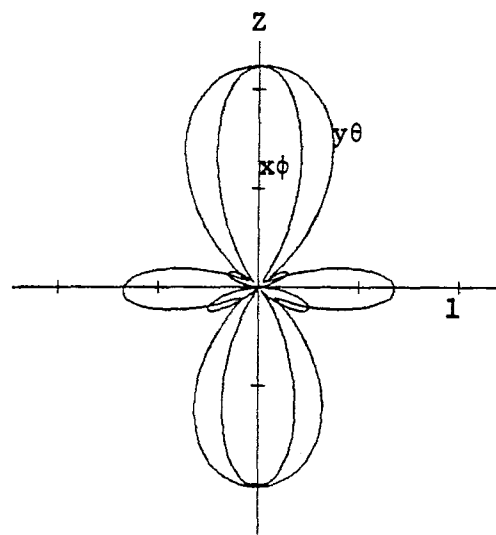
(d)   four mode voltages

Fig. 21.   Bistatic scattering patterns (σ/λ^2) for the wire object of
Fig. 1 loaded for maximum gain in the -z direction. Curves
labeled xϕ denote ϕ polarization in the x=0 plane. Curves
labeled yθ denote θ polarization in the y=0 plane.
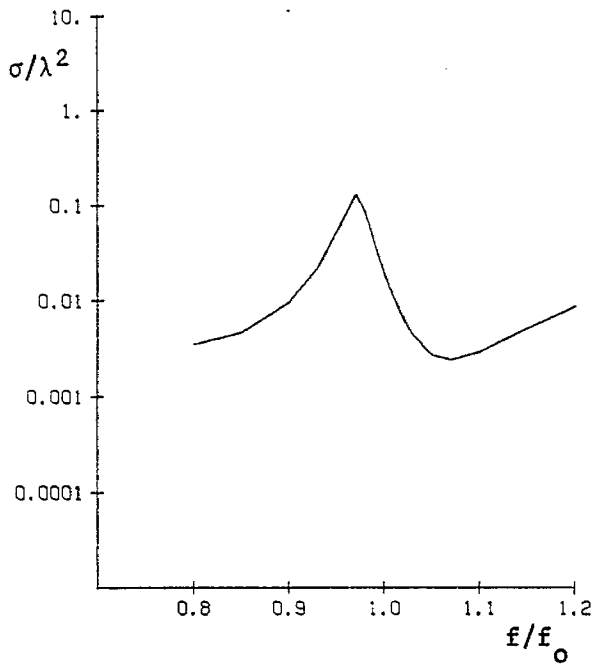
(a)   one mode voltage
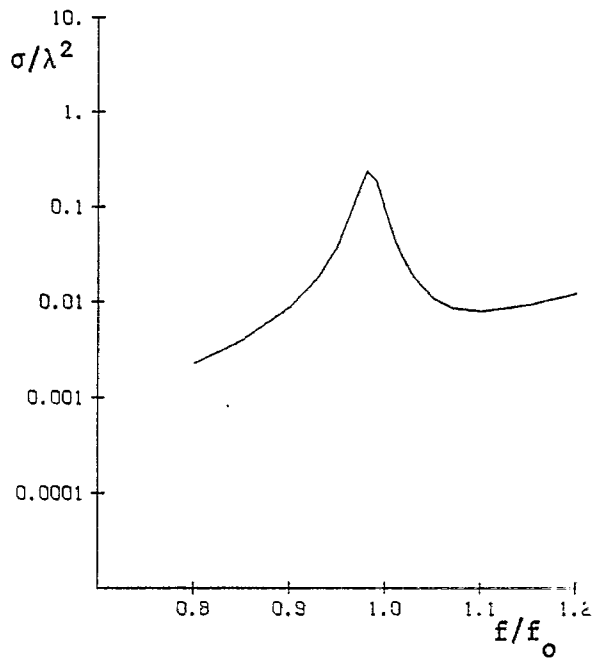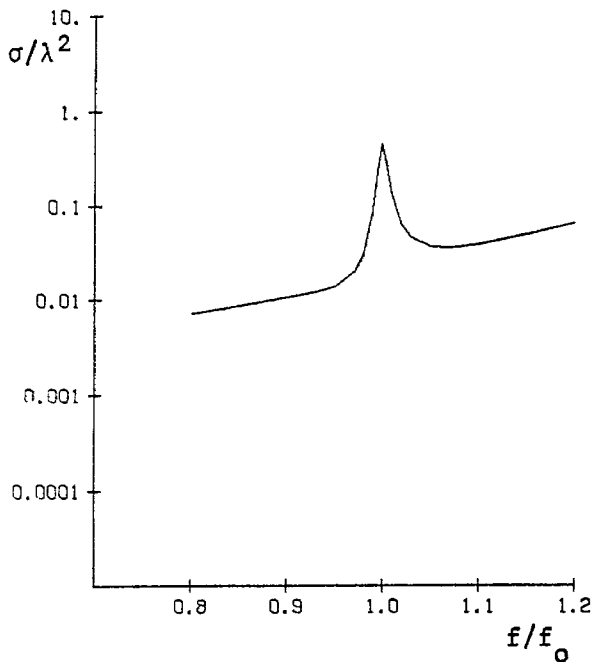
(b)   two mode voltages

(c)   three mode voltages
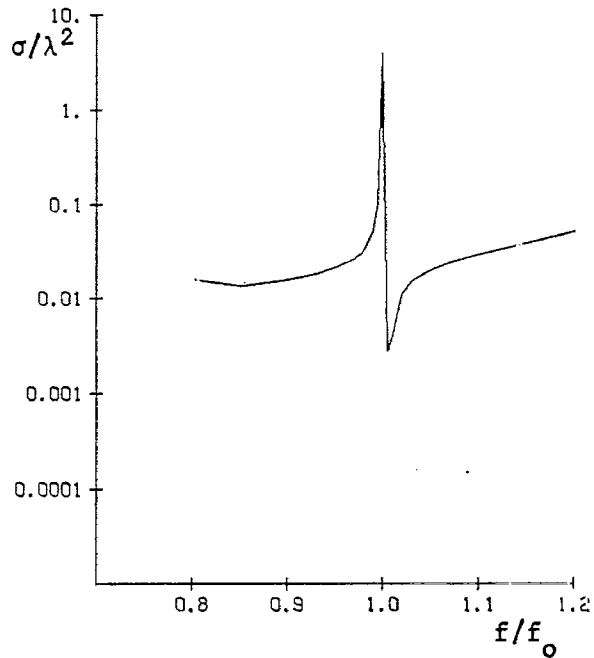
(d)   four mode voltages

Fig. 22.   Backscattering (σ/λ^2) vs. frequency (f/f_o) for the same loaded scatterers as Fig. 21.

$$B_1 = 0.001215$$

$$B_2 = 0.002870$$

$$B_3 = 0.001036$$ (59)

$$B_4 = 0.000483$$

The loads for the cases of Figs. 19a to 19c are, of course, different.

The frequency sensitivity of the loaded scatterers of Fig. 19 is illustrated by Fig. 20. A load B_1 is considered to be a capacitor if positive at f_o, or an inductor if negative at f_o. Note that the one-load optimization case, Fig. 20a, is the same as the one-load synthesis case, Fig. 15a, since the same basis voltage is resonated in both cases.

The second example of the Appendix uses the modal voltages as a basis for the optimization procedure. These mode eigenvalues and eigen-voltages are those listed in Table 4. The gain is optimized using first one mode, then two, then three, and then four, added in the order of increasing magnitude of eigenvalues. The optimum gain voltages are next resonated by the concepts of Section III. The results are summarized in Table 6. It should be noted that we now have loads at all ports of the loaded scatterer for each case, in contrast to the preceding case, Table 5, where loads were only placed at those ports used in the basis, other ports being short circuited.

Table 6. Maximum gain and backscattering cross sections when mode voltages are used as a basis.

Modes Used	Maximum gain	Cross Section
One	0.609	0.01990 λ^2
Two	0.616	0.08658 λ^2
Three	2.003	0.4682 λ^2
Four	3.730	4.044 λ^2

The bistatic radar cross section patterns (σ/λ^2) for the loaded scatterers of Table 6 are shown in Fig. 21. These are labeled in the same manner as are those of Fig. 19. The susceptive loads for the final case, Fig. 21d, are the same as those for the case of Fig. 19d, given by equations (59). This is because the basis was complete in both cases.

Finally, the frequency sensitivity of the loaded scatterers of Fig. 21 is illustrated by Fig. 22. Again a load B_i is considered to be a capacitor if positive at f_o, or an inductor if negative at f_o. Finally, note that the one-mode optimization case, Fig. 22a, is the same as the one-mode synthesis case, Fig. 18a, since the same mode was resonated in both cases.

APPENDIX C

EXAMPLES OF DIFFERENT OPTIMA IN PATTERN SYNTHESIS

The field magnitude pattern synthesis procedure of Section IV is a nonlinear one, and may arrive at different optimum points if different starting points are used. Figure 23 gives some examples of this phenomena. For Fig. 23a, the initial phase angles of the field points were chosen to be 0 and 180°, alternating between adjacent points. The corresponding case for which all initial phase angles were chosen zero is shown in Fig. 5c. Note that the two final patterns are different, although both are reasonable approximations to the desired pattern. A second example is shown in Fig. 23b. In this case the initial phase angles of the field points were chosen to be 0, 90°, 180°, 270°, etc. The corresponding case for which all initial angles were chosen zero is shown in Fig. 5d. An example using a voltage basis is shown in Fig. 23c. In this case the initial angles of the field points were chosen to be 0 and 180°, alternating between adjacent points. The corresponding case for which all initial angles were chosen zero is shown in Fig. 16b. A final example is shown in Fig. 23d. Once again the initial angles of the field points were chosen to be 0 and 180°, alternating between adjacent points. The corresponding case for which all initial angles were chosen zero is shown in Fig. 13c.

54
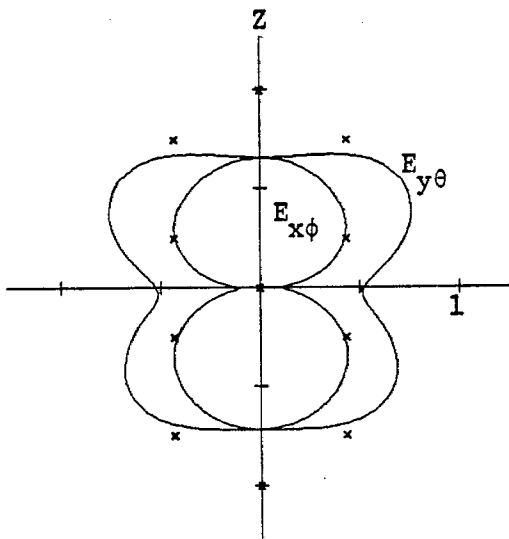
(a) three mode currents,
     compare with Fig. 5c.
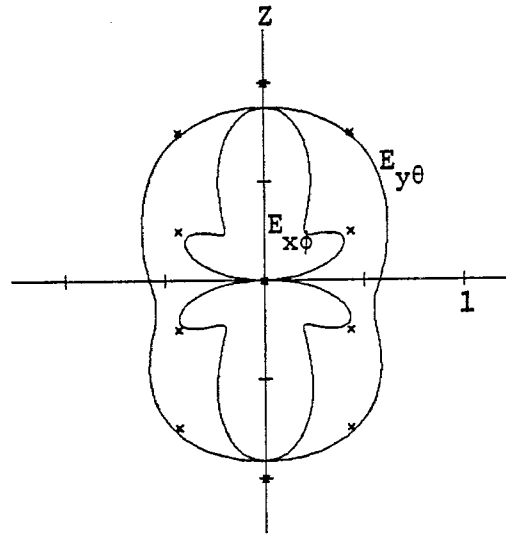
(b) four mode currents,
     compare with Fig. 5d.
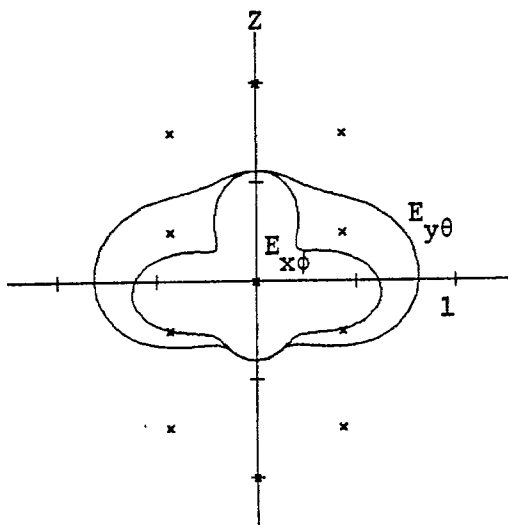
(c) two mode voltages,
     compare with Fig. 16b.
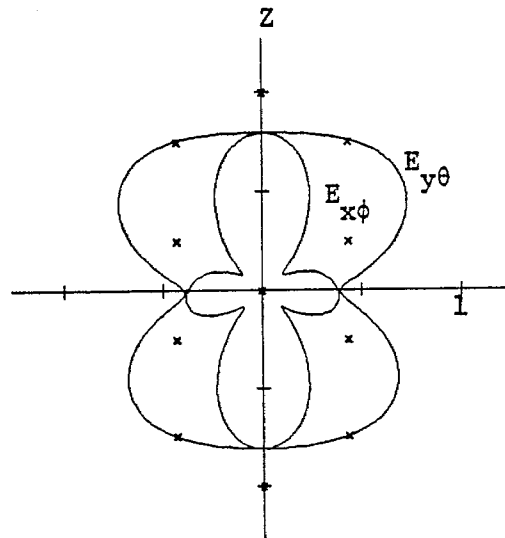
(d) three port voltages,
     compare with Fig. 13c.

Fig. 23. Different optimum points for pattern synthesis due to different
          choices of initial phase angles.

PART TWO

COMPUTER PROGRAMS

I. INTRODUCTION

The programs used to compute the examples of this report are described and listed in this part. Each program is accompanied by an explanation of the input data, a verbal flow chart, and sample input and output data. In general, the input data for the program of a given section depends upon the output of programs of previous sections or of reference [7]. If each program is run with the input data listed in this report, the input data for any one of these programs can be verified in terms of the output of programs previously run. The Calcomp Plotter is used only in Section VIII.

II. PATTERN SYNTHESIS

The program (pattern synthesis program) described in this section requires some data computed by the port parameter program on pages 60-69 of [7]. However, the impedance matrix program on pages 45-52 of [7] and the excitation vector program on pages 53-59 of [7] must precede the port parameter program. The punched card data for the impedance matrix program is exactly the same as in [7]. The punched card data for the excitation vector program is altered slightly to obtain the second and third polarizations (see (103) of [7]) instead of just the third. On the first data card, NPAT is changed from 1 to 2 and on the third data card, NPA(1)=3 is replaced by NPA(1)=2 and NPA(2)=3. Except for NPAT and NPA, the resulting printed output is exactly the same as in [7], but more data is stored on record 2 of data set 6. The port parameter program is run next with NT = 145 replaced by NT = 290 on the first data card. Except for NT, the resulting printed output is exactly the same as in [7].

In the pattern synthesis program, the activity on data sets 1 (punched card input) and 6 (direct access input and output) is as follows.

```
        READ(1,4) ·NF
4       FORMAT(20I3)
        DO 62 MF=1, NF
        READ(1,4) N,M,NT,N6,N8,N9,I2,I3,NIV
        READ(1,7)(RE(I), I=1,M)
7       FORMAT(7E11.4)
        READ(1,4)(NE(I), I=1,M)
        NZ=N*N8
        READ(1,71)(FI(I), I=1,NZ)
71      FORMAT(4E14.7)
        READ(1,4)(NST(I), I=1,N8)
        NTN=I2+(NT-1)*I3+N
        REWIND 6
        SKIP N6 RECORDS ON DATA SET 6
        READ(6)(PP(I), I=1,NTN)
        DO 25 J=1,N8
        IF(NST(J).EQ.0) GO TO 25
        L2=NST(J)
        DO 83 L=1, L2
        READ(1,7)(ANG(I), I=1,M)
83      CONTINUE
25      CONTINUE
62      CONTINUE
```

Virtually all of the main program is contained in DO loop 62. There are N ports at which reactive loads may be placed. The negative of the normalized electric field at the Ith point on the radiation sphere from one ampere at the Jth port is stored in PP(I2+(I-1)*I3+J) for I=1,2...NT. However, the specified pattern consists of the magnitude RE of the electric field at only the NE(1), NE(2),...NE(M)th of these NT points. The basis $\vec{I}_J$ of real port currents appearing in (18) resides in FI((J-1)*N+1) through FI(J*N) for J=1,2,...N8. The iterative procedure for minimizing (21) terminates either as soon as $\vec{\alpha}$ of (23) fails to decrease ε or after (23) has been evaluated N9 times, whichever occurs first.

Although the program is documented in terms of the open circuit impedance formulation which is obtained when NIV≠0, the short circuit admittance formulation can be obtained by setting NIV=0 and by changing I2 so that the normalized electric field from one volt at one of the ports is referenced in PP. The variable NIV is necessary because equations (60) and (52) of [7] are used to obtain $\vec{\underline{E}}^{sc} \cdot \underline{I\ell}_r$ and $-\vec{\underline{E}}^{oc} \cdot \underline{I\ell}_r$ respectively from $\vec{I}^{sc}$ and $\vec{V}^{oc}$ which are stored in PP and appear in the table on page 62 of [7]. The ANG(I) read inside nested DO loops 25 and 83 is the starting value (degrees) of β_I appearing in (21) when only the first second, ..., and J^{th} of the N8 basis functions are used in which case (18) becomes

$$\vec{I} = \sum_{n=1}^{J} \alpha_n \vec{I}_n \qquad \text{(II-1)}$$

For a fixed J, NST(J) different starting values of $\vec{\beta}$ are tried.

Minimum allocations are given by

DIMENSION LR(N8), C(N8*N8)

in the subroutine LINER and in the main program by

COMPLEX PP(I2+(NT-1)*I3+N)
DIMENSION FI(N*N8), NE(M), NST(N8), RE(M),
   E1(M*N8), E2(M*N8), E3(M*N8), E4(M*N8),
   B(N8*(N8+1)/2), BB(N8*N8), E5(M*N8), E6(M*N8),
   E7(M*M), E8(M*M), E9(M*M), E10(M*M), CS(M),
   SN(M), CS2(M), SN2(M), PAT(M), ALP(N8), CUR(N),
   ERR(N9+1)

The logic between statements 85 and 86 prints Y_S, Z_S, $\vec{I}^{sc}$, $\underline{F}^{sc}_{O} \cdot \underline{u}_r$, $\vec{V}^{oc}$, and $\underline{F}^{oc}_{O} \cdot \underline{u}_r$ which are stored in PP and appear in the table on page 62 of [7]. Nested DO loops 20 and 21 store the real and imaginary parts of E of (24) by columns in E1 and E2. Nested DO loops 17 and 67 store the real and imaginary parts of $\tilde{E}F$ (F is an M by M diagonal matrix) by rows in E3 and E4. Nested DO loops 26 and 27 store Re($\tilde{E}$*E) according to the symmetric mode of storage in B.

58

The index J of DO loop 25 indicates that only the first J basis vectors $\vec{I}_n$ appearing in (18) will be used. This means that only the first J columns of E, only the first J rows of $\widetilde{EF}$, and only the upper left hand portion of $Re(\widetilde{E}*E)$ will be considered. Nested DO loops 32 and 33 store $Re(\widetilde{E}*E)$ by columns in BB. Statement 44 inverts $Re(\widetilde{E}*E)$. Nested DO loops 34 and 68 store the real and imaginary parts of $[Re(\widetilde{E}*E)]^{-1}[\widetilde{EF}]$ by rows in E5 and E6.

The column vector $\vec{E}$ of electric fields produced by $\vec{\alpha}$ of (23) can be written as

$$\vec{E} = [E7][\cos \beta] + [E8]\sin \beta + j[E9][\cos \beta] + j[E10][\sin \beta] \qquad (II-2)$$

where

$$[E7] = [Re(E)][Re(\widetilde{E}*E)]^{-1}[Re(\widetilde{EF})]$$

$$[E8] = [Re(E)][Re(\widetilde{E}*E)]^{-1}[Im(\widetilde{EF})]$$

$$\qquad (II-3)$$

$$[E9] = [Im(E)][Re(\widetilde{E}*E)]^{-1}[Re(\widetilde{EF})]$$

$$[E10] = [Im(E)][Re(\widetilde{E}*E)]^{-1}[Im(\widetilde{EF})]$$

and where $[\cos \beta]$ is a column vector whose m^{th} element is $\cos \beta_m$. $[\sin \beta]$ is defined similarly. With (II-2), (22) gives the new $\vec{\beta}$ in terms of the old $\vec{\beta}$.

$$\cos \beta_m = \frac{(E7 \cos \beta)_m + (E8 \sin \beta)_m}{S3} \qquad (II-4)$$

$$\sin \beta_m = \frac{(E9 \cos \beta)_m + (E10 \sin \beta)_m}{S3} \qquad (II-5)$$

where

$$S3 = \sqrt{((E7 \cos \beta)_m + (E8 \sin \beta)_m)^2 + ((E9 \cos \beta)_m + (E10 \sin \beta)_m)^2} \qquad (II-6)$$

The notation $(E7 \cos \beta)_m$ indicates the mth element of the column vector E7 cos β. In (II-4) and (II-5) the old $\vec{\beta}$ is on the right hand side whereas the new $\vec{\beta}$ is on the left hand side. The index L of DO loop 83 indicates the Lth starting value of $\vec{\beta}$. Equations (II-4) and (II-5) are evaluated for the

Ith time in DO loop 47. DO loop 47 stores ε of (21) in ERR, the magnitude of the approximate field in PAT, and $\cos \beta_m$ and $\sin \beta_m$ of (II-4) and (II-5) in CS2 and SN2.

DO loop 55 puts the final $\vec{\alpha}$ of (23) in ALP. Depending upon whether NIV=0 or not, DO loop 58 puts either the port voltages or port currents in CUR. DO loop 80 puts the real and imaginary parts of the approximate electric field in CS and SN.

For the sample input and output, the scatterer is the wire triangle of Fig. 5 of [7]. The magnitude F of the desired electric field pattern is given by

$$F = u_\phi |\cos \theta| \text{ in the x=0 plane} \tag{II-7}$$

$$F = u_\theta |\cos \theta| \text{ in the y=0 plane} \tag{II-8}$$

To obtain a continuous 360° pattern in (II-7), $u_\phi = u_x$ while $\theta=0$ on the positive z axis, $\theta=90°$ on the negative y axis and $\theta=360°$ on the positive z axis. Equation (II-8) is valid for $\theta=0$ on the positive z axis, $\theta=90°$ on the positive x axis, and $\theta=360°$ on the positive z axis. Equation (II-7) is specified at $\theta=0°$, 30°, 60°, 90°, 120°, 150°, and 180° while (II-8) is specified at $\theta=30°$, 60°, 90°, 120°, and 150°. Because of symmetry, it would have been redundant to specify (II-7) at 210°, 240°, 270°, 300°, and 330° or to specify (II-8) at 0°, 180°, 210°, 240°, 270°, 300°, and 330°. The open circuit impedance formulation (NIV≠0) is used with only three basis vectors, the dominant ($\lambda = -0.1552$, $\lambda = -10.12$, and $\lambda = -50.54$) mode currents for the unloaded wire triangle. Seven significant figures were obtained for these mode currents by changing format statement 60 in the eigencurrent program mentioned on pages 72 and 73 of [7].

LISTING OF PATTERN SYNTHESIS PROGRAM

```
//              (0034,FE,20S,2),'MAUTZ,JOE',REGION=200K
// EXEC WATFIV
//GO.FT06F001 DD DSNAME=FE0034.REV1,DISP=OLD,UNIT=2314,         X
//              VOLUME=SER=SU0004,DCB=(RECFM=VS,BLKSIZE=2596,LRECL=2592,X
//              BUFNO=1)
//GO.SYSIN DD *
$JOB            MAUTZ,TIME=1,PAGES=40
       SUBROUTINE LINFR(LL,C)
       DIMENSION LR(4),C(16)
       DO 20 I=1,LL
       LR(I)=I
   20 CONTINUE
       M1=0
       DO 18 M=1,LL
       K=M
       DO 2 I=M,LL
       K1=M1+I
       K2=M1+K
       IF(ABS(C(K1))-ABS(C(K2))) 2,2,6
    6 K=I
    2 CONTINUE
       LS=LR(M)
       LR(M)=LR(K)
       LR(K)=LS
       K2=M1+K
       STOR=C(K2)
       J1=0
       DO 7 J=1,LL
       K1=J1+K
       K2=J1+M
       STO=C(K1)
       C(K1)=C(K2)
       C(K2)=STO/STOR
       J1=J1+LL
    7 CONTINUE
       K1=M1+M
       C(K1)=1./STOR
       DO 11 I=1,LL
       IF(I-M) 12,11,12
   12 K1=M1+I
       ST=C(K1)
       C(K1)=0.
       J1=0
       DO 10 J=1,LL
       K1=J1+I
       K2=J1+M
       C(K1)=C(K1)-C(K2)*ST
       J1=J1+LL
   10 CONTINUE
   11 CONTINUE
       M1=M1+LL
   18 CONTINUE
       J1=0
       DO 9 J=1,LL
       IF(J-LR(J)) 14,8,14
   14 LRJ=LR(J)
       J2=(LRJ-1)*LL
```

```
   21 DO 13 I=1,LL
      K2=J2+I
      K1=J1+I
      S=C(K2)
      C(K2)=C(K1)
      C(K1)=S
   13 CONTINUE
      LR(J)=LR(LRJ)
      LR(LRJ)=LRJ
      IF(J-LR(J)) 14,8,14
    8 J1=J1+LL
    9 CONTINUE
      RETURN
      END
      COMPLEX PP(3236),U2
      DIMENSION FI(16),NE(20),NST(4),RE(20),E1(80),E2(80),E3(80),E4(80)
      DIMENSION B(10),BB(16),E5(80),E6(80),E7(144),E8(144),E9(144)
      DIMENSION E10(144),CS(20),SN(20),CS2(20),SN2(20),PAT(20),ALP(4)
      DIMENSION CUR(4),ERR(100),ANG(20)
      PR=3.141593/180.
      READ(1,4) NF
    4 FORMAT(20I3)
      WRITE(3,61) NF
   61 FORMAT('0 NF'/1X,I3)
      DO 62 MF=1,NF
      READ(1,4) N,M,NT,N6,N8,N9,I2,I3,NIV
      WRITE(3,5) N,M,NT,N6,N8,N9,I2,I3,NIV
    5 FORMAT('0   N   M NT N6 N8 N9 I2 I3 NIV'/1X,8I3,I4)
      READ(1,7)(RE(I),I=1,M)
    7 FORMAT(7E11.4)
      WRITE(3,8)(RE(I),I=1,M)
    8 FORMAT('0RE'/(1X,7E11.4))
      READ(1,4)(NE(I),I=1,M)
      WRITE(3,9)(NE(I),I=1,M)
    9 FORMAT('0NE'/(1X,20I3))
      NZ=N*N8
      READ(1,71)(FI(I),I=1,NZ)
   71 FORMAT(4E14.7)
      WRITE(3,24)(FI(I),I=1,NZ)
   24 FORMAT('0FI'/(1X,4E14.7))
      READ(1,4)(NST(I),I=1,N8)
      WRITE(3,19)(NST(I),I=1,N8)
   19 FORMAT('0NST'/(1X,20I3))
      NTN=I2+(NT-1)*I3+N
      REWIND 6
      IF(N6) 11,11,12
   12 DO 41 J=1,N6
      READ(6)
   41 CONTINUE
   11 READ(6)(PP(I),I=1,NTN)
   85 NN=N*N
      WRITE(3,42)(PP(I),I=1,NN)
   42 FORMAT('0YS'/(1X,5E14.7))
      J1=NN+1
      J2=2*NN
      WRITE(3,84)(PP(I),I=J1,J2)
   84 FORMAT('0ZS'/(1X,5E14.7))
      WRITE(3,87)
   87 FORMAT('0ISC,FSC,VOC,FOC')
      J2=I2-N-1
```

```
      DO 86 J=1,M
      J5=J2+(NE(J)-1)*I3
      J3=J5+1
      J4=J5+I3
      WRITE(3,88)(PP(I),I=J3,J4)
   88 FORMAT(1X,5E14.7)
   86 CONTINUE
      EE=0.
      DO 45 J=1,M
      EE=EE+RE(J)*RE(J)
   45 CONTINUE
      WRITE(3,76) EE
   76 FORMAT('0SUM RE**2=',E14.7)
      ERR(1)=EE
      DO 20 J=1,N8
      J1=(J-1)*M
      J6=(J-1)*N
      DO 21 I=1,M
      J3=I2+(NE(I)-1)*I3
      J2=J1+I
      U2=0.
      DO 22 K=1,N
      J4=J3+K
      J5=J6+K
      U2=U2+PP(J4)*FI(J5)
   22 CONTINUE
      E1(J2)=REAL(U2)
      E2(J2)=AIMAG(U2)
   21 CONTINUE
   20 CONTINUE
      IF(NIV.EQ.0) GO TO 63
      DO 64 J=1,J2
      E1(J)=-E1(J)
      E2(J)=-E2(J)
   64 CONTINUE
   63 WRITE(3,36)(E1(I),I=1,7)
   36 FORMAT('0E1'/(1X,7E11.4))
      WRITE(3,37)(E2(I),I=1,7)
   37 FORMAT('0E2'/(1X,7E11.4))
      J4=0
      DO 17 J=1,N8
      DO 67 I=1,M
      J4=J4+1
      E3(J4)=E1(J4)*RE(I)
      E4(J4)=E2(J4)*RE(I)
   67 CONTINUE
   17 CONTINUE
      J3=0
      DO 26 J=1,N8
      J1=(J-1)*M
      DO 27 I=1,J
      J3=J3+1
      B(J3)=0.
      J6=(I-1)*M
      DO 28 K=1,M
      J4=J1+K
      J5=J6+K
      B(J3)=B(J3)+E1(J4)*E1(J5)+E2(J4)*E2(J5)
   28 CONTINUE
   27 CONTINUE
```

```
   26 CONTINUE
      WRITE(3,18)(B(J),J=1,J3)
   18 FORMAT('0B'/(1X,7E11.4))
      DO 25 J=1,N8
      IF(NST(J).EQ.0) GO TO 25
      J8=0
      DO 32 K=1,J
      J4=(K-1)*J
      DO 33 L=1,K
      J8=J8+1
      J5=J4+L
      J6=(L-1)*J+K
      BB(J5)=B(J8)
      BB(J6)=BB(J5)
   33 CONTINUE
   32 CONTINUE
   44 CALL LINER(J,BB)
      DO 34 K=1,M
      J4=K
      DO 68 I=1,J
      J6=(I-1)*J
      E5(J4)=0.
      E6(J4)=0.
      J7=K
      DO 69 KK=1,J
      J8=J6+KK
      E5(J4)=E5(J4)+BB(J8)*E3(J7)
      E6(J4)=E6(J4)+BB(J8)*E4(J7)
      J7=J7+M
   69 CONTINUE
      J4=J4+M
   68 CONTINUE
   34 CONTINUE
      DO 70 K=1,M
      J4=(K-1)*M
      DO 75 I=1,M
      J5=J4+I
      E7(J5)=0.
      E8(J5)=0.
      E9(J5)=0.
      E10(J5)=0.
      J6=K
      J7=I
      DO 72 KK=1,J
      E7(J5)=E7(J5)+E1(J7)*E5(J6)
      E8(J5)=E8(J5)+E1(J7)*E6(J6)
      E9(J5)=E9(J5)+E2(J7)*E5(J6)
      E10(J5)=E10(J5)+E2(J7)*E6(J6)
      J7=J7+M
      J6=J6+M
   72 CONTINUE
   75 CONTINUE
   70 CONTINUE
      WRITE(3,40)
   40 FORMAT('0E7,E8,E9,E10')
      WRITE(3,14)(E7(I),I=1,7),(E8(I),I=1,7),(E9(I),I=1,7)
      WRITE(3,14)(E10(I),I=1,7)
   14 FORMAT(1X,7E11.4)
      L2=NST(J)
      DO 83 L=1,L2
```

```
      READ(1,7)(ANG(I),I=1,M)
      WRITE(3,16)(ANG(I),I=1,M)
   16 FORMAT('0ANG'/(1X,7E11.4))
      DO 15 K=1,M
      AN=ANG(K)*PR
      CS(K)=COS(AN)
      SN(K)=SIN(AN)
   15 CONTINUE
      DO 47 I=1,N9
      I2=I+1
      ERR(I2)=0.
      DO 50 KK=1,M
      S1=0.
      S2=0.
      J4=KK
      DO 49 K=1,M
      S1=S1+E7(J4)*CS(K)+E8(J4)*SN(K)
      S2=S2+E9(J4)*CS(K)+E10(J4)*SN(K)
      J4=J4+M
   49 CONTINUE
      S8=S1-RF(KK)*CS(KK)
      S9=S2-RE(KK)*SN(KK)
      ERR(I2)=ERR(I2)+S8*S8+S9*S9
      S3=SQRT(S1*S1+S2*S2)
      PAT(KK)=S3
      IF(S3) 51,51,52
   51 CS2(KK)=1.
      SN2(KK)=0.
      GO TO 50
   52 CS2(KK)=S1/S3
      SN2(KK)=S2/S3
   50 CONTINUE
      DO 79 KK=1,M
      CS(KK)=CS2(KK)
      SN(KK)=SN2(KK)
   79 CONTINUE
      IF(ERR(I2).GE.ERR(I)) GO TO 73
   47 CONTINUE
      WRITE(3,53)
   53 FORMAT(' TOO MANY ITERATIONS')
   73 WRITE(3,13)(ERR(I),I=1,I2)
   13 FORMAT('0ERR'/(1X,5E14.7))
      DO 55 I=1,J
      J5=(I-1)*M
      ALP(I)=0.
      DO 56 K=1,M
      J4=J5+K
      ALP(I)=ALP(I)+E5(J4)*CS(K)+E6(J4)*SN(K)
   56 CONTINUE
   55 CONTINUE
      WRITE(3,59)(ALP(I),I=1,J)
   59 FORMAT('0ALPHA'/(1X,4E14.7))
      DO 57 I=1,N
      CUR(I)=0.
      J4=I
      DO 58 K=1,J
      CUR(I)=CUR(I)+ALP(K)*FI(J4)
      J4=J4+N
   58 CONTINUE
   57 CONTINUE
```

```
      WRITE(3,60)(CUR(I),I=1,N)
   60 FORMAT('OPORT QUANTITIES'/(1X,4E14.7))
      WRITE(3,77)(PAT(I),I=1,M)
   77 FORMAT('OAPPROX |E|'/(1X,7E11.4))
      DO 80 K=1,M
      CS(K)=PAT(K)*CS2(K)
      SN(K)=PAT(K)*SN2(K)
   80 CONTINUE
      WRITE(3,81)(CS(K),SN(K),K=1,M)
   81 FORMAT('OAPPROX E'/(1X,7E11.4))
   83 CONTINUE
   25 CONTINUE
   62 CONTINUE
      STOP
      END
$DATA
   1
   4 12290  2   3 60341 10   1
 0.1000E+01 0.8660E+00 0.5000E+00 0.0000E+00 0.5000E+00 0.8660E+00 0.1000E+01
 0.8660E+00 0.5000E+00 0.0000E+00 0.5000E+00 0.8660E+00
   1 13 25 37 49 61 73158170182194206
-0.1338342E+00 0.4326460E+00 0.8418684E+00 0.9999999E+00
-0.6078172E+00 0.9999999F+00 0.8054470E+00-0.6457505E+00
 0.9999996E+00-0.5373682E+00 0.1367921E-01 0.7396740E-01
   0   0   1
 0.0000E+00 0.0000E+00 0.0000E+00 0.0000E+00 0.0000E+00 0.0000E+00 0.0000E+00
 0.0000E+00 0.0000E+00 0.0000E+00 0.0000F+00 0.0000E+00
$STOP
/*
//
```

PRINTED OUTPUT

```
 NF
   1


   N   M  NT N6 N8 N9 I2 I3 NIV
   4 12290  2   3 60341 10   1

 RE
  0.1000E+01 0.8660E+00 0.5000E+00 0.0000E+00 0.5000E+00 0.8660E+00 0.1000E+01
  0.8660E+00 0.5000E+00 0.0000E+00 0.5000E+00 0.8660E+00

 NE
   1 13 25 37 49 61 73158170182194206

 FT
 -0.1338342E+00 0.4326460E+00 0.8418684E+00 0.9999999E+00
 -0.6078172E+00 0.9999999E+00 0.8054470E+00-0.6457505E+00
  0.9999996E+00-0.5373682E+00 0.1367921E-01 0.7396740E-01

 NST
   0   0   1

 YS
  0.1917231E-03 0.3060562E-02-0.3932747E-03-0.3196523E-02-0.6370670E-03
 -0.2576157E-03-0.6627280E-03 0.4244351E-03-0.3932752E-03-0.3196524E-02
  0.1096654E-02 0.3973222E-03 0.1988475E-02 0.1482670E-02 0.2212893E-02
 -0.5016243E-03-0.6370675E-03-0.2576152E-03 0.1988475E-02 0.1482668E-02
  0.3786647E-02 0.1055478E-02 0.4378561E-02 0.2396983E-03-0.6627277E-03
```

```
 0.4244335E-03 0.2212891E-02-0.5016173E-03 0.4378553E-02 0.2397003E-03
 0.5296886E-02 0.1213216E-02


ZS
 0.6553223E+01-0.1816547E+03 0.7365026E+00 0.1965277E+03 0.1112900E+02
-0.3768264E+03-0.1120400E+02 0.2082711E+03 0.7364006E+00 0.1965278E+03
 0.4536248E+01 0.2287910E+03 0.1526020E+02-0.2456085E+03-0.1219231E+01
 0.1319926E+03 0.1112851E+02-0.3768257E+03 0.1526013E+02-0.2456081E+03
 0.7751503E+02-0.4768188E+03 0.4496897E+01 0.4456296E+03-0.1120363E+02
 0.2082705E+03-0.1219147E+01 0.1319923E+03 0.4496399E+01 0.4456296E+03
 0.1117702E+03-0.4224771E+03


ISC,FSC,VOC,FOC
 0.1741995E-01 0.3099880E-02-0.2802336E-01-0.1126636E-01-0.4590483E-01
-0.2377475E-01-0.4625515E-01-0.3972430E-01 0.6376842E+00 0.1247487E-01
-0.2192616E+01 0.8147461E+00-0.6140513E+00-0.1818085E+01-0.7669821E+00
 0.5648457E+00 0.1088376E+02 0.5553505E+01 0.3882574E-01 0.1907506E-01
 0.1868119E-01-0.4495338E-02-0.3718363E-01 0.4325941E-02-0.6177179E-01
 0.5520454E-03-0.6833255E-01-0.8959431E-02 0.6380222E+00-0.3501515E+00
-0.5804261E+00 0.1575368E+01-0.1976346E+00-0.1352030E+01 0.1830723E+01
-0.1114449E+01 0.1174516E+02 0.6294250E+00 0.7380056E+00 0.3092869E+00
 0.4447345E-02-0.2026889E-01-0.1262894E-01 0.4987016E-01-0.2299789E-01
 0.8066756E-01-0.2157412E-01 0.8859092E-01-0.2877145E+00-0.8937255E+00
 0.1530455E+01-0.6922106E+00-0.3141909E+00-0.2119786E+01-0.1572831E+01
-0.9964454E+01 0.3430489E+01-0.8556176E+01 0.1436495E+00-0.9424174E-01
-0.1494673E-01-0.4051365E-02 0.4730245E-01 0.1024298E-01 0.9114552E-01
 0.1087571E-01 0.1071812E+00-0.1665585E-02-0.9120010E+00 0.5829626E+00
-0.1446554E+01-0.1087798E+00-0.2807508E+01 0.1425666E+00-0.1501971E+02
 0.7355479E+00-0.6440857E+01 0.1638210E+01-0.1322157E+00-0.1596093E+00
-0.6673606E-03 0.4352655E-02-0.2714045E-02-0.2889325E-01-0.9360578E-02
-0.7143170E-01-0.1959864E-01-0.9028465E-01 0.7146822E+00 0.6863058E+00
 0.1535620E+01 0.7428402E+00 0.3973961E-02 0.2147792E+01 0.1452603E+00
 0.9687865E+01 0.5625796E+01 0.6814459E+01-0.5010319E-01 0.1602144E+00
-0.1681667E-02-0.3633492E-02-0.1996757E-01 0.4651893E-02-0.5041174E-01
 0.4234578E-02-0.6516790E-01-0.7188669E-03 0.6504440E+00-0.4349312E+00
-0.3145391E+00-0.1839961E+01-0.3052473E-02 0.1035116E+01 0.2411313E+01
-0.8899441E+00 0.9515347E+01-0.2054931E+01 0.1854154E+00 0.1052294E-01
-0.5152740E-02-0.3682023E-02-0.1282415E-01 0.1421350E-01-0.3345026E-01
 0.2893564E-01-0.4674845E-01 0.2653901E-01 0.3086727E+00-0.6145549E+00
-0.2022494E+01-0.1295329E+01-0.5601563E+00 0.1430530E+01-0.1017804E+01
-0.2746825E+01 0.8093803E+01-0.5198156E+01 0.1742824E+00-0.1065023E+00
 0.1431801E-01-0.1658451E-02-0.2404462E-01 0.3820483E-02-0.4434474E-01
 0.5770296E-02-0.5593992E-01-0.5390316E-02 0.4450209E+00-0.3812340E+00
-0.2454308E+01 0.2150214E+01-0.8735202E+00-0.9312153E+00-0.1570337E+01
 0.2811036E+01 0.1159047E+02-0.3117700E+01 0.2114847E-02-0.6987196E-01
 0.5126368E-02 0.1770929E-03 0.3685936E-02 0.7904314E-02 0.8839853E-02
 0.2630038E-01 0.2633312E-03 0.4341792E-01-0.4724065E+00-0.2830663E+00
 0.5215341E+00 0.3669862E+01 0.9594172E+00-0.9879684E-01 0.4000002E+01
 0.4578192E+01-0.5549911E+01-0.1034170E+02-0.2048464E+00 0.9778023E-02
 0.1395519E-01 0.2344323E-02-0.1212004E-01-0.8843843E-02-0.4445191E-02
-0.1745868E-01 0.1498836E-01-0.2014870E-01 0.1217503E+00 0.4513527E+00
 0.3534557E+00 0.7994109E-01 0.1966642E+00-0.2759507E+01 0.9413064E+00
-0.4964129E+01-0.1460495E+01 0.9352454E+01 0.8914864E-01 0.2051381E+00
 0.6843425E-02-0.8706748E-02-0.2662857E-02 0.2066507E-01-0.2947436E-02
 0.2942693E-01-0.1179760E-01 0.2229091E-01 0.1727545E-01-0.3838835E+00
-0.9456767E+00 0.3076982E+01-0.1230765E+01-0.4116199E+00-0.5646402E+01
 0.3176999E+01 0.6015682E+01-0.7440682E+01 0.6830072E+01-0.1706336E+00
 0.1707099E-02 0.4408758E-03 0.1882774E-01-0.1394843E-02 0.4007884E-01
-0.3204998E-02 0.4473817E-01 0.5141165E-02-0.5224348E+00 0.2506838E+00
 0.1954428E+01 0.2486438E+01 0.5895611E+00-0.6433392E+00 0.3815098E+00
```

```
   0.4682909E+01-0.8831078E+01-0.2357099E+01-0.1946359E+00-0.2247558E-01

SUM RF**2= 0.5999821E+01

F1
-0.1027E+02-0.1328E+02-0.1766E+01 0.2011E+02-0.5544E+01-0.1159E+02-0.7265E+01

E2
-0.5133E+01 0.1105E+01 0.1777E+02-0.2334E+01-0.1580E+02 0.2110E+01 0.6718E+01

B
 0.1833E+04-0.2544E+03 0.8790E+03 0.1006E+02-0.2425E+00 0.7154E+02

E7,E8,E9,E10
 0.1108E+00 0.9568E-01 0.8992E-02-0.2236E-01 0.2493E-01 0.7490E-01 0.8747E-01
 0.2542E-01 0.7104E-01 0.8911E-01-/<3858E-03 0.9512F-01 0.5708E-01 0.9009E-02
 0.2542E-01-0.1825E-01-/<5267E-01 0.1368E-01 0.3892E-01 0.1195E-01-0.1515E-01
 0.1079E+00 0.8981E-01-0.1898E-01 0.4106E-02 0.7288E-02-0.9791E-01-0.1075E+00

ANG
 0.0000E+00 0.0000E+00 0.0000E+00 0.0000E+00 0.0000E+00 0.0000E+00 0.0000E+00
 0.0000E+00 0.0000E+00 0.0000E+00 0.0000E+00 0.0000E+00

ERR
 0.5999821E+01 0.4350671E+01 0.1010671E+01 0.9769405E+00 0.9555495E+00
 0.9410038E+00 0.9309457E+00 0.9238821E+00 0.9188403E+00 0.9151857E+00
 0.9124985E+00 0.9104964E+00 0.9089867E+00 0.9078364E+00 0.9069511E+00
 0.9062644E+00 0.9057275E+00 0.9053047E+00 0.9049698E+00 0.9047029E+00
 0.9044896E+00 0.9043177E+00 0.9041796E+00 0.9040670E+00 0.9039757E+00
 0.9039018E+00 0.9038412E+00 0.9037908E+00 0.9037502E+00 0.9037165E+00
 0.9036888E+00 0.9036661E+00 0.9036469E+00 0.9036312E+00 0.9036181E+00
 0.9036076E+00 0.9035987E+00 0.9035910E+00 0.9035851E+00 0.9035797E+00
 0.9035755E+00 0.9035718E+00 0.9035689E+00 0.9035666E+00 0.9035644E+00
 0.9035625E+00 0.9035614E+00 0.9035596E+00 0.9035591E+00 0.9035581E+00
 0.9035573E+00 0.9035565E+00 0.9035563E+00 0.9035559E+00 0.9035555E+00
 0.9035553E+00 0.9035550E+00 0.9035545E+00 0.9035543E+00 0.9035548E+00

ALPHA
-0.3871064E-01 0.3347580E-01 0.1049885E+00

PORT QUANTITIES
 0.8982205E-01-0.3968969E-01-0.4190121E-02-0.5256191E-01

APPROX |E|
 0.7563E+00 0.6898E+00 0.5140E+00 0.3970E+00 0.4464E+00 0.5466E+00 0.5912E+00
 0.8761E+00 0.9036E+00 0.3672E+00 0.7467E+00 0.7089E+00

APPROX E
 0.7414E+00 0.1490E+00 0.6693E+00-0.1667E+00 0.2385E-01-0.5134E+00-0.3830E+00
 0.1046E+00 0.1586E+00 0.4173E+00 0.5384E+00 0.9454E-01 0.5806E+00-0.1117E+00
 0.7884E+00-0.3821E+00-0.2838E+00-0.8579E+00-0.9677E-01 0.3542E+00 0.3287E+00
-0.6705E+00-0.6147E+00-0.3531E+00
```

ONLY THREE MODE CURRENTS APPEAR IN THE ABOVE PRINTED OUTPUT. FOR
REFERENCE, ALL THE MODES OF THE WIRE TRIANGLE ARE LISTED BELOW.

PORT MODE VOLTAGES

EIGENVALUE	PORT(1)	PORT(2)	PORT(3)	PORT(4)
0.1551843E+00	-0.2053680E-01	0.1157823E+00	0.6424825E+00	0.9999995E+00
0.1011907E+02	0.1904054E+00	0.2523626E+00	0.9999999E+00	-0.9255674E+00

```
0.5053986E+02 0.9999996E+00-0.2887278E+00 0.7883916E+00-0.4049708E+00
-0.8162234E+03 0.5313363E+00 0.9999999E+00-0.6748938E+00 0.2066367E+00
```

PORT MODE CURRENTS

EIGENVALUE	PORT(1)	PORT(2)	PORT(3)	PORT(4)
-0.1551809E+00	-0.1338342E+00	0.4326460E+00	0.8418684E+00	0.9999999E+00
-0.1011935E+02	-0.6078172E+00	0.9999999E+00	0.8054470E+00	-0.6457505E+00
-0.5054034E+02	0.9999996E+00	-0.5373682E+00	0.1367921E-01	0.7396740E-01
0.8164128E+03	0.5441235E+00	0.9999999E+00	-0.2839342E+00	0.7781506E-01

III. STORAGE OF SPECIFIED AND SYNTHESIZED PATTERNS

The program of this section stores the specified and synthesized patterns on direct access data set 6 so that they can be plotted by the program on pages 104-110 of [7]. The activity on data sets 1 (punched card input) and 6 (direct access input and output) is as follows:

```
          READ(1,10) N, NT, NPAT, NF, N6, N7, NPP
10        FORMAT(6I3, I4)
          REWIND 6
          SKIP N6 RECORDS ON DATA SET 6
          READ(6)(PP(I), I=1, NPP)
          DO 17 L=1, NF
          READ(1,10) M, I2, I3, N8, NIV
          READ(1,45)(NE(I), I=1,M)
45        FORMAT(20I3)
          READ(1,19)(RE(I), I=1,M)
19        FORMAT(7E11.4)
          READ(1,19)(AE(I), I=1, M)
          DO 22 K=1, N8
          READ(1,23)(CUR(I), I=1, N)
23        FORMAT(5E14.7)
22        CONTINUE
17        CONTINUE
          SKIP N7 RECORDS ON DATA SET 6
          WRITE(6)(G(I), I=1, JG)
```

There are N ports. There are NPAT polarizations and NT angles as described on page 53 of [7]. The same port parameters used by the pattern synthesis program are read in through PP. The real and imaginary parts of the specified desirable electric field pattern are read in through RE and AE. In this instance, the program is more general than necessary because the desirable electric field pattern is specified in magnitude only. This magnitude has been read in through RE and AE has been set equal to zero. For RE(I) and AE(I), NE(I) = (K-1)*NT+J indicates the Kth polarization to be stored in PP

and the Jth angle. I2, I3, and NIV are the same as in the pattern synthesis program. An approximate pattern is defined by its port currents CUR which appear in the printed output of the pattern synthesis program. For each value of L, first the M points on the specified pattern, next the NT*NPAT points on the Kth approximate pattern for K=1,2,...N8 are stored in G.

Minimum allocations are given by

COMPLEX PP(NPP)

DIMENSION ANG(NT), RE(M), AE(M), G(JG),

G2(M), CUR(N), NE(M+1)

where

$$JG = \sum_{L=1}^{NF} (M + N8*NPAT*NT)$$

DO loop 28 stores the specified pattern in both G and G2. DO loop 22 stores in G the synthesized pattern defined by CUR. DO loop 25 is necessary to account for the minus sign in (52) of [7]. DO loop 43 obtains the NPAT polarizations and DO loop 26 the NT angles. DO loop 27 is able to accumulate the normalized electric field in E because PP(J2) is the negative of the normalized electric field from a unit current at the Ith port.

For the sample input data, CUR is the set of port currents which radiate the pattern synthesized by the pattern synthesis program. The synthesized and desirable patterns are printed at the 12 points at which the desirable pattern was specified in the pattern synthesis program plus at the 12 redundant points enumerated in the previous section as well as at 360° for both polarizations for a total of 26 points. The synthesized pattern is stored at every 2.5 degrees in G for a total of 290 points. The contents of G are written on record 4 of direct access data set 6.

```
//                    (0034,EE,20S,1),'MAUTZ,JOE',REGION=200K
// EXEC WATFIV
//GO.FT06F001 DD DSNAME=EE0034.REV1,DISP=OLD,UNIT=2314,                    X
//                  VOLUME=SER=SU0004,DCB=(RECFM=VS,BLKSIZE=2596,LRECL=2592,X
//                  BUFNO=1)`
//GO.SYSIN DD *
$JOB              MAUTZ,TIME=1,PAGES=30
      COMPLEX PP(3236),E
      DIMENSION ANG(145),RE(26),AE(26),G(4692),G2(26),CUR(4),NE(27)
      READ(1,10) N,NT,NPAT,NF,N6,N7,NPP
   10 FORMAT(6I3,I4)
      WRITE(3,11) N,NT,NPAT,NF,N6,N7,NPP
   11 FORMAT('0  N NT NPAT NF N6 N7 NPP'/1X,2I3,I5,3I3,I4)
      REWIND 6
      IF(N6) 12,12,13
   13 DO 14 J=1,N6
      READ(6)
   14 CONTINUE
   12 READ(6)(PP(I),I=1,NPP)
      WRITE(3,16)(PP(I),I=1,2)
   16 FORMAT('0PP'/(1X,4E11.4))
      DEL=360./(NT-1)
      DO 31 J=1,NT
      ANG(J)=(J-1)*DEL
   31 CONTINUE
      JG=0
      DO 17 L=1,NF
      READ(1,10) M,I2,I3,N8,NIV
      WRITE(3,18) M,I2,I3,N8,NIV
   18 FORMAT('0  M I2 I3 N8 NIV'/1X,4I3,I4)
      READ(1,45)(NE(I),I=1,M)
   45 FORMAT(20I3)
      WRITE(3,46)(NE(I),I=1,M)
   46 FORMAT('0NE'/(1X,20I3))
      NE(M+1)=0
      READ(1,19)(RE(I),I=1,M)
   19 FORMAT(7E11.4)
      WRITE(3,20)(RE(I),I=1,M)
   20 FORMAT('0RE'/(1X,7E11.4))
      READ(1,19)(AE(I),I=1,M)
      WRITE(3,21)(AE(I),I=1,M)
   21 FORMAT('0AE'/(1X,7E11.4))
      DO 28 J=1,M
      JG=JG+1
      G(JG)=SQRT(RE(J)*RE(J)+AE(J)*AE(J))
      G2(J)=G(JG)
   28 CONTINUE
      DO 22 K=1,N8
      READ(1,23)(CUR(I),I=1,N)
   23 FORMAT(5E14.7)
      WRITE(3,24)(CUR(I),I=1,N)
   24 FORMAT('0CUR'/(1X,5E14.7))
      IF(NIV) 40,39,40
   39 WRITE(3,37) K
   37 FORMAT('0',3X,'PATTERN OF',I3,'TH SET OF PORT VOLTAGES',8X,'SPECIF
     1IED DESIRABLE PATTERN')
      GO TO 41
   40 WRITE(3,38) K
```

```
   38 FORMAT('0',3X,'PATTERN OF',I3,'TH SET OF PORT CURRENTS',8X,'SPECIF
     1IED DESIRABLE PATTERN')
      DO 25 I=1,N
      CUR(I)=-CUR(I)
   25 CONTINUE
   41 J4=1
      J5=0
      WRITE(3,42)
   42 FORMAT('  ANGLE   REAL(E)',5X,'IMAG(E)',7X,'|E|',7X,'REAL(E)',5X,'
     1IMAG(E)',7X,'|E|')
      DO 43 LL=1,NPAT
      LLK=(LL-1)*I3*NT+I2
      DO 26 J=1,NT
      E=0.
      DO 27 I=1,N
      J2=LLK+I
      E=E+PP(J2)*CUR(I)
   27 CONTINUE
      LLK=LLK+I3
      JG=JG+1
      G(JG)=CABS(E)
      J5=J5+1
      IF(NE(J4).NE.J5) GO TO 26
      WRITE(3,29) ANG(J),E,G(JG),RE(J4),AE(J4),G2(J4)
      J4=J4+1
   29 FORMAT(1X,F6.1,6E12.4)
   26 CONTINUE
   43 CONTINUE
   22 CONTINUE
   17 CONTINUE
      IF(N7) 33,33,34
   34 DO 36 J=1,N7
      READ(6)
   36 CONTINUE
   33 WRITE(6)(G(I),I=1,JG)
      WRITE(3,47)(G(I),I=1,7)
   47 FORMAT('0G'/1X,7E11.4)
      STOP
      END
$DATA
  4145   2   1   2   03236
 26341 10   1   1
  1 13 25 37 49 61 73 85 971091211133145146158170182194206218
230242254266278290
 0.1000E+01 0.8660E+00 0.5000E+00 0.0000E+00 0.5000E+00 0.8660E+00 0.1000E+01
 0.8660E+00 0.5000E+00 0.0000E+00 0.5000E+00 0.8660E+00 0.1000E+01 0.1000E+01
 0.8660E+00 0.5000E+00 0.0000E+00 0.5000E+00 0.8660E+00 0.1000E+01 0.8660E+00
 0.5000E+00 0.0000E+00 0.5000E+00 0.8660E+00 0.1000E+01
 0.0000E+00 0.0000E+00 0.0000E+00 0.0000E+00 0.0000E+00 0.0000E+00 0.0000E+00
 0.0000E+00 0.0000E+00 0.0000E+00 0.0000E+00 0.0000E+00 0.0000E+00 0.0000E+00
 0.0000E+00 0.0000E+00 0.0000E+00 0.0000E+00 0.0000E+00 0.0000E+00 0.0000E+00
 0.0000E+00 0.0000E+00 0.0000E+00 0.0000E+00 0.0000E+00
 0.8982205E-01-0.3968969E-01-0.4190121E-02-0.5256191E-01
$STOP
/*
//
```

PRINTED OUTPUT

   N NT NPAT NF N6 N7 NPP

PP
 0.1917E-03 0.3061E-02-0.3933E-03-0.3197E-02

  M I2 I3 N8 NIV
 26341 10 1   1

NE
   1 13 25 37 49 61 73 85 9710912113314514615817018219420620
230242254266278290

RE
 0.1000E+01 0.8660E+00 0.5000E+00 0.0000E+00 0.5000E+00 0.8660E+00 0.1000E+01
 0.8660E+00 0.5000E+00 0.0000E+00 0.5000E+00 0.8660E+00 0.1000E+01 0.1000E+01
 0.8660E+00 0.5000E+00 0.0000E+00 0.5000E+00 0.8660E+00 0.1000E+01 0.8660E+00
 0.5000E+00 0.0000E+00 0.5000E+00 0.8660E+00 0.1000E+01

AE
 0.0000E+00 0.0000E+00 0.0000E+00 0.0000E+00 0.0000E+00 0.0000E+00 0.0000E+00
 0.0000E+00 0.0000E+00 0.0000E+00 0.0000E+00 0.0000E+00 0.0000E+00 0.0000E+00
 0.0000E+00 0.0000E+00 0.0000E+00 0.0000E+00 0.0000E+00 0.0000E+00 0.0000E+00
 0.0000E+00 0.0000E+00 0.0000E+00 0.0000E+00 0.0000E+00

CUR
 0.8982205E-01-0.3968969E-01-0.4190121E-02-0.5256191E-01

| ANGLE | \multicolumn{3}{c}{PATTERN OF   1TH SET OF PORT CURRENTS} | \multicolumn{3}{c}{SPECIFIED DESIRABLE PATTERN} |

ANGLE	REAL(E)	IMAG(E)	|E|	REAL(E)	IMAG(E)	|E|
0.0	0.7414E+00	0.1489E+00	0.7562E+00	0.1000E+01	0.0000E+00	0.1000E+01
30.0	0.6693E+00	-0.1668E+00	0.6898E+00	0.8660E+00	0.0000E+00	0.8660E+00
60.0	0.2378E-01	-0.5134E+00	0.5140E+00	0.5000E+00	0.0000E+00	0.5000E+00
90.0	-0.3830E+00	0.1046E+00	0.3970E+00	0.0000E+00	0.0000E+00	0.0000E+00
120.0	0.1585E+00	0.4173E+00	0.4464E+00	0.5000E+00	0.0000E+00	0.5000E+00
150.0	0.5384E+00	0.9461E-01	0.5466E+00	0.8660E+00	0.0000E+00	0.8660E+00
180.0	0.5806E+00	-0.1116E+00	0.5912E+00	0.1000E+01	0.0000E+00	0.1000E+01
210.0	0.5384E+00	0.9461E-01	0.5466E+00	0.8660E+00	0.0000E+00	0.8660E+00
240.0	0.1585E+00	0.4173E+00	0.4464E+00	0.5000E+00	0.0000E+00	0.5000E+00
270.0	-0.3830E+00	0.1046E+00	0.3970E+00	0.0000E+00	0.0000E+00	0.0000E+00
300.0	0.2379E-01	-0.5134E+00	0.5140E+00	0.5000E+00	0.0000E+00	0.5000E+00
330.0	0.6693E+00	-0.1668E+00	0.6898E+00	0.8660E+00	0.0000E+00	0.8660E+00
360.0	0.7414E+00	0.1489E+00	0.7562E+00	0.1000E+01	0.0000E+00	0.1000E+01
0.0	0.7414E+00	0.1489E+00	0.7562E+00	0.1000E+01	0.0000E+00	0.1000E+01
30.0	0.7884E+00	-0.3822E+00	0.8762E+00	0.8660E+00	0.0000E+00	0.8660E+00
60.0	-0.2837E+00	-0.8580E+00	0.9036E+00	0.5000E+00	0.0000E+00	0.5000E+00
90.0	-0.9676E-01	0.3541E+00	0.3671E+00	0.0000E+00	0.0000E+00	0.0000E+00
120.0	0.3286E+00	-0.6705E+00	0.7467E+00	0.5000E+00	0.0000E+00	0.5000E+00
150.0	-0.6147E+00	-0.3531E+00	0.7089E+00	0.8660E+00	0.0000E+00	0.8660E+00
180.0	-0.5806E+00	0.1116E+00	0.5912E+00	0.1000E+01	0.0000E+00	0.1000E+01
210.0	-0.6147E+00	-0.3531E+00	0.7090E+00	0.8660E+00	0.0000E+00	0.8660E+00
240.0	0.3286E+00	-0.6705E+00	0.7467E+00	0.5000E+00	0.0000E+00	0.5000E+00
270.0	-0.9675E-01	0.3541E+00	0.3671E+00	0.0000E+00	0.0000E+00	0.0000E+00
300.0	-0.2837E+00	-0.8579E+00	0.9036E+00	0.5000E+00	0.0000E+00	0.5000E+00
330.0	0.7884E+00	-0.3822E+00	0.8762E+00	0.8660E+00	0.0000E+00	0.8660E+00
360.0	0.7414E+00	0.1489E+00	0.7562E+00	0.1000E+01	0.0000E+00	0.1000E+01

G
 0.1000E+01 0.8660E+00 0.5000E+00 0.0000E+00 0.5000E+00 0.8660E+00 0.1000E+01

IV. LOADS FOR MODAL RESONANCE

The program (modal resonance program) of this section calculates the set of reactive loads (14) which makes a given real port current an eigencurrent whose eigenvalue is zero. The activity on data sets 1 (punched card input) and 6 (direct access input and output) is as follows.

```
          READ(1,10) NF
10        FORMAT(I3)
          DO 12 L=1, NF
          READ(1,13) N, N6, N8, I2
13        FORMAT(3I3, I4)
          NZ = N*N
          NPP = I2 + NZ
          REWIND 6
          SKIP N6 RECORDS ON DATA SET 6
          READ(6)(PP(I), I=1, NPP)
          DO 20 J=1, N8
          READ(1,21)(CUR(I), I=1, N)
21        FORMAT(5E14.7)
20        CONTINUE
12        CONTINUE
```

The reactance matrix X_S in (14) is the imaginary part of the impedance matrix found in PP(I2+1) through PP(I2+N*N). The Jth set of real port currents $\vec{I}$ of (14) is read in through CUR.

Minimum allocations are given by

```
          COMPLEX PP(NPP)
          DIMENSION X(N*N), CUR(N), XL(N)
```

DO loop 19 stores $[X_S]$ of (14) in X. DO loop 26 puts the largest $|I_i|$ of (14) in CU. DO loop 23 stores X_I of (14) in XL(I). Statement 27 ensures that I_i in the denominator of (14) is at least CU*1.E-8.

The sample output XL is the set of reactive loads for modal resonance of the set of real port currents which radiate the pattern synthesized by the pattern synthesis program.

```
//              (0034,EE,10S,1),'MAUTZ,JOE',REGION=200K
// EXEC WATFIV
//GO.FT06F001 DD DSNAME=EE0034.REV1,DISP=OLD,UNIT=2314,              X
//              VOLUME=SER=SU0004,DCB=(RECFM=VS,BLKSIZE=2596,LRECL=2592,X
//              BUFNO=1)
//GO.SYSIN DD *
$JOB              MAUTZ,TIME=1,PAGES=20
      COMPLEX PP(900)
      DIMENSION X(900),CUR(30),XL(30)
      READ(1,10) NF
   10 FORMAT(I3)
      WRITE(3,11) NF
   11 FORMAT('ONF=',I3)
      DO 12 L=1,NF
      READ(1,13) N,N6,N8,I2
   13 FORMAT(3I3,I4)
      WRITE(3,14) N,N6,N8,I2
   14 FORMAT('0  N N6 N8   I2'/1X,3I3,I4)
      NZ=N*N
      NPP=I2+NZ
      REWIND 6
      IF(N6) 15,15,16
   16 DO 17 J=1,N6
      READ(6)
   17 CONTINUE
   15 READ(6)(PP(I),I=1,NPP)
      WRITE(3,18)(PP(I),I=1,3)
   18 FORMAT('OPP'/(1X,10E11.4))
      DO 19 I=1,NZ
      J2=I2+I
      X(I)=AIMAG(PP(J2))
   19 CONTINUE
      DO 20 J=1,N8
      READ(1,21)(CUR(I),I=1,N)
   21 FORMAT(5E14.7)
      WRITE(3,22)(CUR(I),I=1,N)
   22 FORMAT('OCUR'/(1X,5E14.7))
      CU=0.
      DO 26 I=1,N
      S1=ABS(CUR(I))
      IF(S1.GT.CU) CU=S1
   26 CONTINUE
      CU8=CU*1.E-8
      DO 23 I=1,N
      J1=(I-1)*N
      S1=0.
      DO 24 K=1,N
      J2=J1+K
      S1=S1+X(J2)*CUR(K)
   24 CONTINUE
      S2=CUR(I)
   27 IF(ABS(S2).LT.CU8) S2=CU8
      XL(I)=-S1/S2
   23 CONTINUE
      WRITE(3,25)(XL(I),I=1,N)
   25 FORMAT('OXL'/(1X,5E14.7))
   20 CONTINUE
   12 CONTINUE
```

```
        STOP
        END
$DATA
   1
   4   2   1   16
  0.8982205E-01-0.3968969E-01-0.4190121E-02-0.5256191E-01
$STOP
/*
//
```

PRINTED OUTPUT

NF=   1

```
  N  N6  N8    I2
  4   2   1    16
```

PP
  0.1917E-03 0.3061E-02-0.3933E-03-0.3197E-02-0.6371E-03-0.2576E-03

CUR
  0.8982205E-01-0.3968969E-01-0.4190121E-02-0.5256191E-01

XL
  0.3727910E+03 0.6710123E+02-0.1086468E+05 0.6431934E+03

V. RADAR CROSS SECTION

The program (σ/λ^2 versus angle program) of this section calculates the radar cross section per wavelength squared σ/λ^2 of the N-port loaded scatterer. For a given incident plane wave, this program obtains patterns of σ/λ^2 in one or more of the coordinate planes. The activity on data sets 1 (punched card input) and 6 (direct access input and output) is as follows.

```
         READ(1,10) NF, N6W
10       FORMAT(2I3)
         DO 12 JF=1, NF
         READ(1,13)N, N6, NQ, NS, NL, NT, NA, NPAT, NIV, NZ, I2, I3, BK
13       FORMAT(9I3, 3I4, E14.7)
         REWIND 6
         SKIP N6 RECORDS ON DATA SET 6
         NPP = I2+I3*(NT*NPAT-1) + N+1
         READ(6)(PP(I), I=1, NPP)
         DO 22 JL = 1, NL
         READ(1,24)(XL(J), J=1, N)
24       FORMAT(5E14.7)
22       CONTINUE
12       CONTINUE
         SKIP N6W RECORDS ON DATA SET 6
         WRITE(6)(SIG(I), I=1, J7)
```

Virtually all of the main program is inside DO loop 12. Referring to the table on page 62 of [7], the given incident plane wave is specified by $\vec{V}^{oc}$ and $\vec{F}^{oc}_{\sim 0} \cdot \underset{\sim r}{u}$ which reside in PP(I2+(NA-1)*I3+1) through PP(I2+(NA-1)*I3+N+1). For each of NPAT patterns, σ/λ^2 is evaluated at NT points but is printed at only the first, the (NS+1)th, the (2*NS+1)th,... of these points. The N-port impedance matrix Z_S at propagation constant BK resides in PP(NZ+1) through PP(NZ+N*N) while $\vec{V}^{oc}$ and $\vec{F}^{oc}_{\sim 0} \cdot \underset{\sim r}{u}$ are in PP(I2+((J-1)*NT+I-1)*I3+1) through PP(I2+((J-1)*NT+I-1)*I3+N+1) for the Ith value σ/λ^2 on the Jth pattern. The

JLth set of reactive loads is read into XL inside DO loop 22. NIV $\neq$ 0 obtains the open circuit impedance formulation while NIV = 0 obtains the dual short circuit admittance formulation. If NQ is neither 1 nor 2, both $\sqrt{\sigma/\lambda^2}$ and σ/λ^2 are stored in SIG. If NQ = 1, only $\sqrt{\sigma/\lambda^2}$ is stored in SIG. If NQ = 2, only σ/λ^2 is stored in SIG. All of the data (either $\sqrt{\sigma/\lambda^2}$ or σ/λ^2) for a given set of loads is stored in a block in SIG. For the first set of loads, $\sqrt{\sigma/\lambda^2}$ at the Ith point on the Jth pattern is put in SIG((J-1)*NT+I) and the corresponding σ/λ^2 is put in SIG(NT*NPAT+(J-1)*NT+I) provided NQ is neither 1 nor 2.

Minimum allocations are given by

COMPLEX C(N*N)

DIMENSION LR(N)

in the subroutine LINEQ and in the main program by

COMPLEX PP(I2+I3*(NT*NPAT-1)+N+1), ZS(N*N), Z(N*N), CUR(N)

DIMENSION ANG(NT), XL(N), ND(N), D(N), E1(NT*NPAT),

E2(NT*NPAT), SIG(J7)

DO loop 21 puts Z_S of (1) in ZS. The JL^{th} set of loads is considered in DO loop 22. DO loop 23 puts ZS in Z. DO loop 26 adds the loads to the diagonal elements of Z. If the ratio of $|XL(J)|$ to the magnitude of the Jth diagonal element of ZS is greater than 10, then DO loop 29 divides the Jth row and the Jth column of Z by the square root of this ratio. Statement 28 inverts Z. DO loop 32 is similar to DO loop 29. DO loops 29 and 32 scale [11] the matrix Z to avoid excessive round off error in the subroutine LINEQ. Do loops 29 and 32 have no net effect in the absence of round off error. DO loop 34 puts $[Z_S + Z_L]^{-1} \vec{V}^{oc}$ of (1) in CUR. DO loop 50 is necessary because (1) is combined with (52) of [7] while, for the dual short circuit admittance formulation, (7) is combined with (60) of [7]. The Jth σ/λ^2 on the LLth pattern is obtained in nested DO loops 38 and 39. In DO loop 39, PP(J5) represents $\underset{\sim}{E}^{oc}_O$ of (1). DO loop 39 stores σ/λ^2 in E2 and $\sqrt{\sigma/\lambda^2}$ in E1.

The loads XL for the sample input data are taken from the printed output of the modal resonance program. The incident electric field is an x polarized plane wave traveling in the z direction. According to the figure on page 42 of [7], this plane wave is incident on the tip of the wire triangle. The two

patterns appearing in the printed output are the second and third polarizations of (103) of [7]. For proper comparison with the $|E|$ patterns of the pattern symthesis program, only $\sqrt{\sigma/\lambda^2}$ is stored on record 5 of data set 6. The $\sqrt{\sigma/\lambda^2}$ patterns on record 5 of data set 6 can be plotted by the program on pages 104-110 of [7].

LISTING OF SIGMA OVER LAMBDA SQUARED VERSUS ANGLE PROGRAM

```
//              (0034,EE,20S,1),'MAUTZ,JOE',REGION=200K
// EXEC WATFIV
//GO.FT06F001 DD DSNAME=EE0034.REV1,DISP=OLD,UNIT=2314,            X
//              VOLUME=SER=SU0004,DCB=(RECFM=VS,BLKSIZE=2596,LRECL=2592,X
//              BUFNO=1)
//GO.SYSIN DD *
$JOB             MAUTZ,TIME=1,PAGES=40
      SUBROUTINE LINEQ(LL,C)
      COMPLEX C(100),STOR,STO,ST,S
      DIMENSION LR(40)
      DO 20 I=1,LL
      LR(I)=I
   20 CONTINUE
      M1=0
      DO 18 M=1,LL
      K=M
      DO 2 I=M,LL
      K1=M1+I
      K2=M1+K
      IF(CABS(C(K1))-CABS(C(K2))) 2,2,6
    6 K=I
    2 CONTINUE
      LS=LR(M)
      LR(M)=LR(K)
      LR(K)=LS
      K2=M1+K
      STOR=C(K2)
      J1=0
      DO 7 J=1,LL
      K1=J1+K
      K2=J1+M
      STO=C(K1)
      C(K1)=C(K2)
      C(K2)=STO/STOR
      J1=J1+LL
    7 CONTINUE
      K1=M1+M
      C(K1)=1./STOR
      DO 11 I=1,LL
      IF(I-M) 12,11,12
   12 K1=M1+I
      ST=C(K1)
      C(K1)=0.
      J1=0
      DO 10 J=1,LL
      K1=J1+I
      K2=J1+M
      C(K1)=C(K1)-C(K2)*ST
      J1=J1+LL
   10 CONTINUE
   11 CONTINUE
      M1=M1+LL
   18 CONTINUE
      J1=0
      DO 9 J=1,LL
      IF(J-LR(J)) 14,8,14
   14 LRJ=LR(J)
      J2=(LRJ-1)*LL
```

```
21 DO 13 I=1,LL
   K2=J2+I
   K1=J1+I
   S=C(K2)
   C(K2)=C(K1)
   C(K1)=S
13 CONTINUE
   LR(J)=LR(LRJ)
   LR(LRJ)=LRJ
   IF(J-LR(J)) 14,8,14
 8 J1=J1+LL
 9 CONTINUE
   RETURN
   END
   COMPLEX U,PP(3236),ZS(100),Z(100),CUR(10),E,CONJG
   DIMENSION ANG(145),XL(10),ND(10),D(10),E1(290),E2(290),SIG(4640)
   ETA=376.730
   PI=3.141593
   C1=.25*ETA/SQRT(PI*PI*PI)
   U=(0.,1.)
   READ(1,10) NF,N6W
10 FORMAT(2I3)
   WRITE(3,11) NF,N6W
11 FORMAT('0 NF N6W'/1X,I3,I4)
   J7=0
   DO 12 JF=1,NF
   READ(1,13) N,N6,NQ,NS,NL,NT,NA,NPAT,NIV,NZ,I2,I3,BK
13 FORMAT(9I3,3I4,E14.7)
   WRITE(3,14) N,N6,NQ,NS,NL,NT,NA,NPAT,NIV,NZ,I2,I3,BK
14 FORMAT('0  N N6 NQ NS NL NT NA NPAT NIV   NZ   I2   I3',6X,'BK'/1X,7I
  13,I5,4I4,E14.7)
   NP1=N+1
   JP=I2+(NA-1)*I3
   NTP=NT*NPAT
   DEL=360./(NT-1)
   DO 15 J=1,NT
   ANG(J)=(J-1)*DEL
15 CONTINUE
   C2=BK*BK*C1
   REWIND 6
   IF(N6) 16,16,17
17 DO 18 J=1,N6
   READ(6)
18 CONTINUE
16 NPP=I2+I3*(NT*NPAT-1)+NP1
   READ(6)(PP(I),I=1,NPP)
   WRITE(3,19)(PP(I),I=1,2)
19 FORMAT('0PP'/(1X,4E11.4))
   NTP=NT*NPAT
   NN=N*N
   DO 21 J=1,NN
   J1=NZ+J
   ZS(J)=PP(J1)
21 CONTINUE
   DO 22 JL=1,NL
   DO 23 J=1,NN
   Z(J)=ZS(J)
23 CONTINUE
   READ(1,24)(XL(J),J=1,N)
24 FORMAT(5E14.7)
```

```
      WRITE(3,25)(XL(J),J=1,N)
   25 FORMAT('0XL'/(1X,5E14.7))
      J1=1
      J2=0
      DO 26 J=1,N
      Z(J1)=Z(J1)+U*XL(J)
      S1=ABS(XL(J))/CABS(ZS(J1))
      J1=J1+NP1
      IF(S1-10.) 26,26,27
   27 J2=J2+1
      ND(J2)=J
      D(J2)=1./SQRT(S1)
   26 CONTINUE
      IF(J2.EQ.0) GO TO 28
      DO 29 J=1,J2
      J1=ND(J)
      J3=(J1-1)*N
      DO 30 I=1,N
      J3=J3+1
      Z(J3)=Z(J3)*D(J)
      Z(J1)=Z(J1)*D(J)
      J1=J1+N
   30 CONTINUE
   29 CONTINUE
   28 CALL LINEQ(N,Z)
      IF(J2.EQ.0) GO TO 31
      DO 32 J=1,J2
      J1=ND(J)
      J3=(J1-1)*N
      DO 33 I=1,N
      J3=J3+1
      Z(J3)=Z(J3)*D(J)
      Z(J1)=Z(J1)*D(J)
      J1=J1+N
   33 CONTINUE
   32 CONTINUE
   31 DO 34 J=1,N
      J3=(J-1)*N
      CUR(J)=0.
      DO 35 I=1,N
      J2=I+JP
      J4=J3+I
      CUR(J)=CUR(J)+Z(J4)*PP(J2)
   35 CONTINUE
   34 CONTINUE
      IF(NIV.EQ.0) GO TO 49
      DO 50 J=1,N
      CUR(J)=-CUR(J)
   50 CONTINUE
   49 WRITE(3,36) JL
   36 FORMAT('0SCATTERING PATTERN FOR THE',I3,'TH SET OF LOADS')
      WRITE(3,37)
   37 FORMAT('  ANGLE   REAL(E)',5X,'IMAG(E)',7X,'|E|',6X,'SIG/(LAM)**2'
     1)
      J1=I2
      J6=0
      DO 38 LL=1,NPAT
      DO 39 J=1,NT
      J5=J1+NP1
      E=PP(J5)
```

```
            DO 40 I=1,N
            J2=J1+I
            E=E-CUR(I)*PP(J2)
      40 CONTINUE
            E=E*C2
            J6=J6+1
            E2(J6)=E*CONJG(E)
            E1(J6)=SQRT(E2(J6))
            J3=J-1
            J1=J1+I3
            IF(J3/NS*NS.NE.J3) GO TO 39
            WRITE(3,41) ANG(J),E,E1(J6),E2(J6)
      41 FORMAT(1X,F6.1,4E12.4)
      39 CONTINUE
      38 CONTINUE
            IF(NQ.EQ.2) GO TO 42
            DO 43 J=1,NTP
            J7=J7+1
            SIG(J7)=E1(J)
      43 CONTINUE
      42 IF(NQ.EQ.1) GO TO 22
            DO 45 J=1,NTP
            J7=J7+1
            SIG(J7)=E2(J)
      45 CONTINUE
      22 CONTINUE
      12 CONTINUE
            IF(N6W) 46,46,47
      47 DO 48 J=1,N6W
            READ(6)
      48 CONTINUE
      46 WRITE(6)(SIG(I),I=1,J7)
            WRITE(3,51)(SIG(I),I=1,6)
      51 FORMAT('OSIG'/(1X,6E11.4))
            STOP
            END
   $DATA
     1  1
     4   2   1 12   1145 73   2   1   16 341   10 0.1963495E+00
    0.3727910E+03 0.6710123E+02-0.1086468E+05 0.6431934E+03
   $STOP
   /*
   //
```

PRINTED OUTPUT

```
   NF N6W
    1   1


   N N6 NQ NS NL NT NA NPAT NIV   NZ   I2   I3        BK
   4   2   1 12   1145 73    ?    1   16 341   10 0.1963495E+00


   PP
    0.1917E-03 0.3061E-02-0.3933E-03-0.3197E-02


   XL
    0.3727910E+03 0.6710123E+02-0.1086468E+05 0.6431934E+03


   SCATTERING PATTERN FOR THE  1TH SET OF LOADS
    ANGLE   REAL(E)      IMAG(E)        |E|      SIG/(LAM)**2
```

```
  0.0   0.6517E+00  -0.5051E-01   0.6537E+00   0.4273E+00
 30.0   0.5390E+00  -0.2790E+00   0.6069E+00   0.3684E+00
 60.0  -0.1260E-01  -0.4830E+00   0.4831E+00   0.2334E+00
 90.0  -0.3864E+00   0.3767E-01   0.3882E+00   0.1507E+00
120.0   0.1109E+00   0.4222E+00   0.4366E+00   0.1906E+00
150.0   0.5461E+00   0.5942E-01   0.5493E+00   0.3017E+00
180.0   0.5669E+00  -0.1850E+00   0.5963E+00   0.3556E+00
210.0   0.5461E+00   0.5942E-01   0.5493E+00   0.3017E+00
240.0   0.1109E+00   0.4222E+00   0.4366E+00   0.1906E+00
270.0  -0.3864E+00   0.3767E-01   0.3882E+00   0.1507E+00
300.0  -0.1260E-01  -0.4830E+00   0.4831E+00   0.2334E+00
330.0   0.5390E+00  -0.2790E+00   0.6069E+00   0.3684E+00
360.0   0.6517E+00  -0.5051E-01   0.6537E+00   0.4273E+00
  0.0   0.6517E+00  -0.5051E-01   0.6537E+00   0.4273E+00
 30.0   0.5789E+00  -0.5292E+00   0.7843E+00   0.6151E+00
 60.0  -0.4713E+00  -0.6832E+00   0.8300E+00   0.6889E+00
 90.0   0.4228E-01   0.3540E+00   0.3565E+00   0.1271E+00
120.0   0.1833E+00  -0.7520E+00   0.7740E+00   0.5991E+00
150.0  -0.6782E+00  -0.2552E+00   0.7246E+00   0.5251E+00
180.0  -0.5669E+00   0.1850E+00   0.5963E+00   0.3556E+00
210.0  -0.6782E+00  -0.2552E+00   0.7246E+00   0.5251E+00
240.0   0.1832E+00  -0.7520E+00   0.7740E+00   0.5991E+00
270.0   0.4229E-01   0.3540E+00   0.3565E+00   0.1271E+00
300.0  -0.4713E+00  -0.6832E+00   0.8300E+00   0.6889E+00
330.0   0.5789E+00  -0.5292E+00   0.7843E+00   0.6151E+00
360.0   0.6517E+00  -0.5051E-01   0.6537E+00   0.4273E+00
```

SIG
```
 0.6537E+00  0.6533E+00  0.6524E+00  0.6508E+00  0.6485E+00  0.6456E+00
```

VI. OPTIMUM GAIN

The program (optimum gain program) of this section obtains the set of real port currents (50) which maximizes (55). The activity on data sets 1 (punched card input) and 6 (direct access input and output) is as follows.

```
        READ(1,7) NF
7       FORMAT(20I3)
        DO 9 JF = 1, NF
        READ(1,10) N, N6, N8, NPP, NZ, NV, BK
10      FORMAT(3I3, 3I4, E14.7)
        READ(1,7)(NST(I), I = 1, N8)
        REWIND 6
        SKIP N6 RECORDS ON DATA SET 6
        READ(6)(PP(I), I = 1, NPP)
        NN8 = N*N8
        READ(1,17)(FI(I), I = 1, NN8)
17      FORMAT(4E14.7)
9       CONTINUE
```

Virtually all of the main program is inside DO loop 9. For propagation constant BK, the N-port impedance matrix Z_s of (1) is in PP(NZ+1) through PP(NZ+N*N) while $\vec{V}^{oc}$ of (36) is in PP(NV+1) through PP(NV+N). The nth basis vector $\vec{I}_n$ of port currents resides in FI((n-1)*N+1) through FI(n*N). If NST(J) = 0, then the optimization of (55) with J basis vectors (II-1) is omitted.

Minimum allocations are given by

```
        DIMENSION LR(N8), C(N8*N8)
```

in the subroutine LINER and in the main program by

```
        COMPLEX PP(NPP), VC(N8)
        DIMENSION NST(N8), FI(N*N8), R(N*N),
            RI(N*N8), RCS(N8*(N8+1)/2), V1(N8),
            V2(N8), RC(N8*N8), A1(N8), A2(N8),
            ALP(N8), CR1(N), CR2(N), CUR(N)
```

DO loop 19 puts [R] of (54) in R. DO loop 20 puts $[R]\vec{I}_n$ of (54) in RI((n-1)*N+1) through RI(n*N). DO loop 23 puts [$\hat{R}$] of (55) in RCS using the symmetric mode of storage [12]. DO loop 27 puts the real and imaginary parts of $\hat{V}^{OC}$ of (55) in V1 and V2.

DO loop 30 maximizes (55) using J basis vectors (II-1). DO loop 31 puts $\hat{R}$ in RC by columns. Statement 52 inverts $\hat{R}$. DO loop 33 puts the real and imaginary parts of $[\hat{R}]^{-1}\hat{V}^{OC}$ in A1 and A2. DO loop 35 and statement 53 put the maximum gain for complex $\vec{\alpha}$ in GC. The constant $\frac{k^2\eta}{4\pi}$ appearing in (40) resides in C1. The maximum gain for real $\vec{\alpha}$ will be put in GR. If all of the elements of either $\mathrm{Re}(\hat{V}^{OC})$ or $\mathrm{Im}(\hat{V}^{OC})$ are zero, then GR = GC, C = 1, and the evaluation of (45) is avoided. It was permissible to set C = 1 because (42) does not depend on C when $\hat{V}^{OC}$ is constant phase. The logic between statements 36 and 38 puts (44) in C and, with the help of (42), puts the maximum gain for real $\vec{\alpha}$ in GR. Upon exit from DO loop 40, the real $\vec{\alpha}$ for maximum gain is in ALP while the real and imaginary parts of the complex $\vec{\alpha}$ for maximum gain are in A1 and A2. DO loop 48 puts the real port current $\vec{I}$ for maximum gain in CUR after storing the real and imaginary parts of the complex port current $\vec{I}$ for maximum gain in CR1 and CR2.

For the sample input data, $\vec{V}^{OC}$ is the set of open circuit port voltages for an x polarized unit plane wave traveling in the positive z direction. The basis vectors (II-1) are the three dominant ($\lambda = -0.1552$, $\lambda = -10.12$, and $\lambda = -50.54$) mode currents for the unloaded wire triangle.

LISTING OF OPTIMUM GAIN PROGRAM

```
//                (0034,EE,20S,1),'MAUTZ,JOE',REGION=200K
// EXEC WATFIV
//GO.FT06F001 DD DSNAME=EE0034.REV1,DISP=OLD,UNIT=2314,              X
//               VOLUME=SER=SU0004,DCB=(RECFM=VS,BLKSIZE=2596,LRECL=2592,X
//               BUFNO=1)
//GO.SYSIN DD *
$JOB              MAUTZ,TIME=1,PAGES=30
C     THIS PROGRAM CALLS THE MATRIX INVERSION SUBROUTINE LINER LISTED
C        WITH THE PATTERN SYNTHESIS PROGRAM OF SECTION II
       COMPLEX PP(3236),VC(4)
       DIMENSION NST(4),FI(16),R(16),RI(16),RCS(10),V1(4),V2(4),RC(16)
       DIMENSION A1(4),A2(4),ALP(4),CR1(4),CR2(4),CUR(4)
       PI=3.141593
       ETA=376.730
       C2=ETA/(4.*PI)
       READ(1,7) NF
     7 FORMAT(20I3)
       WRITE(3,8) NF
     8 FORMAT('ONF=',I3)
       DO 9 JF=1,NF
       READ(1,10) N,N6,N8,NPP,NZ,NV,BK
    10 FORMAT(3I3,3I4,E14.7)
       WRITE(3,11) N,N6,N8,NPP,NZ,NV,BK
    11 FORMAT('0   N N6 N8 NPP   NZ   NV',6X,'BK'/1X,3I3,3I4,E14.7)
       READ(1,7)(NST(I),I=1,N8)
       WRITE(3,12)(NST(I),I=1,N8)
    12 FORMAT('ONST'/(1X,20I3))
       REWIND 6
       IF(N6) 13,13,14
    14 DO 15 J=1,N6
       READ(6)
    15 CONTINUE
    13 READ(6)(PP(I),I=1,NPP)
       WRITE(3,16)(PP(I),I=1,3)
    16 FORMAT('OPP'/(1X,6E11.4))
       NN8=N*N8
       READ(1,17)(FI(I),I=1,NN8)
    17 FORMAT(4E14.7)
       WRITE(3,18)(FI(I),I=1,NN8)
    18 FORMAT('OFI'/(1X,4E14.7))
       NN=N*N
       DO 19 J=1,NN
       J1=J+NZ
       R(J)=REAL(PP(J1))
    19 CONTINUE
       DO 20 J=1,N8
       J1=(J-1)*N
       DO 21 I=1,N
       J3=(I-1)*N
       J2=J1+I
       RI(J2)=0.
       DO 22 K=1,N
       J4=J3+K
       J5=J1+K
       RI(J2)=RI(J2)+R(J4)*FI(J5)
    22 CONTINUE
    21 CONTINUE
    20 CONTINUE
```

```
      J1=0
      DO 23 J=1,N8
      J2=(J-1)*N
      DO 24 I=1,J
      J1=J1+1
      RCS(J1)=0.
      J4=(I-1)*N
      DO 25 K=1,N
      J3=J2+K
      J5=J4+K
      RCS(J1)=RCS(J1)+FI(J5)*RI(J3)
   25 CONTINUE
   24 CONTINUE
   23 CONTINUE
      WRITE(3,26)(RCS(I),I=1,J1)
   26 FORMAT('ORCS'/(1X,7E11.4))
      DO 27 I=1,N8
      VC(I)=0.
      J1=(I-1)*N
      DO 28 K=1,N
      J2=J1+K
      J3=NV+K
      VC(I)=VC(I)+FI(J2)*PP(J3)
   28 CONTINUE
      V1(I)=REAL(VC(I))
      V2(I)=AIMAG(VC(I))
   27 CONTINUE
      WRITE(3,29)(VC(I),I=1,N8)
   29 FORMAT('OVC'/(1X,7E11.4))
      C1=C2*BK*BK
      DO 30 J=1,N8
      IF(NST(J).EQ.0) GO TO 30
      J2=0
      DO 31 K=1,J
      J3=(K-1)*J
      J5=K
      DO 32 I=1,K
      J2=J2+1
      J4=J3+I
      RC(J4)=RCS(J2)
      RC(J5)=RC(J4)
      J5=J5+J
   32 CONTINUE
   31 CONTINUE
   52 CALL LINER(J,RC)
      S1=0.
      S2=0.
      DO 33 K=1,J
      A1(K)=0.
      A2(K)=0.
      J3=(K-1)*J
      DO 34 I=1,J
      J1=J3+I
      A1(K)=A1(K)+RC(J1)*V1(I)
      A2(K)=A2(K)+RC(J1)*V2(I)
   34 CONTINUE
      S1=S1+ABS(A1(K))
      S2=S2+ABS(A2(K))
   33 CONTINUE
      GC=0.
```

```
      DO 35 K=1,J
      GC=GC+V1(K)*A1(K)+V2(K)*A2(K)
   35 CONTINUE
   53 GC=GC*C1
      IF(S1*S2.NE.0.) GO TO 36
      GR=GC
      C=1.
      GO TO 38
   36 S1=0.
      S2=0.
      S3=0.
      DO 39 K=1,J
      S1=S1+V1(K)*A1(K)
      S2=S2+V2(K)*A2(K)
      S3=S3+V1(K)*A2(K)
   39 CONTINUE
      A=(S1-S2)/(2.*S3)
      SA=SQRT(A*A+1.)
      C=-A+SIGN(SA,S3)
      GR=C1*(S1+C*S3)
   38 DO 40 K=1,J
      ALP(K)=A1(K)+C*A2(K)
      A2(K)=-A2(K)
   40 CONTINUE
      WRITE(3,45) GR,GC
   45 FORMAT('0',5X,'GR',9X,'GC'/1X,2E11.4)
      WRITE(3,46)(ALP(K),K=1,J)
   46 FORMAT('OREAL ALPHA FOR MAXIMUM GAIN'/(1X,5E14.7))
      WRITE(3,47)(A1(K),A2(K),K=1,J)
   47 FORMAT('OCOMPLEX ALPHA FOR MAXIMUM GAIN'/(1X,4E14.7))
      DO 48 K=1,N
      CR1(K)=0.
      CR2(K)=0.
      J1=K
      DO 49 I=1,J
      CR1(K)=CR1(K)+FI(J1)*A1(I)
      CR2(K)=CR2(K)+FI(J1)*A2(I)
      J1=J1+N
   49 CONTINUE
      CUR(K)=CR1(K)-C*CR2(K)
   48 CONTINUE
      WRITE(3,50)(CUR(K),K=1,N)
   50 FORMAT('OREAL PORT QUANTITIES FOR MAXIMUM GAIN'/(1X,4E14.7))
      WRITE(3,51)(CR1(K),CR2(K),K=1,N)
   51 FORMAT('OCOMPLEX PORT QUANTITIES FOR MAXIMUM GAIN'/(1X,4E14.7))
   30 CONTINUE
    9 CONTINUE
      STOP
      END
$DATA
  1
  4  2  31066   161061 0.1963495E+00
  0  0  1
-0.1338342E+00 0.4326460E+00 0.8418684E+00 0.9999999E+00
-0.6078172E+00 0.9999999E+00 0.8054470E+00-0.6457505E+00
 0.9999996E+00-0.5373682E+00 0.1367921E-01 0.7396740E-01
$STOP
/*
//
```

PRINTED OUTPUT

NF= 1

```
   N N6 N8 NPP   NZ   NV       BK
   4  2  31066    161061 0.1963495E+00
```

NST
```
   0   0   1
```

PP
```
  0.1917E-03 0.3061E-02-0.3933E-03-0.3197E-02-0.6371E-03-0.2576E-03
```

FI
```
-0.1338342E+00 0.4326460E+00 0.8418684E+00 0.9999999E+00
-0.6078172E+00 0.9999999E+00 0.8054470E+00-0.6457505E+00
 0.9999996E+00-0.5373682E+00 0.1367921E-01 0.7396740E-01
```

RCS
```
  0.1857E+03-0.2441E-03 0.1047E+03-0.5817E-04-0.2823E-03 0.6226E+01
```

VC
```
  0.7265E+01-0.6718E+01-0.5377E+01 0.3362E+01-0.1137E+01-0.2486E+01
```

```
      GR         GC
  0.1554E+01 0.2440E+01
```

REAL ALPHA FOR MAXIMUM GAIN
```
-0.1090493E+01 0.9509159E+00-0.1265057E+02
```

COMPLEX ALPHA FOR MAXIMUM GAIN
```
 0.3912077E-01 0.3617598E-01-0.5133666E-01-0.3209720E-01
-0.1825690E+00 0.3992882E+00
```

REAL PORT QUANTITIES FOR MAXIMUM GAIN
```
-0.1308260E+02 0.7277129E+01-0.3251898E+00-0.2640278E+01
```

COMPLEX PORT QUANTITIES FOR MAXIMUM GAIN
```
-0.1566013E+00 0.4139557E+00 0.6369549E-01-0.2310105E+00
-0.1091181E-01 0.1006477E-01 0.5876725E-01 0.8643705E-01
```

Next, the set of real port currents listed under the heading "Real port quantities for maximum gain" in the printed output of the optimum gain program was fed into the modal resonance program of section IV. The loads appearing in the printed output of the modal resonance program were then fed into the σ/λ^2 versus angle program of section V with the variables NQ and N6W changed so as to store σ/λ^2 on record 6 of data set 6. The following printed output resulted.

PRINTED OUTPUT OF THE MODAL RESONANCE PROGRAM

NF= 1

```
  N N6 N8   I2
  4  2  1   16
```

PP
```
 0.1917E-03 0.3061E-02-0.3933E-03-0.3197E-02-0.6371E-03-0.2576E-03
```

CUR
```
-0.1308260E+02 0.7277129E+01-0.3251898E+00-0.2640278E+01
```

XL
```
 0.2583062E+03 0.1614346E+03 0.6522367E+04-0.3005938E+03
```

PRINTED OUTPUT OF THE SIGMA/LAMBDA SQUARED VERSUS ANGLE PROGRAM
```
 NF N6W
  1   2
```

```
  N N6 NQ NS NL NT NA NPAT NIV  NZ  I2  I3      BK
  4  2  2 12  1145 73    2   1  16 341  10 0.1963495E+00
```

PP
```
 0.1917E-03 0.3061E-02-0.3933E-03-0.3197E-02
```

XL
```
 0.2583062E+03 0.1614346E+03 0.6522367E+04-0.3005938E+03
```

SCATTERING PATTERN FOR THE 1TH SET OF LOADS

ANGLE	REAL(E)	IMAG(E)	|E|	SIG/(LAM)**2
0.0	0.8329E+00	-0.3128E-01	0.8335E+00	0.6947E+00
30.0	0.7219E+00	-0.4781E+00	0.8659E+00	0.7497E+00
60.0	-0.2990E+00	-0.7010E+00	0.7621E+00	0.5808E+00
90.0	-0.4324E-01	0.3059E+00	0.3090E+00	0.9547E-01
120.0	0.2382E+00	-0.6192E+00	0.6634E+00	0.4401E+00
150.0	-0.6800E+00	-0.3753E+00	0.7767E+00	0.6033E+00
180.0	-0.7510E+00	0.4409E-01	0.7523E+00	0.5659E+00
210.0	-0.6800E+00	-0.3753E+00	0.7767E+00	0.6033E+00
240.0	0.2382E+00	-0.6192E+00	0.6634E+00	0.4401E+00
270.0	-0.4324E-01	0.3059E+00	0.3090E+00	0.9547E-01
300.0	-0.2990E+00	-0.7010E+00	0.7621E+00	0.5808E+00
330.0	0.7219E+00	-0.4781E+00	0.8659E+00	0.7497E+00
360.0	0.8329E+00	-0.3128E-01	0.8335E+00	0.6947E+00
0.0	0.8329E+00	-0.3128E-01	0.8335E+00	0.6947E+00
30.0	0.6287E+00	-0.8528E-01	0.6345E+00	0.4025E+00
60.0	0.4398E+00	0.2292E+00	0.4960E+00	0.2460E+00
90.0	0.9456E+00	0.1046E+00	0.9514E+00	0.9051E+00
120.0	0.6271E+00	-0.3244E+00	0.7061E+00	0.4986E+00
150.0	0.5874E+00	-0.6249E-01	0.5907E+00	0.3489E+00
180.0	0.7510E+00	-0.4409E-01	0.7523E+00	0.5659E+00
210.0	0.5873E+00	-0.6251E-01	0.5907E+00	0.3489E+00
240.0	0.6271E+00	-0.3244E+00	0.7061E+00	0.4986E+00
270.0	0.9456E+00	0.1046E+00	0.9514E+00	0.9051E+00
300.0	0.4398E+00	0.2292E+00	0.4959E+00	0.2459E+00
330.0	0.6287E+00	-0.8533E-01	0.6345E+00	0.4025E+00
360.0	0.8329E+00	-0.3128E-01	0.8335E+00	0.6947E+00

SIG
```
 0.6947E+00 0.6952E+00 0.6967E+00 0.6993E+00 0.7027E+00 0.7071E+00
```

VII. BACKSCATTERING VERSUS FREQUENCY

The program (σ/λ^2 versus frequency program) of this section requires the port parameters Z_S, $\vec{V}^{OC}$, and $\vec{F}^{OS}_{\sim O} \cdot \underset{\sim r}{u}$ at the frequencies of interest. As a preliminary step, the impedance matrix program, the excitation vector program and the port parameter programs on pages 45-69 of [7] were run after insertion of the statements

```
          DO 200 I = 1, KV1
          V(I) = CONJG(V(I))
200       CONTINUE
```

just after statement 37 in the main program of the excitation vector program. These 3 additional statements change the incident field from a plane wave traveling in the minus z direction to a plane wave traveling in the positive z direction. The impedance matrix program and the port parameter program were run with the G level compiler but the excitation vector program was run with WATFIV. It has been observed that the particular propagation constant read in as 0.1963495 is printed correctly by the WATFIV compiler but is printed as 0.1963494 by the G level compiler.

PRINTED OUTPUT OF IMPEDANCE MATRIX PROGRAM

```
NF N6 NP NW      RAD
19  6 94  6 0.1600000E+00
```

PX
```
  2.0706   1.8117   1.5529   1.2941   1.0353   0.7765   0.5176   0.2588   0.0000  -0.2588
 -0.5176  -0.7765  -1.0353  -1.2941  -1.5529  -1.8117  -2.0706  -1.5529  -1.8117  -2.0706
 -1.0353   0.0000   1.0353   2.0706   1.8117   1.5529  -4.6587  -4.3999  -4.1411  -3.1058
 -2.0706  -1.0353   0.0000   1.0353   2.0706   3.1058   4.1411   4.3999   4.6587  -4.1411
 -4.3999  -4.6587  -4.9176  -5.1764  -5.4352  -5.6940  -5.9528  -6.2117  -5.1764  -4.1411
 -3.1058  -2.0706  -1.0353   0.0000   1.0353   2.0706   3.1058   4.1411   5.1764   6.2117
  5.9528   5.6940   5.4352   5.1764   4.9176   4.6587   4.3999   4.1411   2.0706   3.1058
  4.1411   3.8823   3.6235   3.3646   3.1058   2.8470   2.5882   2.3294   2.0706   1.0353
  0.0000   0.0000  -1.0353  -2.0706  -2.3294  -2.5882  -2.8470  -3.1058  -3.3646  -3.6235
 -3.8823  -4.1411  -3.1058  -2.0706
```

PY
```
  0.0000   0.0000   0.0000   0.0000   0.0000   0.0000   0.0000   0.0000   0.0000   0.0000
  0.0000   0.0000   0.0000   0.0000   0.0000   0.0000   0.0000   0.0000   0.0000   0.0000
  0.0000   0.0000   0.0000   0.0000   0.0000   0.0000   0.0000   0.0000   0.0000   0.0000
  0.0000   0.0000   0.0000   0.0000   0.0000   0.0000   0.0000   0.0000   0.0000   0.0000
  0.0000   0.0000   0.0000   0.0000   0.0000   0.0000   0.0000   0.0000   0.0000   0.0000
  0.0000   0.0000   0.0000   0.0000   0.0000   0.0000   0.0000   0.0000   0.0000   0.0000
  0.0000   0.0000   0.0000   0.0000   0.0000   0.0000   0.0000   0.0000   0.0000   0.0000
  0.0000   0.0000   0.0000   0.0000   0.0000   0.0000   0.0000   0.0000   0.0000   0.0000
  0.0000   0.0000   0.0000   0.0000   0.0000   0.0000   0.0000   0.0000   0.0000   0.0000
  0.0000   0.0000   0.0000   0.0000
```

PZ
```
  7.7274   6.7615   5.7956   4.8296   3.8637   2.8978   1.9319   0.9659   0.0000   0.9659
  1.9319   2.8978   3.8637   4.8296   5.7956   6.7615   7.7274   5.7956   6.7615   7.7274
  7.7274   7.7274   7.7274   7.7274   6.7615   5.7956  17.3867  16.4207  15.4548  15.4548
 15.4548  15.4548  15.4548  15.4548  15.4548  15.4548  15.4548  16.4207  17.3867  15.4548
 16.4207  17.3867  18.3526  19.3185  20.2844  21.2504  22.2163  23.1822  23.1822  23.1822
 23.1822  23.1822  23.1822  23.1822  23.1822  23.1822  23.1822  23.1822  23.1822  23.1822
 22.2163  21.2504  20.2844  19.3185  18.3526  17.3867  16.4207  15.4548  15.4548  15.4548
 15.4548  14.4889  13.5230  12.5570  11.5911  10.6252   9.6593   8.6933   7.7274   7.7274
  7.7274   7.7274   7.7274   7.7274   8.6933   9.6593  10.6252  11.5911  12.5570  13.5230
 14.4889  15.4548  15.4548  15.4548
```

LL
```
  1 18 27 40 69 82
```

BKK
```
 0.1570796E+00 0.1668971E+00 0.1767145E+00 0.1826050E+00 0.1865320E+00
 0.1904590E+00 0.1924224E+00 0.1943859E+00 0.1953678E+00 0.1963494E+00
 0.1973312E+00 0.1983130E+00 0.2002766E+00 0.2022399E+00 0.2061670E+00
 0.2100939E+00 0.2159845E+00 0.2258018E+00 0.2356192E+00
```

IMPEDANCE MATRIX OF ORDER 38
```
 0.1962E+01-0.6556E+03 0.1943E+01 0.2897E+03 0.1886E+01 0.5413E+02 0.1286E+00
 0.1962E+01-0.1606E+01-0.1383E+02
```

IMPEDANCE MATRIX OF ORDER 38
```
 0.2214E+01-0.6138E+03 0.2189E+01 0.2744E+03 0.2117E+01 0.5148E+02 0.1447E+00
 0.1880E+01-0.1799E+01-0.1332E+02
```

PLUS 17 MORE APPEARANCES OF IMPEDANCE MATRIX OF ORDER 38

PRINTED OUTPUT OF EXCITATION VECTOR PROGRAM

```
NF N6 NP NW NT NPAT
19 25 94  6  1  1
```

HK
```
 0.1570796E+00  0.1668971E+00  0.1767145E+00  0.1826050F+00  0.1865320E+00
 0.1904590E+00  0.1924225E+00  0.1943860F+00  0.1953678E+00  0.1963495E+00 ·
 0.1973312E+00  0.1983130E+00  0.2002766E+00  0.2022399E+00  0.2061670E+00
 0.2100939E+00  0.2159845E+00  0.2258018E+00  0.2356193E+00
```

NPA
```
 ?
```

PX
```
  2.0706   1.8117   1.5529   1.2941   1.0353   0.7765   0.5176   0.2588   0.0000  -0.2588
 -0.5176  -0.7765  -1.0353  -1.2941  -1.5529  -1.8117  -2.0706  -1.5529  -1.8117  -2.0706
 -1.0353   0.0000   1.0353   2.0706   1.8117   1.5529  -4.6587  -4.3999  -4.1411  -3.1058
 -2.0706  -1.0353   0.0000   1.0353   2.0706   3.1058   4.1411   4.3999   4.6587  -4.1411
 -4.3999  -4.6587  -4.9176  -5.1764  -5.4352  -5.6940  -5.9528  -6.2117  -5.1764  -4.1411
 -3.1058  -2.0706  -1.0353   0.0000   1.0353   2.0706   3.1058   4.1411   5.1764   6.2117
  5.9528   5.6940   5.4352   5.1764   4.9176   4.6587   4.3999   4.1411   2.0706   3.1058
  4.1411   3.8823   3.6235   3.3646   3.1058   2.8470   2.5882   2.3294   2.0706   1.0353
  0.0000   0.0000  -1.0353  -2.0706  -2.3294  -2.5882  -2.8470  -3.1058  -3.3646  -3.6235
 -3.8823  -4.1411  -3.1058  -2.0706
```

PY
```
  0.0000   0.0000   0.0000   0.0000   0.0000   0.0000   0.0000   0.0000   0.0000   0.0000
  0.0000   0.0000   0.0000   0.0000   0.0000   0.0000   0.0000   0.0000   0.0000   0.0000
  0.0000   0.0000   0.0000   0.0000   0.0000   0.0000   0.0000   0.0000   0.0000   0.0000
  0.0000   0.0000   0.0000   0.0000   0.0000   0.0000   0.0000   0.0000   0.0000   0.0000
  0.0000   0.0000   0.0000   0.0000   0.0000   0.0000   0.0000   0.0000   0.0000   0.0000
  0.0000   0.0000   0.0000   0.0000   0.0000   0.0000   0.0000   0.0000   0.0000   0.0000
  0.0000   0.0000   0.0000   0.0000   0.0000   0.0000   0.0000   0.0000   0.0000   0.0000
  0.0000   0.0000   0.0000   0.0000   0.0000   0.0000   0.0000   0.0000   0.0000   0.0000
  0.0000   0.0000   0.0000   0.0000   0.0000   0.0000   0.0000   0.0000   0.0000   0.0000
  0.0000   0.0000   0.0000   0.0000
```

PZ
```
  7.7274   6.7615   5.7956   4.8296   3.8637   2.8978   1.9319   0.9659   0.0000   0.9659
  1.9319   2.8978   3.8637   4.8296   5.7956   6.7615   7.7274   5.7956   6.7615   7.7274
  7.7274   7.7274   7.7274   7.7274   6.7615   5.7956  17.3867  16.4207  15.4548  15.4548
 15.4548  15.4548  15.4548  15.4548  15.4548  15.4548  15.4548  16.4207  17.3867  15.4548
 16.4207  17.3867  18.3526  19.3185  20.2844  21.2504  22.2163  23.1822  23.1822  23.1822
 23.1822  23.1822  23.1822  23.1822  23.1822  23.1822  23.1822  23.1822  23.1822  23.1822
 22.2163  21.2504  20.2844  19.3185  18.3526  17.3867  16.4207  15.4548  15.4548  15.4548
 15.4548  14.4889  13.5230  12.5570  11.5911  10.6252   9.6593   8.6933   7.7274   7.7274
  7.7274   7.7274   7.7274   7.7274   8.6933   9.6593  10.6252  11.5911  12.5570  13.5230
 14.4889  15.4548  15.4548  15.4548
```

LL
```
  1 18 27 40 69 82
 0.3056983F+01-0.5124519E+03
-0.2141947E+00-0.4635820E+00
 0.1917231E-03  0.3060562F-02
 0.1000000E+01  0.8659999E+00
 0.4113738E+00  0.4117785E+00
 0.1692279E+00  0.1695610E+00
 0.1962249E+01-0.6555750E+03
 0.2213690E+01-0.6137673F+03
 0.2479986E+01-0.5764236E+03
 0.2646889E+01-0.5558608E+03
 0.2761129E+01-0.5428396E+03
 0.2877709E+01-0.5303284E+03
 0.2936877E+01-0.5242546E+03
 0.2996636E+01-0.5182971E+03
 0.3026734E+01-0.5153604E+03
 0.3056983E+01-0.5124519F+03
 0.3087398E+01-0.5095703E+03
 0.3117905E+01-0.5067163E+03
 0.3179434E+01-0.5010867E+03
 0.3241521E+01-0.4955605E+03
 0.3367495E+01-0.4848052E+03
 0.3495778E+01-0.4744280E+03
 0.3692583E+01-0.4595256E+03
 0.4032207E+01-0.4363062E+03
 0.4386234E+01-0.4148894E+03
```

V
-0.3148E+00-0.4053E+00-0.4215E+00-0.2927E+00-0.4898E+00-0.1534E+00-0.5132E+00
-0.5862E-01-0.4898E+00-0.1534E+00

PRINTED OUTPUT OF PORT PARAMETER PROGRAM

```
NF NT   M   N N6V N6Z N6P NVT
19  1  38   4  25 -20   1   1
```

BK
```
0.1570796E+00 0.1668971E+00 0.1767145E+00 0.1826050E+00 0.1865320E+00
0.1904590E+00 0.1924224E+00 0.1943859E+00 0.1953678E+00 0.1963494E+00
0.1973312E+00 0.1983130E+00 0.2002766E+00 0.2022399E+00 0.2061670E+00
0.2100939E+00 0.2154845E+00 0.2258018E+00 0.2356192E+00
```

N4
```
 4   9 13 22  1  2  3  5  6  7  8 10 11 12 14 15 16 17 18 19
20 21 23 24 25 26 27 28 29 30 31 32 33 34 35 36 37 38
```

```
NY NZ MIV MII MISC NISC KESC MIOC NVOC KEOC
 1  1  0   0   0    1    1    0    1    1
0.3057E+01-0.5125E+03 0.3011E+01 0.2382E+03
-0.2142E+00-0.4636E+00-0.3706E+00-0.3513E+00
0.1917E-03 0.3061E-02-0.3933E-03-0.3197E-02
0.1000E+01 0.8660E+00 0.5000E+00 0.0000E+00
0.4114E+00 0.4118E+00 0.4130E+00 0.4150E+00
0.1692E+00 0.1696E+00 0.1706E+00 0.1722E+00
0.1962E+01-0.6556E+03 0.1943E+01 0.2897E+03
0.2214E+01-0.6138E+03 0.2189E+01 0.2744E+03
0.2480E+01-0.5764E+03 0.2449E+01 0.2609E+03
0.2647E+01-0.5559E+03 0.2612E+01 0.2536E+03
0.2761E+01-0.5428E+03 0.2723E+01 0.2489E+03
0.2878E+01-0.5303E+03 0.2837E+01 0.2445E+03
0.2937E+01-0.5243E+03 0.2894E+01 0.2424E+03
0.2997E+01-0.5183E+03 0.2952E+01 0.2403E+03
0.3027E+01-0.5154E+03 0.2981E+01 0.2393E+03
0.3057E+01-0.5125E+03 0.3011E+01 0.2382E+03
0.3087E+01-0.5096E+03 0.3040E+01 0.2372E+03
0.3118E+01-0.5067E+03 0.3070E+01 0.2362E+03
0.3179E+01-0.5011E+03 0.3129E+01 0.2343E+03
0.3242E+01-0.4956E+03 0.3189E+01 0.2324E+03
0.3367E+01-0.4848E+03 0.3311E+01 0.2286E+03
0.3496E+01-0.4744E+03 0.3435E+01 0.2251E+03
0.3693E+01-0.4595E+03 0.3625E+01 0.2200E+03
0.4032E+01-0.4363E+03 0.3952E+01 0.2121E+03
0.4386E+01-0.4149E+03 0.4291E+01 0.2050E+03
```

V
-0.3148E+00 0.4053E+00-0.4215E+00 0.2927E+00-0.4898E+00 0.1534E+00

Z
0.1962E+01-0.6556E+03 0.1943E+01 0.2897E+03 0.1886E+01 0.5413E+02

Z
0.2214E+01-0.6138E+03 0.2189E+01 0.2744E+03 0.2117E+01 0.5148E+02

PLUS 17 MORE APPEARANCES OF Z.   THE FINAL 2 LINES OF PRINTED OUTPUT ARE

PP
0.1064E-03 0.1373E-02-0.1728E-03-0.3332E-02-0.2692E-03-0.6069E-03

According to the preceding printed output, impedance matrices are on records 7 to 25 of data set 6. The excitation vectors and port parameters are on records 26 and 27 respectively.

In the σ/λ^2 versus frequency program, the activity on data sets 1 (punched card input) and 6 (direct access input and output) is as follows.

```
        READ(1,10) NC,N6W
10      FORMAT(20I3)
        DO 12 JC = 1, NC
        READ(1,13) N, NF, N6, NL, NIV, NZ, NV, I3, B
13      FORMAT(5I3, 3I4, E14.7)
        READ(1,15)(BK(I), I = 1, NF)
15      FORMAT(5E14.7)
        REWIND 6
        SKIP N6 RECORDS ON DATA SET 6
        NPP = NV + (NF-1)*I3 + N+1
        READ(6)(PP(I), I=1, NPP)
        DO 22 JL = 1, NL
        READ(1, 23)(XL(J), J=1, N)
23      FORMAT(5E14.7)
22      CONTINUE
12      CONTINUE
        SKIP N6W RECORDS ON DATA SET 6
        WRITE(6)(SIG(I), I = 1, J7)
```

Virtually all of the main program is inside DO loop 12. Of all the propagation constants BK, B is the particular propagation constant at which the load reactances XL are evaluated. The N-port parameter Z_S at the Jth frequency resides in PP(NZ + (J-1)*I3+1) through PP(NZ+(J-1)*I3+N*N) while $\vec{V}^{oc}$ and $F_{\sim O}^{oc} \cdot \underset{\sim}{u}_r$ reside in PP(NV+(J-1)*I3+1) through PP(NV+(J-1)*I3+N+1). For the open circuit impedance formulation, NIV $\neq$ 0 whereas NIV = 0 for the dual short circuit admittance formulation. The JL^{th} set of reactive loads is read into XL inside DO loop 22.

Minimum allocations are given by

```
        COMPLEX C(N*N)

        DIMENSION LR(N)
```

in the subroutine LINEQ and in the main program by

```
        COMPLEX PP(NV+(NF-1)*I3+N+1), Z(N*N), V(N)

        DIMENSION BK(NF), C2(NF), XL(N), ND(N), D(N),
```

$$SIG(\sum_{JC=1}^{NC} NL*NF)$$

The index JF of DO loop 25 denotes the JF^{th} frequency. DO loop 26 puts Z_S in Z. DO loop 27 adds the reactive loads to the diagonal elements of Z. If the ratio of the magnitude of the $ND(J)^{th}$ reactive load to the magnitude of the $ND(J)^{th}$ diagonal element of Z_S is greater than 10, then DO loop 33 divides the $ND(J)^{th}$ row and the $ND(J)^{th}$ column of Z by the square root of this ratio. Statement 35 inverts Z. DO loop 37 is similar to DO loop 33. DO loops 33 and 37 scale [11] the matrix Z to avoid excessive round off error in the subroutine LINEQ. DO loops 33 and 37 have no net effect in the absence of round off error.

DO loop 39 puts $\vec{V}^{oc}$ in V. DO loop 40 accumulates $\vec{V}^{oc}[Z_S+Z_L]^{-1}\vec{V}^{oc}$ of (68) of [7] in EL. In statement 43, PP(J3) is $\underset{\sim}{F_O^{oc}} \cdot \underset{\sim}{u_r}$ of (68) of [7]. The constant $C2(JF) = \dfrac{k^2\eta}{4\pi^{3/2}}$ is necessary to obtain σ/λ^2 which is subsequently stored in $SIG((JL-1)*NF+JF)$ for the JL^{th} set of loads and the JF^{th} frequency.

There are two sets of reactive loads in the sample input data. The first set of reactive loads resonates the set of port currents which radiates the pattern synthesized by the pattern synthesis program of section II. The second set of reactive loads resonates the set of port currents generated by the optimum gain program of section VI. The 38 values of σ/λ^2 appearing in the printed output are put on record 28 of data set 6. The center frequency mentioned in the printed output is the frequency at which the propagation constant is B. Note that σ/λ^2 at the center frequency is the same as σ/λ^2 at 180° on the pattern printed by the σ/λ^2 versus angle program of section V.

LISTING OF THE SIGMA OVER LAMBDA SQUARED VERSUS FREQUENCY PROGRAM

```
//              (0034,EE,20S,1),'MAUTZ,JOE',REGION=200K
// EXEC WATFIV
//GO.FT06F001 DD DSNAME=EE0034.REV1,DISP=OLD,UNIT=2314,              X
//              VOLUME=SER=SU0004,DCB=(RECFM=VS,BLKSIZE=2596,LRECL=2592,X
//              BUFNO=1)
//GO.SYSIN DD *
$JOB            MAUTZ,TIME=1,PAGES=40
C     THIS PROGRAM CALLS THE MATRIX INVERSION SUBROUTINE LINEQ LISTED
C     WITH THE SIGMA OVER LAMBDA SQUARED VERSUS ANGLE PROGRAM OF SECTION V
      COMPLEX U,PP(798),Z(100),V(4),EL,CUR,E,CONJG
      DIMENSION BK(19),C2(19),XL(4),ND(4),D(4),SIG(608)
      ETA=376.730
      PI=3.141593
      C1=.25*ETA/SQRT(PI*PI*PI)
      U=(0.,1.)
      READ(1,10) NC,N6W
   10 FORMAT(20I3)
      WRITE(3,11) NC,N6W
   11 FORMAT('0 NC N6W'/1X,I3,I4)
      J7=0
      DO 12 JC=1,NC
      READ(1,13) N,NF,N6,NL,NIV,NZ,NV,I3,B
   13 FORMAT(5I3,3I4,E14.7)
      WRITE(3,14) N,NF,N6,NL,NIV,NZ,NV,I3,B
   14 FORMAT('0   N NF N6 NL NIV  NZ   NV  I3',6X,'B'/1X,4I3,4I4,E14.7)
      READ(1,15)(BK(I),I=1,NF)
   15 FORMAT(5E14.7)
      WRITE(3,16)(BK(I),I=1,NF)
   16 FORMAT('0BK'/(1X,5E14.7))
      REWIND 6
      IF(N6) 17,17,18
   18 DO 19 J=1,N6
      READ(6)
   19 CONTINUE
   17 NP1=N+1
      NPP=NV+(NF-1)*I3+NP1
      READ(6)(PP(I),I=1,NPP)
      WRITE(3,20)(PP(I),I=1,2)
   20 FORMAT('0PP'/(1X,4E11.4))
      DO 21 J=1,NF
      C2(J)=C1*BK(J)*BK(J)
      BK(J)=BK(J)/B
   21 CONTINUE
      NN=N*N
      DO 22 JL=1,NL
      READ(1,23)(XL(J),J=1,N)
   23 FORMAT(5E14.7)
      WRITE(3,24)(XL(J),J=1,N)
   24 FORMAT('0XL'/(1X,5E14.7))
      WRITE(3,51) JL
   51 FORMAT('0BACKSCATTERING VERSUS RATIO OF FREQUENCY TO'/'  CENTER FR
     1EQUENCY FOR THE',I3,'TH SET OF LOADS')
      WRITE(3,52)
   52 FORMAT('    FREQ',3X,'REAL(E)',5X,'IMAG(E)',7X,'|E|',6X,'SIG/(LAM)*
     1*2')
      KZ=NZ
      KV=NV
      DO 25 JF=1,NF
```

```
      DO 26 J=1,NN
      J2=J+KZ
      Z(J)=PP(J2)
   26 CONTINUE
      J2=0
      J1=1
      DO 27 J=1,N
      IF(XL(J)) 28,28,29
   28 X=XL(J)/BK(JF)
      GO TO 30
   29 X=XL(J)*BK(JF)
   30 S1=ABS(X)/CABS(Z(J1))
      Z(J1)=Z(J1)+U*X
      J1=J1+NP1
      IF(S1-10.) 27,27,31
   31 J2=J2+1
      ND(J2)=J
      D(J2)=1./SQRT(S1)
   27 CONTINUE
      IF(J2.EQ.0) GO TO 35
      DO 33 J=1,J2
      J1=ND(J)
      J3=(J1-1)*N
      DO 34 I=1,N
      J3=J3+1
      Z(J3)=Z(J3)*D(J)
      Z(J1)=Z(J1)*D(J)
      J1=J1+N
   34 CONTINUE
   33 CONTINUE
   35 CALL LINEQ(N,Z)
      IF(J2.EQ.0) GO TO 36
      DO 37 J=1,J2
      J1=ND(J)
      J3=(J1-1)*N
      DO 38 I=1,N
      J3=J3+1
      Z(J3)=Z(J3)*D(J)
      Z(J1)=Z(J1)*D(J)
      J1=J1+N
   38 CONTINUE
   37 CONTINUE
   36 DO 39 J=1,N
      J2=J+KV
      V(J)=PP(J2)
   39 CONTINUE
      EL=0.
      DO 40 J=1,N
      J3=(J-1)*N
      CUR=0.
      DO 41 I=1,N
      J4=J3+I
      CUR=CUR+Z(J4)*V(I)
   41 CONTINUE
      EL=EL+CUR*V(J)
   40 CONTINUE
      J3=KV+NP1
      IF(NIV) 43,42,43
   42 E=(PP(J3)-EL)*C2(JF)
      GO TO 53
```

```
   43 E=(PP(J3)+EL)*C2(JF)
   53 J7=J7+1
      SIG(J7)=F*CONJG(E)
      E1=SQRT(SIG(J7))
      WRITE(3,54) BK(JF),E,E1,SIG(J7)
   54 FORMAT(1X,F6.3,4E12.4)
      KZ=KZ+I3
      KV=KV+I3
   25 CONTINUE
   22 CONTINUE
   12 CONTINUE
      IF(N6W) 47,47,48
   48 DO 49 J=1,N6W
      READ(6)
   49 CONTINUE
   47 WRITE(6)(SIG(I),I=1,J7)
      WRITE(3,50)(SIG(I),I=1,6)
   50 FORMAT('0SIG'/(1X,6E11.4))
      STOP
      END
$DATA
  1  0
  4 19 26  2  1  16  37  42 0.1963495E+00
 0.1570796E+00 0.1668971E+00 0.1767145E+00 0.1826050E+00 0.1865320E+00
 0.1904590E+00 0.1924225E+00 0.1943860E+00 0.1953678E+00 0.1963495E+00
 0.1973312E+00 0.1983130E+00 0.2002766E+00 0.2022399E+00 0.2061670E+00
 0.2100939E+00 0.2159845E+00 0.2258018E+00 0.2356193E+00
 0.3727910E+03 0.6710123E+02-0.1086468E+05 0.6431934E+03
 0.2583062E+03 0.1614346E+03 0.6522367E+04-0.3005938E+03
$STOP
/*
//
```

PRINTED OUTPUT

```
 NC N6W
  1   0


 N NF N6 NL NIV  NZ   NV  I3       B
 4 19 26  2    1  16   37  42 0.1963495E+00


BK
 0.1570796E+00 0.1668971E+00 0.1767145E+00 0.1826050E+00 0.1865320E+00
 0.1904590E+00 0.1924225E+00 0.1943860E+00 0.1953678E+00 0.1963495E+00
 0.1973312E+00 0.1983130E+00 0.2002766E+00 0.2022399E+00 0.2061670E+00
 0.2100939E+00 0.2159845E+00 0.2258018E+00 0.2356193E+00


PP
 0.1064E-03 0.1373E-02-0.1728E-03-0.3332E-02


XL
 0.3727910E+03 0.6710123E+02-0.1086468E+05 0.6431934E+03


BACKSCATTERING VERSUS RATIO OF FREQUENCY TO
CENTER FREQUENCY FOR THE  1TH SET OF LOADS
 FREQ   REAL(E)      IMAG(E)       |E|      SIG/(LAM)**2
 0.800 -0.6733E-02  0.9202E-01  0.9227E-01  0.8514E-02
 0.850  0.1096E+00  0.1412E+00  0.1787E+00  0.3194E-01
 0.900 -0.2062E+00 -0.2498E+00  0.3239E+00  0.1049E+00
 0.930 -0.1360E+00  0.8386E-01  0.1598E+00  0.2552E-01
```

```
0.950  -0.5849E-01   0.1732E+00   0.1828E+00   0.3342E-01
0.970   0.7587E-01   0.2658E+00   0.2764E+00   0.7639E-01
0.980   0.2212E+00   0.3001E+00   0.3728E+00   0.1390E+00
0.990   0.4712E+00   0.2128E+00   0.5171E+00   0.2674E+00
0.995   0.5796E+00   0.4336E-01   0.5812E+00   0.3378E+00
1.000   0.5669E+00  -0.1850E+00   0.5963E+00   0.3556E+00
1.005   0.4275E+00  -0.3480E+00   0.5512E+00   0.3038E+00
1.010   0.2646E+00  -0.3971E+00   0.4772E+00   0.2277E+00
1.020   0.6259E-01  -0.3390E+00   0.3447E+00   0.1188E+00
1.030  -0.1761E-01  -0.2594E+00   0.2600E+00   0.6760E-01
1.050  -0.6257E-01  -0.1596E+00   0.1714E+00   0.2939E-01
1.070  -0.6923E-01  -0.1088E+00   0.1289E+00   0.1662E-01
1.100  -0.6765E-01  -0.7074E-01   0.9788E-01   0.9580E-02
1.150  -0.6775E-01  -0.4406E-01   0.8082E-01   0.6532E-02
1.200  -0.7760E-01  -0.2744E-01   0.8231E-01   0.6774E-02
```

XL

```
0.2583062E+03 0.1614346E+03 0.6522367E+04-0.3005938E+03
```

BACKSCATTERING VERSUS RATIO OF FREQUENCY TO
CENTER FREQUENCY FOR THE   2TH SET OF LOADS

```
 FREQ    REAL(E)      IMAG(E)       |E|       SIG/(LAM)**2
0.800   0.2503E-02   0.8414E-01   0.8417E-01   0.7085E-02
0.850   0.5783E-01   0.8861E-01   0.1058E+00   0.1120E-01
0.900   0.1205E+00   0.4872E-01   0.1300E+00   0.1690E-01
0.930   0.1513E+00  -0.7158E-02   0.1515E+00   0.2295E-01
0.950   0.1614E+00  -0.6851E-01   0.1754E+00   0.3075E-01
0.970   0.1433E+00  -0.1756E+00   0.2266E+00   0.5134E-01
0.980   0.9220E-01  -0.2734E+00   0.2885E+00   0.8324E-01
0.990  -0.1124E+00  -0.4315E+00   0.4459E+00   0.1989E+00
0.995  -0.4309E+00  -0.4385E+00   0.6148E+00   0.3780E+00
1.000  -0.7510E+00   0.4410E-01   0.7522E+00   0.5659E+00
1.005  -0.3540E+00   0.4775E+00   0.5944E+00   0.3533E+00
1.010  -0.3072E-01   0.4151E+00   0.4162E+00   0.1732E+00
1.020   0.1517E+00   0.2160E+00   0.2639E+00   0.6966E-01
1.030   0.1898E+00   0.1039E+00   0.2164E+00   0.4681E-01
1.050   0.1952E+00  -0.2097E-01   0.1964E+00   0.3856E-01
1.070   0.1746E+00  -0.1003E+00   0.2014E+00   0.4057E-01
1.100   0.1189E+00  -0.1854E+00   0.2202E+00   0.4850E-01
1.150  -0.2448E-01  -0.2612E+00   0.2623E+00   0.6880E-01
1.200  -0.2026E+00  -0.2384E+00   0.3128E+00   0.9787E-01
```

SIG
```
0.8514E-02 0.3194E-01 0.1049E+00 0.2552E-01 0.3342E-01 0.7639E-01
```

VIII. PLOTS

The synthesized pattern, the scattering pattern of the wire triangle
loaded by the set of reactive loads that resonate the set of port currents
which radiate the synthesized pattern, and the scattering pattern of the
wire triangle loaded by the set of reactive loads that resonate the set of
port currents which radiate the optimum gain pattern are plotted from
records 4, 5, and 6 of data set 6 by the plot program on pages 104-110
of [7].

PRINTED OUTPUT OF PLOT PROGRAM ON PAGES 104-110 OF REFERENCE 7

NF
 3

 NT NE NEP NS N6
145 4   3 12 3

N1
  0   0   1 1

N2
  1   3 4

N3
  0   0   1

NSBL
  4   0   0

SCAL
 0.2000E+01 0.2000E+01 0.2000E+01
 0.3057E+01-0.5125E+03 0.3011E+01 0.2382E+03
-0.2142E+00-0.4636E+00-0.3706E+00-0.3513E+00
 0.1917E-03 0.3061E-02-0.3933E-03-0.3197E-02

SIG
 0.1000E+01 0.8660E+00 0.5000E+00 0.0000E+00

 NT NE NEP NS N6
145 2   2 12 4

```
N1
   1   1

N2
   1   2

N3
   0   1

NSBL
   4   4

SCAL
  0.2000E+01  0.2000E+01
  0.3057E+01-0.5125E+03  0.3011E+01  0.2382E+03
 -0.2142E+00-0.4636E+00-0.3706E+00-0.3513E+00
  0.1917E-03  0.3061E-02-0.3933E-03-0.3197E-02
  0.1000E+01  0.8660E+00  0.5000E+00  0.0000E+00

SIG
  0.6537E+00  0.6533E+00  0.6524E+00  0.6508E+00

  NT  NE  NEP  NS  N6
 145   2    2  12   5

N1
   1   1

N2
   1   2

N3
   0   1

NSBL
   4   4

SCAL
  0.2000E+01  0.2000E+01
  0.3057E+01-0.5125E+03  0.3011E+01  0.2382E+03
 -0.2142E+00-0.4636E+00-0.3706E+00-0.3513E+00
  0.1917E-03  0.3061E-02-0.3933E-03-0.3197E-02
  0.1000E+01  0.8660E+00  0.5000E+00  0.0000E+00
  0.6537E+00  0.6533E+00  0.6524E+00  0.6508E+00

SIG
  0.6947E+00  0.6952E+00  0.6967E+00  0.6993E+00
```

A new plot program (σ/λ^2 versus frequency plot program) has been written to plot the data stored on record 28 of data set 6 by the σ/λ^2 versus frequency program of section VII. The σ/λ^2 versus frequency plot program accepts input data on data sets 1 (punched cards) and 6 (direct access) in the following manner.

```
        READ(1,10) NC
10      FORMAT(20I3)
        DO 12 JC = 1, NC
        READ(1,13) NF, N6, NE, NEP, B
13      FORMAT(4I3, E14.7)
        READ(1,10)(N2(I), I=1, NEP)
        READ(1,10)(N3(I), I=1, NEP)
        READ(1,17)(BK(I), I=1, NF)
17      FORMAT(5E14.7)
        REWIND 6
        SKIP N6 RECORDS ON DATA SET 6
        NEF = NE*NF
        READ(6)(SIG(J), J=1, NEF)
12      CONTINUE
```

Virtually all of the program is inside DO loop 12. The quantity σ/λ^2 for the Jth set of loads and the Ith frequency is in SIG((J-1)*NF+I) where J=1,2,...NE and I=1,2,...NF. Among the propagation constants BK, B is the propagation constant corresponding to the center frequency. The Ith curve to be plotted is that of σ/λ^2 for the N2(I)[th] load set. If N3(I) > 0, the pen draws the horizontal and vertical axes and moves to the next frame after plotting the Ith curve. If N3(I) $\le$ 0, the pen neither plots any axis nor moves to the next frame after plotting the Ith curve.

Minimum allocations are given by

        DIMENSION N2(NEP), N3(NEP), BK(NF), SIG(NE*NF), Y(NF)

Do loop 19 prepares the horizontal coordinates BK for plotting. The index L of DO loop 24 denotes the Lth curve to be plotted. DO loop 25 puts

the vertical coordinates in Y. Statement 31 plots σ/λ^2 versus frequency by drawing straight lines between data points. Statement 27 draws the vertical axis. The logic between and including statements 28 and 29 puts the scale on the vertical axis. Statement 30 draws the horizontal axis. DO loop 26 puts the scale on the horizontal axis.

LISTING OF SIGMA OVER LAMBDA SQUARED VERSUS FREQUENCY PLOT PROGRAM

```
//              (0034,EF,1,1,,10),'MAUT7,JOE',REGION=140K
// MSG 1, MAKE ONE COPY OF PLOT NOW AND HOLD OTHER FOR BLACK INDIA INK
// EXEC FORTGCLG,PARM.FORT='MAP'
//FORT.SYSIN DD *
      DIMENSION AREA(400),N2(100),N3(100),BK(50),X1(4),Y1(4),SIG(608)
      DIMENSION Y(50)
      CALL PLOTID
      CALL PLOTS(AREA,400)
      READ(1,10) NC
   10 FORMAT(20I3)
      WRITE(3,11) NC
   11 FORMAT('ONC=',I3)
      DO 12 JC=1,NC
      READ(1,13) NF,N6,NE,NEP,B
   13 FORMAT(4I3,E14.7)
      WRITE(3,14) NF,N6,NE,NEP,B
   14 FORMAT('O NF N6 NE NEP',6X,'B'/1X,3I3,I4,E14.7)
      READ(1,10)(N2(I),I=1,NEP)
      WRITE(3,15)(N2(I),I=1,NEP)
   15 FORMAT('ON2'/(1X,20I3))
      READ(1,10)(N3(I),I=1,NEP)
      WRITE(3,16)(N3(I),I=1,NEP)
   16 FORMAT('ON3'/(1X,20I3))
      READ(1,17)(BK(I),I=1,NF)
   17 FORMAT(5E14.7)
      WRITE(3,18)(BK(I),I=1,NF)
   18 FORMAT('OBK'/(1X,5E14.7))
      S1=10./B
      DO 19 J=1,NF
      BK(J)=S1*BK(J)-6.
   19 CONTINUE
      X1(1)=1.
      X1(2)=1.
      Y1(1)=1.
      Y1(2)=7.
      X1(3)=1.
      X1(4)=6.
      Y1(3)=1.
      Y1(4)=1.
      REWIND 6
      IF(N6) 20,20,21
   21 DO 22 J=1,N6
      READ(6)
   22 CONTINUE
   20 NEF=NE*NF
      READ(6)(SIG(J),J=1,NEF)
      WRITE(3,23)(SIG(J),J=1,6)
   23 FORMAT('OSIG'/(1X,6E11.4))
      DO 24 L=1,NEP
      J1=(N2(L)-1)*NF
      DO 25 J=1,NF
      J2=J+J1
      Y(J)=SIG(J2)
      IF(Y(J).LT..00001) Y(J)=.00001
      Y(J)=6.+ALOG10(Y(J))
   25 CONTINUE
   31 CALL LINE(BK(1),Y(1),NF,1,0,0)
      IF(N3(L)) 24,24,27
```

```
   27 CALL LINE(X1,Y1,2,1,0,0)
   28 CALL NUMBER(.52,6.93,.14,10.,0.,0)
      CALL SYMBOL(1.,7.,.14,13,90.,-1)
      CALL NUMBER(.64,5.93,.14,1.,0.,0)
      CALL SYMBOL(1.,6.,.14,13,90.,-1)
      CALL NUMBER(.52,4.93,.14,.1,0.,1)
      CALL SYMBOL(1.,5.,.14,13,90.,-1)
      CALL NUMBER(.40,3.93,.14,.01,0.,2)
      CALL SYMBOL(1.,4.,.14,13,90.,-1)
      CALL NUMBER(.28,2.93,.14,.001,0.,3)
      CALL SYMBOL(1.,3.,.14,13,90.,-1)
      CALL NUMBER(.16,1.93,.14,.0001,0.,4)
   29 CALL SYMBOL(1.,2.,.14,13,90.,-1)
   30 CALL LINE(X1(3),Y1(3),2,1,0,0)
      XA=6.
      XB=1.2
      DO 26 J=1,5
      XC=XA-.16
      CALL NUMBER(XC,.72,.14,XB,0.,1)
      CALL SYMBOL(XA,1.,.14,13,0.,-1)
      XA=XA-1.
      XB=XB-.1
   26 CONTINUE
      CALL PLOT(7.,0.,-3)
   24 CONTINUE
   12 CONTINUE
      CALL PLOT(5.,0.,-3)
      STOP
      END
/*
//GO.FT06F001 DD DSNAME=EE0034.REV1,DISP=OLD,UNIT=2314,              X
//             VOLUME=SER=SU0004,DCB=(RECFM=VS,BLKSIZE=2596,LRECL=2592,X
//             BUFNO=1)
//GO.SYSIN DD *
  1
 19 27   2   2 0.1963495E+00
  1  2
  1  1
 0.1570796E+00 0.1668971E+00 0.1767145E+00 0.1826050E+00 0.1865320E+00
 0.1904590E+00 0.1924225E+00 0.1943860E+00 0.1953678E+00 0.1963495E+00
 0.1973312E+00 0.1983130E+00 0.2002766E+00 0.2022399E+00 0.2061670E+00.
 0.2100939E+00 0.2159845E+00 0.2258018E+00 0.2356193E+00
/*
//
```

PRINTED OUTPUT

NC=   1

 NF N6 NE NEP   B
 19 27   2   2 0.1963494E+00

N2
  1 2

N3
  1 1

BK
  0.1570796E+00 0.1668971E+00 0.1767145E+00 0.1826050E+00 0.1865320E+00

  0.1904590E+00 0.1924224E+00 0.1943859E+00 0.1953678E+00 0.1963494E+00
  0.1973312E+00 0.1983130E+00 0.2002766E+00 0.2022399E+00 0.2061670E+00
  0.2100939E+00 0.2159845E+00 0.2258018E+00 0.2356192E+00

SIG
  0.8514E-02 0.3194E-01 0.1049E+00 0.2552E-01

REFERENCES

[1] J. K. Schindler, R. B. Mack, and P. Blacksmith, Jr., "The Control of Electromagnetic Scattering by Impedance Loading," Proc. IEEE, vol. 53, No. 8, August 1965, pp. 993-1004.

[2] R. F. Harrington, "Theory of Loaded Scatterers," Proc. Inst. Elect. Eng., vol. 111, April 1964, pp. 617-623.

[3] R. F. Harrington and J. R. Mautz, "Radiation and Scattering from Loaded Bodies of Revolution," Appl. Sci. Res., vol. 26, 1971. See also: R. F. Harrington and J. R. Mautz, "Computation of Radiation and Scattering from Loaded Bodies of Revolution," Scientific Report No. 4 on Contract No. F19628-68-C-0180 between Syracuse University and Air Force Cambridge Research Laboratories, AFCRL-70-0046, January 1970.

[4] R. F. Harrington and J. R. Mautz, "Control of Radar Scattering by Reactive Loading," IEEE Trans. on Antennas and Propagation, vol. AP-20, No. 4, July 1972, pp. 446-454. See also: J. R. Mautz and R. F. Harrington, "Control of Radar Scattering by Reactive Loading," Scientific Report No. 13 on Contract No. F19628-68-C-0180 between Syracuse University and Air Force Cambridge Research Laboratories, AFCRL-71-0429, August 1971.

[5] R. J. Garbacz and R. H. Turpin, "A Generalized Expansion for Radiated and Scattered Fields," IEEE Trans. on Antennas and Propagation, vol. AP-19, No. 3, May 1971, pp. 348-358.

[6] R. F. Harrington and J. R. Mautz, "Theory of Characteristic Modes for Conducting Bodies," IEEE Trans. on Antennas and Propagation, vol. AP-19, No. 5, September 1971, pp. 622-628.

[7] R. F. Harrington and J. R. Mautz, "Modal Analysis of Loaded N-Port Scatterers," Scientific Report No. 16 on Contract No. F19628-68-C-0180 between Syracuse University and Air Force Cambridge Research Laboratories, AFCRL-72-0179, March 1972.

[8] L. D. Bakhrakh and V. I. Troytskiy, "Mixed Problems of Antenna Synthesis," Radio Engineering and Electronic Physics, vol. 12, No. 3, March 1967, pp. 404-414.

[9] Y. I. Choni, "Synthesis of an Antenna According to a Given Amplitude Radiation Pattern," Radio Engineering and Electronic Physics, vol. 16, No. 5, May 1971, pp. 770-778.

[10] R. F. Harrington, Field Computation by Moment Methods, Macmillan Co., New York, 1968, Chap. 10.

110

[11] G. F. Forsythe and C. B. Moler, Computer Solution of Linear Algebraic Systems, Prentice-Hall, 1967, Sec. 11.

[12] IBM System/360 Scientific Surboutine Package (360A-CM-03X) Version III, Programmer's Manual, pages 4-5.